MULTIBAND AND CONCURRENT MATCHING NETWORK DESIGN

SERKAN YILDIZ

IŞIK UNIVERSITY
2020

MULTIBAND AND CONCURRENT MATCHING NETWORK DESIGN

SERKAN YILDIZ
B.S., Electrical-Electronics Engineering, Istanbul University, 2009
M.Sc., Telecommunication Engineering, Istanbul Technical University, 2011

Submitted to the Graduate School of Science and Engineering
in partial fulfillment of the requirements for the degree of
Doctorate in Philosophy
in
Electronics Engineering

IŞIK UNIVERSITY
2020

IŞIK UNIVERSITY
GRADUATE SCHOOL OF SCIENCE AND ENGINEERING

MULTIBAND AND CONCURRENT MATCHING NETWORK DESIGN

SERKAN YILDIZ

APPROVED BY:

Prof. Dr. Ahmet Aksen (Thesis Advisor)	Işık University
Prof. Dr. Sıddık B. Yarman (Thesis Co-Advisor)	İstanbul University-Cerrahpaşa
Prof. Dr. İbrahim Akduman	İstanbul Technical University
Dr. Öğr. Üyesi Ramazan Köprü	Işık University
Prof. Dr. Serdar Özoğuz	İstanbul Technical University
Prof. Dr. Ece Olcay Güneş	İstanbul Technical University

APPROVAL DATE: 05./02./2020

MULTIBAND AND CONCURRENT MATCHING NETWORK DESIGN

Abstract

Multiband network design has become a big issue due to the current improvements in RF and MW technologies. Since the new wireless protocols come up fast such as 3G, 4G, 5G etc., the RF and MW hardware must be designed to provide services to all distinct technologies in simultaneous regimes. To avoid interference, noise, harmonics, etc., the use of multiband matching or filtering at the front-end or back-end of RF/MW devices is an inevitable work. Particularly multiband matching in a multiband system is always necessary to be sure of proper power transfer between each multiband units.

In this thesis, the multiband matching network design problem is addressed under the analytical perspective. Therefore, a deep investigation on network theoretical foundations is performed. In addition, only passive networks are concerned for providing concurrent operation. One of the well-known semi-analytical network design methods, which is called real frequency technique, is taken as a main domain to develop the thesis contributions.

Two main approaches are elaborated. The first approach is the generation of proper frequency mapping functions and determination of prototype networks to design multiband matching network. The proposed frequency transformation approach is useful and practical for multiband filter and matching network designs.

As a second research track of the thesis; a synthesis based approach is aimed to be developed for generalized multiband matching network designs. A proper integration of the proposed approach with RFT matching techniques and examination of the implementation results are provided.

Keywords: Multiband matching, frequency mapping, real frequency technique, Brune functions, network synthesis

ÇOKLUBAND VE EŞ ZAMANLI EMPEDANS UYDURMA DEVRESİ TASARIMI

Özet

RF ve Mikrodalga teknolojilerindeki gelişmelerle birlikte çokluband devre tasarımı önemli bir konu olmuştur. 3G, 4G, 5G gibi yeni kablosuz iletişim protokollerinin hızlı bir şekilde ortaya çıkmasıyla, RF ve Mikrodalga donanımlarının tüm ayrı teknolojilere eş zamanlı servis sağlayacak şekilde tasarlanması gerekmektedir. Enterferans, gürültü, harmonikler vb. etkilerden kaçınmak için RF ve Mikrodalga cihazlarının giriş-sonunda veya çıkış-sonunda çokluband empedans uydurma veya filtreleme yapılması kaçınılmaz bir iştir. Özellikle, çokluband empedans uydurma, çokluband sistemlerdeki ayrık çokluband birimler arasındaki uygun güç aktarımından emin olmak için daima gereklidir.

Bu tezde, çokluband empedans uydurma devresi tasarım problemi analitik bakış açısıyla ele alınmıştır. Bu yüzden, devre teorisinin temelleri üzerine derin bir inceleme yapılmıştır. Buna ek olarak, eş zamanlı operasyon sağlamak için sadece pasif devreler düşünülmüştür. İyi bilinen yarı analitik devre tasarım metodları olan reel frekans tekniği tezin katkılarını geliştirmek için temel zemin olarak alınmıştır.

İki temel yaklaşım üzerine durulmuştur. İlk yaklaşım, uygun frekans haritalama fonksiyonlarının ve prototip devrelerinin belirlenmesidir. Önerilen frekans dönüştürme yaklaşımı, çokluband filtre ve empedans uydurma devre tasarımları için kullanışlı ve pratiktir.

Tezin ikinci araştırma yolu olarak, genelleştirilmiş çokluband devrenin empedans uydurma tasarımları için sentez tabanlı bir yaklaşım geliştirilmesi amaçlanmıştır. Önerilen yaklaşımın, reel frekans teknikleriyle uygun entegrasyonu ve uygulama sonuçlarının incelemesi sunulmuştur.

Anahtar kelimeler: Çokluband empedans uydurma, frekans haritalama, reel frekans tekniği, Brune fonkisyonları, devre sentezi

Acknowledgements

First, I would like to thank my advisor Prof. Dr. Ahmet Aksen and my co-advisor Prof. Dr. Sıddık B. Yarman for their constant supports, guidance, patience and encouragements throughout my PhD work. Their insights on network theory and many years of experiences contributed to my comprehension to understand tedious theoretical literature. I am deeply greateful to have been one of their PhD students.

I am also thankfull to scientific committee members of the thesis, Prof. Dr. İbrahim Akduman, Dr. Öğr. Üyesi Ramazan Köprü for their great contributions and supports.

I would like to thank to my friend and colleague Sedat Kılınç who gave great supports for manufacturing and measuring the dual band pass, dual band stop and triple band pass filters in the application works of the thesis.

Lastly, I thank to my family and my parents for their deepest patience, tolerance and supports.

To My Family...

Table of Contents

List of Tables

List of Figures

List of Abbreviations

EDGE	**E**nhanced **D**ata **G**SM **E**nvironment
WCDMA	**W**ideband **C**ode **D**ivision **M**ultiple **A**ccess
TD-SCDMA	**T**ime **D**ivision **S**ynchronous **C**ode **D**ivision **M**ultiple **A**ccess
GSM	**G**lobal **S**ystem for **M**obile
CDMA2000	**C**ode **D**ivision **M**ultiple **A**ccess **2000**
HSPA	**H**igh **S**peed **P**acket **A**ccess
LTE	**L**ong **T**erm **E**volution
IS-95	**I**nterim **S**tandard **95**
RF	**R**adio **F**requency
UWB	**U**ltra-**W**ide **B**and
GSM900	**G**lobal **S**ystem for **M**obile **9000**
GSM1800	**G**lobal **S**ystem for **M**obile **1800**
GPS	**G**lobal **P**ositioning **S**ystem
RFT	**R**eal **F**requency **T**echnique
DCS1800	**D**igital **C**ellular **S**ystem **1800**
PCS1900	**P**ersonal **C**ommunications **S**ervice **1900**
LNA	**L**ow **N**oise **A**mplifier
LP	**L**ow **P**ass
BP	**B**and **P**ass
PCB	**P**rinted **C**ircuit **B**oard
MOSFET	**M**etal-**O**xide **S**emiconductor **F**ield-**E**ffect **T**ransistor
ADC	**A**nalog to **D**igital **C**onverter
MOS-HBT	**M**etal-**O**xide **S**emiconductor **H**eterojunction **B**ipolar **T**ransistor
MEMS	**M**icro-**E**lectro **M**echanical **S**ystems

MMIC	**M**onolithic **M**icrowave **I**ntegrated **C**ircuit
MIM	**M**etal-**I**nsulator-**M**etal
GaN	**Ga**llium **N**itride
IC	**I**ntegrated **C**ircuit
US-PCS	**U**nited **S**tates- **P**ersonal **C**ommunications **S**ervice
FTZs	**F**inite **T**ransmission **Z**eros
TPG	**T**ransducer **P**ower **G**ain
CAD	**C**omputer **A**ided **D**esign
RFLST	**R**eal **F**requency **L**ine **S**egment **T**echnique
RFDCT	**R**eal **F**requency **D**irect **C**omputational **T**echnique
SRFT	**S**implified **R**eal **F**requency **T**echnique
RHP	**R**ight **H**and-side **P**ole
LHP	**L**eft **H**and-side **P**ole
DC	**D**irect **C**urrent
LPtoBP	**L**ow **P**ass **to** **B**and **P**ass
LPtoDB	**L**ow **P**ass **to** **D**ual **P**ass
LPtoQB	**L**ow **P**ass **to** **Q**uad **P**ass
MB	**M**ulti-**B**and
HP	**H**igh **P**ass
PIFA	**P**lanar **I**nverted-**F** **A**ntenna
UMTS	**U**niversal **M**obile **T**elecommunications **S**ystem
DBS	**D**ual **B**and **S**top
FR4	**F**lame **R**etardant **4**
EM	**E**lectro**M**agnetic
ADS	**A**dvanced **D**esign **S**ystem

Chapter 1

Introduction

1.1 Motivation for Multiband Matching

Due to fast development in RF and MW technology, there has been a huge demand on multi-standard products, which are capable of providing services to different technologies such as, EDGE, WCDMA, TD-SCDMA, Bluetooth, GSM, CDMA2000, HSPA, LTE, IS-95, etc. RF hardware behind these technologies has to perform at all distinct frequency bands.

One of the solution for this issue is, expanding the bandwidth capabilities of RF devices to cover all required bands. This is also called UWB systems. UWB systems may cover unnecessary bands between aimed frequency bands. As an example if it is needed to provide services only for GSM900 and GSM1800 bands but it will be inevitable to cover GPS bands between these two bands. This brings several disadvantages such as interference, noise, size etc. [1].

Beside of UWB systems, multiband systems can also perform distinct frequency bands without covering unnecessary bands by employing multiband RF units in hardware. This provides many benefits such as; size reduction, better harmonic performance, less cross-talk, less interference etc. [2]. Multiband RF units can be filters, antennas, amplifiers, etc. Employment of multiband components also requires incorporation of multiband matching network between each discrete unit for proper power flow.

In most of applications, multiband systems are demanded to perform simultaneously over the entire intended frequency bands. Therefore, multiband matching networks must also provide concurrent operation. This automatically restrict the topology of multiband networks with the use of passive elements only.

Although the multiband networks have been evaluated by many scientists of the field, there has been not much effort given to multiband matching applications. Moreover, the analytical solution of multiband matching network design problem has not been completely resolved.

In this thesis, several novel analytical design approaches are developed to establish a concrete solution to multiband concurrent matching network design problem.

1.2 Impedance Matching Theory

Since the crucial RF components such as; transmitters, receivers, antennas, etc. come into place of human life, engineers have faced with the problem of impedance matching. The fundamental concept of impedance matching lies on maximum power transfer theorem, which is developed by Thevenin. A robust RF network requires proper power flow between each RF units. Thus at the interface of each RF unit there must be placed a proper matching network.

The theoretical foundation of impedance matching have begun to development since 1930s. Foster reactance theorem was one of the breakthrough to give a mathematical basis of matching network [3]. Bode presented gain-bandwidth theory for restricted load topologies [4]. This gave the idea of limit of matching frequency bandwidth for specified load topologies. Fano and Youla gave more generalized form of gain-bandwidth theory for arbitrary loads [5, 6]. Afterwards, many researcher have investigated on analytical approach to extend their understanding of the matching network design problem.

The main goal is transferring maximum power from a complex generator to a complex load trough a matching network. In addition, the SNR of the whole

system can be improved by employing matching network. As given in the Figure (1.1), the absorbed power from load is related with the incident and reflected power at the input of matching network (i.e.$|a_1|^2 - |b_1|^2 = |b_2|^2 - |a_2|^2$]).

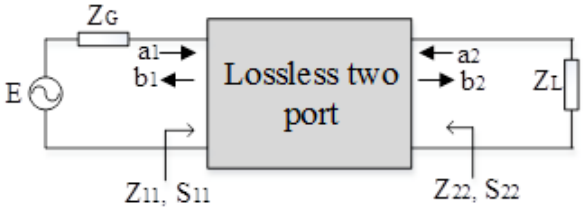

Figure 1.1: Lossless two-port with complex terminations.

When $Z_{11} = Z_{22}^*$ (complex conjugate of Z_{22}), the available power at the input of lossless matching network is transferred to load in maximum otherwise there will be some mismatch as;

$$MM = \left|\frac{Z_{11} - Z_G^*}{Z_{11} + Z_G}\right| = \left|\frac{Z_{22} - Z_L^*}{Z_{22} + Z_L}\right| \tag{1.1}$$

The reflected power can be also formulated as return loss as

$$RL = -20\log(MM) \tag{1.2}$$

This is so-called conjugate matching. Even though the conjugate matching can be obtainable for single frequencies, it is not possible for over a specified band of interest [7]. However, this is the most common case for matching network design. To overcome this issue, more circuit elements are incorporated in design.

Several design methodologies can be classified in matching network design problem [8]:

(a) Single Matching: This is the case when the source is resistive and the load network is a complex impedance, which is aimed to match to the resistive source

by employing a matching network. This is the most common scenario for antenna matching problems.

(b) Double Matching: in this case, both source and load impedance are complex and the matching network is needed to hand impedance matching at the input and output port of it. This scenario is a generalized case for most of matching problem.

(c) Active matching: If an active device is in concern for matching problem, then it can be classified as active matching. This case more complex form of the double matching problem.

Once the matching problem is defined, the next part is choosing proper network topology for the interested application. The matching network may include lumped elements, distributed elements, combination of lumped and distributed elements also called mixed topology or some ad-hoc circuitry may include lattice structures [9].

The element values should be chosen accordingly with the complex load and source network. This opens another main aspect of design and there are mainly two methods exist. First method is the analytical approach and the second is using computer aided design tools.

The analytical approach requires explicit model for the load and generator networks. However, this may not be possible in practical applications. One can get measurements data of complex load or source network and determine an approximate circuit model. A transfer function can be written in terms of approximate load/source model and theoretical gain-bandwidth limit is derived by solving a set of integral equations [4]. This method can be applicable for simple impedance model but not efficient if the number of elements in approximate impedance model are increased. Therefore, the analytic approach for matching network design is not applicable for today's engineering problems.

On the other hand, computer aided design tools provide a large scale of solutions for complex matching problems by employing numerical optimization techniques [10, 11]. In these techniques, mainly circuit components of matching circuitry are optimized over a frequency band of interest to maximize the transferred power. One of the famous method in this family is Real Frequency Techniques (RFT), which yields a semi-analytical design procedure to establish realizable driving point impedance or admittance [12].

1.3 Basic Impedance Matching Network Topologies

Generally, matching networks are assumed to be composed of lossless reactive components. Several basic network topologies are mostly used for many matching problems. The main idea is the elimination and equalization of the complex and real part impedance of load over a frequency band.

1.3.1 Lumped Element Matching

Lossless lumped reactive components are widely used in matching networks. One of the simple topology is so called L-type network. There are eight different variations of L-type network, which are composed of a serial, and a shunt LC component as illustrated in Figure (1.2).

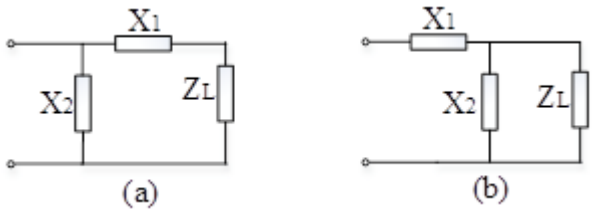

Figure 1.2: L-type matching network topologies.

The different configurations are chosen according to the impedance characteristic of the load network. The X1 and X2 can be either a capacitor or an inductor.

Generally, first element eliminated imaginary part of load impedance and the second element equalizes the real part of load impedance to the resistive source network. These topologies are effective only for narrow band matching applications.

Adding a third element to the L-type network will generate Pi or T-type networks. These networks provide the adjustment capability of quality factor to designers. If numbers of elements are increased the bandwidth of matching operation is inherently increased. In addition, the reactive components store more energy. Thus, a rule of thumb is concluded as "sufficient bandwidth minimum stored energy" [13]. The specific choice of network topology is determined according to the application of interest.

Using lumped components in matching network brings some advantages and disadvantages. These are summarized [14] in Table (1.1).

Advantages	**Disadvantages**
Easy footprint	Lower sensitivity
Small size	Not applicable above 10GHz
Wide bandwidth	Lossy
Simple circuit model	Not easy to repeat same value
High reactance value	Limited power handling
Low cost	
Robust against coupling effects	
Easy to apply different circuit topologies	

Table 1.1: Lumped elements advantages and disadvantages.

1.3.2 Distributed Element Matching

Impedance response of distributed network element varies along with physical length. Distributed elements with proper termination and length have special impedance characteristic. Thus, these elements are incorporated in design as a network component. Mostly distributed elements are designed as transmission lines or replacement structures of lumped components [15]. Especially transmission lines are extensively used in matching networks. This is so called stub

matching. Open, short termination of series and shunt stubs are used to eliminate reactive part and equalize real part impedance of the complex load as in lumped element matching. The quality factors of stubs are higher than their lumped counterparts. Therefore, narrow-band matching operation can be effectively obtained. Bandwidth of the matching network can be extended by increasing number of stubs or cascading transmission lines. The advantages and disadvantages of distributed element matching are summarized [16] in Table (1.2).

Advantages	**Disadvantages**
Easy to adjust reactance value	Narrow bandwidth
Reasonable size at high frequencies	Expensive dielectric costs
Easy for PCB applications	Big size at low frequencies
Higher sensitivity	Limited power handling capacity
Less parasitic	High vulnerability to couplings
Easy to produce same elements	

Table 1.2: Distributed elements advantages and disadvantages.

1.3.3 Mixed Element Matching

One of the well-established matching network design technique is so called "mixed matching". This technique is involved with lumped and distributed elements together in matching network design. It is very effective in squeezing powers to desired bands [9].

From the practical point of view, lumped elements are connected to each other through a transmission line over a printed circuit board. At higher frequencies these transmission lines creates parasitic effects and they must be included in design process. Therefore, mixed element circuit topologies are a practical and robust way of matching network design [17].

Many of study investigates cascaded configuration of lumped elements with an ideal transmission line called unit elements [18]. Matching network application with mixed network topology provides better harmonic rejection characteristics.

1.4 Literature Review on Multiband Matching Networks

Multiband matching network design is strongly related with the technology that the system is involved with. Frequency bands, linearity, phase concerns and bandwidth or the size of circuit board are some of design prerequisites [19]. Many methods have been presented in literature to meet some of these requirements. If there would be a classifications of these methods, it might be the one with made according to used elements.

1.4.1 Multiband Matching with Lumped Elements

One of these techniques is about using lumped circuit elements. With proper design structures of LC tuner elements, it is possible to accomplish multiband characteristics. S. F. Chang et. all [20] have designed a concurrent triple band gain amplifier. The design employs three resonators to provide matching at 2.4 GHz, 5.8 GHz and 9.0 GHz frequencies. Yiqun Li et all [21] designed a multiband matching network for GSM cell phone. They also used three sections of resonator circuitry to match the antenna of a cell phone to resistive generator over GSM900, DCS1800 and PCS1900 bands.

Several applications are involved with LNAs. One of them is done by H. Hashemi et. all [22]. They used lumped elements in their design for the minimum size and concurrent operation concerns. Dual band matching network is established by applying input and output matching networks in LNA design. Conjugate matching principle is used. The input matching network consists of a single parallel LC while the output-matching network includes two resonators.

N. Nallam and S. Chatterjee presented a general technique [23] for synthesis of concurrent multi-band matching networks with lumped elements. The technique is based on LP to BP transformation. An LP filter is transformed to a BP filter and the new structure brings two resonance frequencies. If second transformation is applied then four different resonance frequencies are occurred. Even if the

technique is promising; the resulted resonance frequencies are in relation with previous resonance frequencies in geometric mean. As a result, it is not easy to make matching in predefined frequencies.

In several lumped matching studies are involved with using PCB waveguide. J.-S. Lee et all [24] have designed a matching circuit for a mobile phone antenna that include lumped elements and co-planar waveguide. The idea behind the study is placing a lumped element band reject matching filter on co-planar wave-guide with a proper distance from the antenna. This distance is determined according to the place where the impedance into the antenna is set to short circuit. Resonant frequencies can be controlled by lumped elements values. Even if it gives good matching results, using co-planar wave-guide in PCB increases the size of circuit board.

1.4.2 Multiband Matching with Tunable Varactors and Inductors

Another technique for matching network design is that using tunable varactor or inductor as matching elements. A study is presented by W. C. Edmund Neo et all [25]. Including varactors in matching network provides a re-configurable structure. Two control voltages at input and output of the amplifier perform the tuning of matching network. A center-tap voltage controls each varactor.

Another study is presented by C.-S. Lee and C.-L. Yang [26]. They attached a tunable matching network before a UWB antenna to tune the operation frequency with one single control. The design is good at suppressing unwanted frequencies. The matching network is a T-type structure and includes two capacitors and one tunable inductor that include a varactor. Tuning operation is provided by applying a bias voltage to varactor. Although matching performance is promising, there is not concurrent operation.

1.4.3 Multiband Matching with Switches

Several matching network design are involved with switches. Using switches makes impedance matching automatically re-configurable. These switches are generally used for putting several varactors, inductors or separated passive networks into use or withdrawing from operation. One example of these kind of matching structure is presented by X. Yu and N. M. Neihart [27]. A reconfigurable multimode LNA design is presented. Design included switchable multi-tap transformers as input matching circuitry. This provides multi-mode operation. The transformer includes several multi-tap inductors and several parasitic capacities realized by MOSFETs. The switch configuration of MOSFETs determines the input impedance of the LNA and generates new resonance frequencies at the overall characteristic of the LNA. Unfortunately, parasitic capacities cannot be controlled at lower frequencies therefore, the matching at low frequencies is poor.

Another study [28] presents a multi-band multi-mode antenna matching tuner. This module consists of a tunable antenna matching network, a detector, a microcontroller combined with an ADC and a driver. The working principle is based on detection of phase mismatch at the input of matching network and changing the varactor capacitance values in tunable matching module to ensure the performance requirements. The micro-controller hosts the automatic tuning algorithm, ensures protocol synchronization and controls power management of the tuner system. Even if the system gives good transducer power gain but it is expensive and complicated. However, concurrent operation is very restricted.

One of MOS-HBT switched matching network design study is done by M. Kaynak et all [29]. They designed a multi-band, Class A, power amplifier. Multiband characteristic of the amplifier was obtained by using MOS based switching network. They did not use varactors in their design due to high frequency operation. Matching network is composed of four elements LC ladder structure with switches. Switches are used to control capacitance values by taking in and out the different

capacitors. This design is strongly depended on measured load impedance value and requires certain adjustment time. Thus, concurrency is not provided.

R. Malmqvist at all [30] designed RF MEMS and MMIC based re-configurable matching networks for adaptive multiband RF front-ends. The matching network consists of two shunt connected MEMS switches and four MIM capacitors. The resonance frequency can be changed by using the MEMS switches. After the load data measurement, the MEMS switches are positioned for desired frequency band. This study does not also provide concurrent application.

1.4.4 Multiband Matching with Transmission Lines

Lumped elements have several poor characteristic as summarized in Table (1.1). However, transmission lines have many superior properties as listed in Table (1.2). Therefore, in several studies on multiband matching network design employs transmission lines circuitry in their design. Yongle Wu et all [31] presented a dual frequency transformer for two arbitrary complex frequency-dependent impedance. Transmission lines with different characteristic impedance are used in the cascaded configuration in the matching networks design at each arm of the divider.

In several studies, transmission lines are incorporated at input and output impedance matching network design of amplifiers. R. Fagotti et all [32] presented a hex-band GaN power amplifier employing cascaded transmission lines. They chose this approach since re-configurable structure cannot be driven in concurrent mode. They derived the formulation for multi section transmission lines, which has a specific characteristic impedance and length, overall system is terminated with load impedance, which is a function of the frequency, and the goal of the transformer is to match this frequency-dependent termination to the system impedance at an assigned number of design frequencies. They defined reflection coefficients in between each section. Then they include electrical length finally they conclude the generic form of i^{th} section impedance which is dependent on next impedance

of transmission line, frequency and electrical length. They set the number of section and matching frequency then for each frequency they solved the electrical length by setting reflection coefficient to zero. They solve this by using Gauss-Newton method based algorithm. Eventually they get a good gain at output by using this matching method at eight different frequencies. The method needs complex computational steps when the number of transmission line sections and the number of matching frequencies are increased. Another matching network design example with transmission lines is presented by A. Fukuda et all [33]. They used multi-section transformer for dealing with multiband operation of power amplifiers. Designed matching network is composed of a combination of T-shaped transmission line network and a shunt tank block. The reactance of the shunt blocks are tuned to assigned resonance frequencies. This characteristic of the T-shaped network is not clarified.

F. Chiadini and V. Fiumara [34] present another example of transmission line impedance transformer for matching application. They presented a method to multi-section quarter-wave transformer. They optimize the delivered power between each section in order to determine the characteristic impedance and the frequency of the section. The presented method is useful when load and source impedance are real.

1.4.5 Multiband Matching with ICs

Several researchers studied on adaptive impedance matching using IC unit. There are many publications. The main drawback of this kind of work is not being concurrent. One of the examples is presented by H. Song at all [35]. They introduced an adaptive antenna tuner module that operated from 850MHz to 2GHz. The idea is sensing the mismatch signal and re-configuring the matching network. The re-configurable matching network is in PI configuration and consists of one fixed value inductor and several switchable capacitors. Matching performance of this

system is very promising. However, it does not offer concurrent operation and it is a costly solution.

1.4.6 Multiband Matching with Mixed Networks

Using distributed structure in matching network design is also another design aspect. There are many studies in this tack. While in several studies only distributed elements are used, in some of them incorporates mixed structures such as lumped and distributed elements in the design of matching network. Zhebin Wang and Chan-Wang Parket [36] designed a novel multiband matching network. They proposed a novel configuration that employs a multi-section transformer. Based on the proposed structure, a triple-band PA prototype was also presented. Each section of the transformer matches one of the required operation bands without deviation in the matching in other matched bands. The matching network includes transmission lines and shunt subs in cascade configuration. The idea behind the matching network is setting each unit, which includes a fixed characteristic impedance transmission line and a shunt stubs, to the characteristic impedance at specified frequency. It gives good results at resonance frequencies but does not clarify the bandwidth requirements.

Distributed structures can be used as parasitic elements in multiband design technology. One of the examples is presented by H. Rhyu at all [37]. They try to design an internal cell phone antenna, which covers GSM 900, DCS and US-PCS bands. The antenna mainly consists of three parts: a radiating patch, which is connected to a feed line, and a parasitic open stub in parallel configuration to the feed line. The quarter-wavelength parasitic open stub acts as a band reject filter to shift the resonance frequency of the antenna without any modification in radiating patch. However, there is still in difficulty to realize the wide bandwidth in lower resonance frequencies.

Making desired filtering between two defined terminals with distributed elements is a popular approach in this field. In one study, P. Sarkar at all [38] presented

a dual band filter, which incorporates a UWB structure with dual notch band open stubs. This study gives a good projection for creating multiband response by inserting notch bands at overall response. However, there is not a systematic approach in the presented study.

Technological evolution will always bring new generations, many devices will be in need to support old, and new technologies in same time since human comprehension is slower. There are some ways to design a multiband matching network. Many of them has been purposed to solve today technology. However future technologies will be performing at the higher frequency bands for many reasons. Because of that, developing new matching concept for future application is the main aspect for my thesis.

1.5 Thesis Objectives

Multiband matching network design has been evaluated in many studies. Most of study provides operational based solutions. Several studies shows glimpse of analytical solutions [19] at least for filter design problems. In current literature, there are two main approaches for multiband filter or matching network design problems. The first approach uses frequency mapping functions to produce a multiband gain response. There have been presented many mapping functions to design multiband networks especially for filters [39]. There are a few studies for multiband matching network design issue. These methods require complex computational steps for the generation of mapping functions.

One track of this thesis is to evaluate a generalized multiband mapping function for matching and filter network design problems. The well-known LP to BP transformation is applied sequentially to produce multiband network responses. A new generalized form of multiband frequency mapping function, which is based on sequential application of LP to BP transformation, is proposed.

The second solution is using a complete network model of lossless two-port and including Finite Transmission Zeros (FTZs) in network impedance function to create multiband response. Even if this solution is one of the most straightforward way to shape the the gain response, create notches and pass bands on overall characteristic, there is a big synthesis issue exist for the synthesis of FTZs as realizable network. Generally, negative elements come up in the synthesis routine of FTZs. Even if it is possible to eliminate these negative elements as coupled coil equivalencies, it may not applicable for RF filter or matching network design problem due to difficulties of design and realization of high frequency transformers. In literature, several studies have been presented for the solution of this issue. However, there is still not a solution for generalized problems especially for matching problems.

Therefore, the second track of this thesis is on the realizable ladder synthesis of multiband matching networks, which have FTZs in their impedance or admittance functions. Several circuit transformation techniques or manipulations on the network element extraction order is employed to eliminate the unrealizable element in this track. In addition, a new parametric representation of Brune function [40] is proposed. By employing the presented parametric construction algorithm of driving point impedance of multiband network, it is possible to achieve multiband ladders without use of coupled coils.

1.6 Thesis Organization

In Chapter 1, an introduction to matching problem, including brief information is presented. The motivation of the multiband matching network design problem is stated. Main solution tracks are classified and current literature is reviewed. The main objectives of the thesis are mentioned.

In Chapter 2, the parametric representation of lossless two-port network is presented under the multiband network design perspective. Real Frequency Techniques (RFT) is summarized since the proposed methods in the thesis are integrated with the general RFT optimization philosophy.

In Chapter 3, the frequency transformation based approach is investigated. The generalized multiband frequency transformation is proposed. Generation of prototype network is explained. The synthesis procedure is introduced. The incorporation algorithm of the proposed technique with RFT is underlined. Several multiband matching and filter design examples are provided.

In Chapter 4, the synthesis based approach is presented. The parametric characterization of multiband network is explained. The network synthesis of FTZs is introduced. The attempts for transformer-free network synthesis in literature are mainly mentioned. Network transformations for the elimination of unrealizable elements are obtained thorough a multiband matching network design example. A parametric design approach for multiband ladder network synthesis is presented. The application of the proposed technique on a low pass filter is provided.

In Chapter 5, the applications of the proposed methods on multiband RF network are presented.

In Chapter 6, several concluding remarks and suggestions for prospective research are stated.

Chapter 2

Multiband Matching of Complex Terminations

2.1 Multiband Matching Problem

In general, matching network design problem is related with the power transfer between two terminations through a lossless two-port network over a specified frequency band as illustrated in Figure (2.1). The power transfer characteristic is generally considered as Transducer Power Gain (TPG) [8], which is a ratio of delivered power to available power as given in (2.1). The lossless two-port can be a filter if both terminations are resistive and matched or a matching network if one or both terminations are complex.

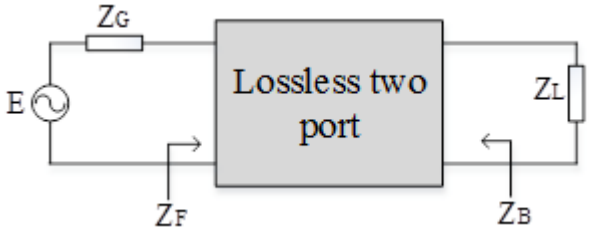

Figure 2.1: Matching network design problem with lossless two-port and complex terminations.

$$TPG(w) = 1 - |\rho_{in}(w)|^2; \quad \rho_{in}(w) = \frac{Z_F(w) - Z_G^*(w)}{Z_F(w) + Z_G(w)} \tag{2.1}$$

where $Z_F(w)$ is the input driving point impedance of matching network and $Z_G(w)$ is the complex impedance of generator.

The TPG characteristic of the matching network depends on designer preferences. In most of studies however, it is aimed to be broadband or wideband form. Recently multiband characteristic is investigated by many scientist. This is more challenging issue since it has to cover lower and upper limits of several frequency bands as in broadband applications and also has to have notch bands at desired frequencies. An illustrative TPG characteristic of multiband matching network is given in Figure (2.2).

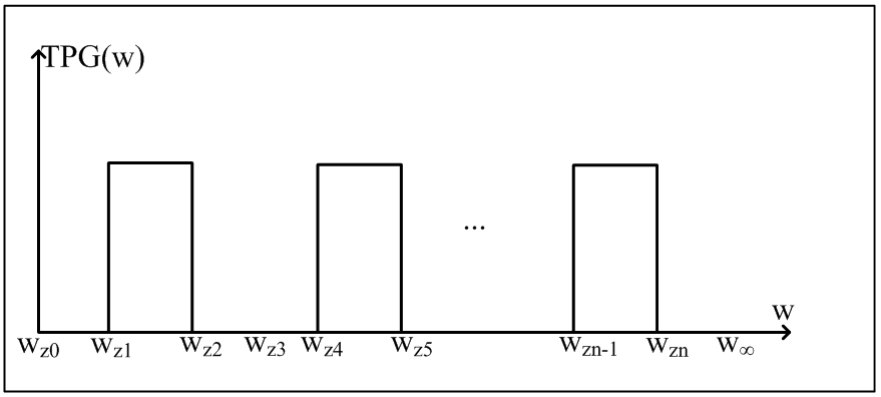

Figure 2.2: General multiband TPG characteristic.

As it can be interpreted from the figure above, there has to be FTZs at the TPG characteristics of the matching network. By changing the locations of these FTZs, the TPG characteristic can be controlled. In this regard, a complete analytical representation of the matching network is required. This may be driving point impedance or admittance of the lossless two-port. Even if the analytical representation can be established it is also necessary to employ an efficient matching network design technique to optimize the network function for most generalized multiband matching problems. In this regard, in the following section the matching network design techniques are briefly discussed.

2.2 Real Frequency Multiband Matching

Matching network design problem has been approached from many different points. Various formulations of lossless two-port network are incorporated. As mentioned before, one of the first attempt was made by Bode [4]. He established a gain-bandwidth limitation for resistive generator and a restrictive load topology. Later Fano extended the theory for arbitrary load networks [5]. Nevertheless, it is always necessary to establish a network model for the load. However, this may not be possible for practical applications. As an example, in the most of antenna matching problem, it may not be possible to give an explicit network topology for the antenna. Even if there might be approximate models for load network, it might not be easy and efficient.

It is always possible to incorporate Computer Aided Design (CAD) tools to optimize the element values of a pre-assigned matching network [10]. However, these tools require an initial start value of the network elements. This might be supplied by ad-hoc choices and can give acceptable designs if number of elements in matching network is reasonable [41, 42]. However, if the number of elements is increased then the optimization gets more difficult and it cannot converge to a global optimum. In practice CAD tools are efficient for final fine tuning of the element values.

As a conclusion, purely numeric methods or analytical theory can give solution for simple matching problems. Therefore, there is a need for special techniques to bypass both analytical theory and CAD tools. This technique should produce analytically best possible component values for an arbitrarily chosen matching network topology and should be applicable for all matching problems regardless the number of element values and load or generator networks topology.

Thankfully, in 1977 Carlin [12] established such a method named Real Frequency Technique, which resolves the issues of analytical theory and CAD tools. Carlin used measured data of the load or generator network instead of modeling them

with explicit network topologies. It has been proved that Carlin's technique gives better solution rather than obtained with analytical theory [43–45]. RFT is evolved by many researcher of the field [46–51] and generalized for all matching problems.

RFT utilizes realizable positive real functions in parametric representation and optimizes over a frequency band to approach a target performance characteristic. In literature, RFT generally is used for broadband matching network problems [44, 46, 49]. However RFT can be employed for multiband matching problem as well. Since the analytical representation of driving point impedance or admittance functions are already used in RFT, the FTZs of the multiband TPG form can also be incorporated into RFT routine. By incorporating a multiband optimization process in RFT, multiband matching problem can be solved.

The objective of the multiband matching is, finding a lossless two-port network that maximizes the TPG level at the multiple pass bands and minimizes at the multiple notch bands. Depending on the terminal impedance in Figure (2.1), the problem can be double matching, single matching or active matching as mentioned in Chapter 1.

Real frequency techniques have been grouped in four categories by Yarman as in [52];

- Real Frequency Line Segment Technique (RFLST)
- Real Frequency Direct Computational Technique (RFDCT)
- Real Frequency Parametric Approach
- Simplified Real Frequency Technique (SRFT)

RFLST [12, 44, 53, 54] method employs a piecewise liner approximation of the back-end impedance of matching network and provides a good estimate to the analytical gain-bandwidth limit.

RFDCT [43,55,56] is similar with RFLST but instead of using linear approximation, it employs even part of back-end impedance with unknown coefficients to be optimized. The complete form of complex back-end driving point impedance can be constructed uniquely from its even part by employing Gewertz procedure. This technique provides a good insight to double matching problems. The main drawback is the need for Hurwitz factorization to determine the denominator polynomial of back-end impedance and using Gewertz procedure to construct impedance at the each step of the optimization routine.

Real Frequency Parametric Approach and SRFT are most evolved methods in the RFT family. In the context of this thesis, it has been preferred to use these two methods for specific matching problems. In the following sections two main RFT approaches will be outlined under the consideration of multiband matching problem.

2.2.1 Real Frequency Parametric Approach

This technique [45, 57–61] is established by Fettwise to resolve the issues comes with RFLST and RFDCT. In this method, the parametric representation of Brune functions are incorporated in design as back-end or front-end driving point impedance of the matching network. Since the explicit equations of the impedance or admittance is obtained, the matching problem is reduced to only optimization of the poles of the back-end impedance or admittance function over a band of interest. There is no need for a linear piecewise modeling or neither Hurwitz factorization and Gewertz procedures to employ. Consider the single matching problem as illustrated in Figure (2.3);

The back-end impedance function $Z(p)$ can be written as [58];

$$Z(p) = B_0 + \sum_{i=1}^{n} \frac{B_i}{p - p_i} = \frac{N(p)}{D(p)} \tag{2.2}$$

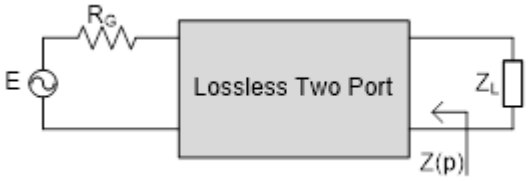

Figure 2.3: Single matching problem.

Here the B_0 is non-zero real constant, and B_i are non-zero complex constants and p_i are complex LHP (Left-Hand Plane) poles.

A realizable driving point impedance $Z(p)$ in (2.2) is called Brune function or positive real function and must fulfill the following properties [40];

- The degree of numerator and denominator polynomial of $Z(p)$ is differs by one.
- $Z(p)$ is real for real values of p.
- Both numerator and denominator polynomials are Hurwitz.
- All residues at poles must be positive.

The even part of the back-end impedance $Z(p)$ can be written as;

$$Ev\left\{Z(p)\right\} = \frac{Z(p) + Z(-p)}{2} = \frac{f(p)f(-p)}{d(p)d(-p)} \tag{2.3}$$

Here the $d(p)$ polynomial must be a strictly Hurwitz and the f(p) is a real monic polynomial. Since the poles of $Z(p)$ and the roots of $d(p)$ are same then $d(p)$ can be written as;

$$d(p) = D_n \prod_{i=1}^{n} (p - p_i) \tag{2.4}$$

Here D_n is a real non-zero constant. Regarding the zeros of $d(p)$ polynomial, which must be all distinct and complex poles, have to be in conjugate form as [9];

$$\left\{ \begin{array}{l} p_i = -\alpha_i + j\beta_i \\ p_i^* = -\alpha_i - j\beta_i \end{array} \right\}, \quad i = 1, 2, ..., n_2 \tag{2.5}$$

Here $p_n = \{-\alpha_0\}$ for odd n where $\alpha_i > 0$ and

$$n_2 = \left\{ \begin{array}{l} \dfrac{n}{2}, \quad n \quad is \quad even \\ \dfrac{n-1}{2}, \quad n \quad is \quad odd \end{array} \right\} \tag{2.6}$$

The complex coefficients B_i are derived as;

$$B_i = -\frac{f(p_i)f(-p_i)}{p_i D_n^2 \prod\limits_{\substack{k=1 \\ k\neq i}}^{n} (p_k^2 - p_i^2)}, \quad i = 1, 2, ..., n; B_0 = \left\{ \begin{array}{l} 0, \quad \deg(f) < n \\ {}^{1}\!/_{D_n^2}, \quad \deg(f) = n \end{array} \right\} \tag{2.7}$$

By setting $p = jw$, the real and imaginary parts of $Z(p) = R(w) + jX(w)$ can be derived as [9];

$$R(w) = -\sum_{i=1}^{n} \frac{p_i B_i}{w^2 + p_i^2} + B_0, \qquad X(w) = -w \sum_{i=1}^{n} \frac{B_i}{w^2 + p_i^2} \tag{2.8}$$

Thus, the positive real impedance $Z(p)$ is defined fully in terms of $f(p)$ and $d(p)$ polynomials in parametric form.

Here the zeros of $f(p)$ polynomial correspond to the zeros of the TPG function. Signal transmission stops at the locations of these zeros. The functional form of $f(p)$ imposes the special circuit topologies [8] such as;

- If $f_{DC}(p) = p^k$; it correspond a network with multiple zeros at DC.
- If $f_w(p) = \prod\limits_{r=1}^{n_w} (p^2 + w_r^2)$; it correspond a network with finite zeros.

- If $f_\sigma(p) = \prod_{r=1}^{n_\sigma} (\sigma_r - p)$; it correspond a network with pure real RHP (Right-Hand Plane) zeros.

- If $f_{MLHP}(p) = (-1)^{n_\delta} \prod_{r=1}^{n_\delta} (\delta_r^2 - p^2)$ it correspond a network with pure real LHP zeros then it means there are its mirror image complex RHP zeros pairs in network; $f_{CRHP}(p) = \prod_{r=1}^{n_R} \left[(\delta_r - p)^2 + \beta_r^2\right]$.

- If $f_{MCLHP}(p) = \prod_{r=1}^{n_L} \left[(\delta_r - p)^2 + \beta_r^2\right] \left[(\delta_r + p)^2 + \beta_r^2\right]$,

It correspond a network with complex LHP zeros with its mirror image.Then, the general form of $f(p)$ may be given as;

$f(p) = f_{DC}(p) f_w(p) f_\sigma(p) f_{MLHP}(p) f_{MCLHP}(p) f_{CRHP}(p)$. The proper generic form of $f(p)$ is given by

$$f(p) = p^k \prod_{r=1}^{n_w} (p^2 + w_r^2) \prod_{r=1}^{n_\delta} (\delta_r^2 - p^2) \prod_{r=1}^{n_L} \left[(\delta_r - p)^2 + \beta_r^2\right] \left[(\delta_r + p)^2 + \beta_r^2\right] \quad (2.9)$$

The full form of $f(p)$ corresponds to a highly complicated network structure which may be impractical to realize. In practice however, generally lossless reciprocal ladder forms are in concern whose $f(p)$ polynomial is composed of only first two terms of the above equation, which is;

$$f(p) = p^k \prod_{r=1}^{n_w} (p^2 + w_r^2) \quad (2.10)$$

The outlined parametric representation provides full description of the lossless two-port in terms of its poles and transmission zeros. Thus $Z(p)$ can be written in terms of $\{\alpha_i, \beta_i, n, B_0\}$. The TPG of the matching network in Figure (2.3) can be written as ;

$$TPG(w) = \frac{4R(w) R_L(w)}{(R(w) + R_L(w))^2 + (X(w) + X_L(w))^2} \quad (2.11)$$

Here $R(w)$ and $X(w)$ are the real and imaginary part of $Z(w)$ as given in (2.8). The $R_L(w)$ and $X_L(w)$ are the real and imaginary part impedance of complex load termination. If $TPG(w)$ is optimized to approach to a multiband gain form $T_0(w)$ as illustrated in Figure (2.2) then the objective function to be minimized can be

$$\zeta = \sum_{k=0}^{N_w} [TPG(w_k, \theta_j) - T_0(w_k)]^2 \tag{2.12}$$

Here the N_w is number of breaking point frequency.

The $\theta_j = \{\alpha_j, \beta_j\}, \quad j = 1, 2, ..., n$ are the optimization parameters, which are the real and imaginary parts of the zeros of $d(p)$ as given in (2.5).

Therefore, Real Frequency Parametric Approach utilizes a preassigned network complexity and the roots of the impedance denominator are taken as the unknowns of the matching problem to be optimized for an intended TPG characteristic, which can be arbitrary over the frequency band of interest.

Once the optimized back-end impedance $Z(p)$ is obtained, then by employing Darlington sense pole zero extraction routines the synthesis of the impedance can be established.

2.2.2 Simplified Real Frequency Technique (SRFT)

The complete description of back-end or front-end impedance of lossless two-port leads to establish a scattering parameters based formulations for matching problem, which is so called Simplified Real Frequency Technique (SRFT) [9, 62–64]. In SRFT, Belevitch canonic form of scattering polynomials is employed. This method provides better numeric stability and convergence in optimization. SRFT is very suitable for the design of matching network between cascaded units [8]. One disadvantage is that SRFT also uses Hurwitz factorization within the optimization process [9]. Consider the double matching problem illustrated in Figure (2.4).

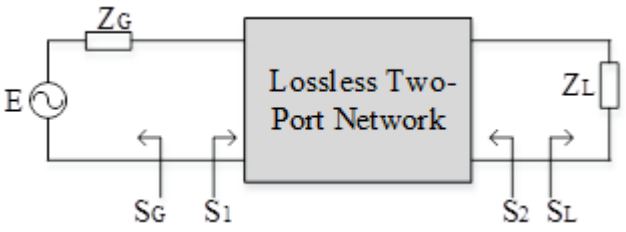

Figure 2.4: Double matching problem.

The normalized scattering parameters of lossless two-port can be expressed as;

$$\begin{aligned} S_{11}(p) &= \frac{h(p)}{g(p)}, \quad S_{12}(p) = \pm\frac{f(-p)}{g(p)} \\ S_{21}(p) &= \frac{f(p)}{g(p)} \quad S_{22}(p) = \mp\frac{h(-p)}{g(p)} \end{aligned} \tag{2.13}$$

Here the p is the complex frequency variable, the $h(p)$ is an arbitrary polynomial and the $g(p)$ is a strictly Hurwitz polynomial. The $g(p)$ is a real monic polynomial whose zeros are also transmission zeros of the lossless two-port network. If the network consists of transmission zeros only at DC, infinity and finite frequencies, then the $f(p)$ polynomial can be given as;

$$f(p) = a_0 p^k \prod_{i=1}^{n_z} (p^2 + w_i^2) \tag{2.14}$$

Here the k and n_z represent the number of transmission zeros at DC and at finite frequencies respectively. The parameter is an arbitrary real constant.

The $f(p)$ polynomial also characterize the topology of the network.

If $f(p) = 1$ which correspond to a low pass ladder structure which consists of shunt capacitors and series inductors.

If $f(p) = p^k$, then the network is in a high pass ladder topology which includes shunt inductors and series capacitors.

If $f(p) = \prod_{i=1}^{n_z} (p^2 + w_i^2)$ then the network must possess series/shunt resonators or Brune/Type-C sections [65].

The following losslessness condition must be held [8] between these polynomials as;

$$g(p)g(-p) = h(p)h(-p) + f(p)f(-p) \tag{2.15}$$

Which also imposes the relation between polynomial degrees as;

$$\deg(h) \leq n, \quad \deg(f) \leq n \ , \quad n = \deg(g) \tag{2.16}$$

In SRFT, once the location of transmission zeros, so the zeros of $f(p)$ polynomial, which also corresponds to the complexity of the lossless two-port is set then auxiliary $h(p)$ polynomial is initiated in ad-hoc basis, then by using the losslessness condition in (2.15) and employing Hurwitz factorization the strictly Hurwitz $g(p)$ polynomial is generated. Since the $f(p)$,$g(p)$ and $h(p)$ are polynomials are determined, then the TPG function of the filter can be computed at real frequencies as

$$TPG(w) = \frac{(1 - |S_G|^2)|S_{21}|^2(1 - |S_L|^2)}{|1 - S_1 S_G|^2 |1 - S_2 S_L|^2} \tag{2.17}$$

Here the S_1 and S_2 represent the unit normalized input and output reflection coefficients of the lossless two-port when it is terminated with the complex load impedance Z_L and Z_G respectively. The S_G and S_L are the reflection coefficients of generator and the load networks respectively. The explicit relations are given as [9];

$$\begin{aligned} S_1 &= S_{11} + \frac{S_{12}^2 S_L}{1 - S_{11} S_L} \ , \quad S_2 = S_{22} + \frac{S_{21}^2 S_G}{1 - S_{11} S_G} \ , \\ S_G &= \frac{Z_G - 1}{Z_G + 1} \ , \quad S_L = \frac{Z_L - 1}{Z_L + 1} \end{aligned} \tag{2.18}$$

Through a numeric optimization routine the coefficients of $h(p)$ polynomial are iterated, $g(p)$ polynomial and TPG function in (2.17) are calculated at each step.

By employing an objective function as;

$$\delta = \sum_{j=0}^{N_j} \left[TPG(w_j, h_i) - T_0(w_j) \right]^2 \tag{2.19}$$

and minimizing this over an interested frequency band the suitable $h(p)$ and $g(p)$ polynomials can be achieved. Here the N_j represents number of breaking point frequencies. The $T_0(w_j)$ is the target gain characteristic which can be chosen as arbitrary form. However if multiband matching problem is in concern then it is suitable to choose the $T_0(w_j)$ characteristic according to the band specifications of pass bands and notch bands of multiband TPG form as illustrated in Figure (2.2).

As a conclusion, real frequency techniques are excellent tools for matching network design applications. They provide very strong analytical basis to characterization of the matching network and says a lot for performance optimization of matching network for arbitrary complex terminations. The analytical solution of the multiband matching problem can be evaluated by using these techniques as well. By employing one of these two RFT method and choosing a multiband target gain form as illustrated in Figure (2.2), the parametric form of multiband matching network can be achieved.

However, RFT tools does not provide a synthesis routine. Therefore, even if a multiband matching network function can be achieved in terms of explicit driving point impedance or unit normalized scattering polynomials, it may not be possible to synthesize it. In the proceeding sections of the thesis multiband matching network design problem is investigated both design and the synthesis perspectives by integrating novel methods with RFT routines.

Chapter 3

Multiband Matching with A Generalized Frequency Transformations

3.1 Introduction

Using frequency transformations or frequency mapping functions is one of the most preferred way to design multiband networks especially multiband filters in literature [19, 66–76]. This method provides a strong analytical basis for the solution of multiband design. In this method, special mapping functions are employed to generate multiband networks via application of the mapping functions on a pre-assigned prototype network. The characteristic of the prototype network is preserved but bandwidths are scaled [39].

In this method, it is most critical to define a suitable mapping function for the concerned application. The mapping function is used as a frequency variable to transform the prototype network to its multiband correspondence. Therefore, it should be defined in terms of gain characteristic of the concerned multiband application. For this manner, several multiband mapping functions are proposed in literature. In one of the major study [77], the finite transmission zeros at stop band are generated with a presented dual band mapping function. This technique results with coupled cavity structures. In [78], a multi-resonance mapping function which is based on Foster reactance function, is presented. The reactance function of multiband matching network is generated by employing a proposed

mapping function. The presented technique is not suitable for multiband matching applications since the bandwidths of each resonance are only depend on the element tolerances. In [39], a multiband mapping function, which requires an intermediate unsymmetrical transformation, is presented. The mapping function is suitable to generated arbitrary number of pass bands but it requires complex computational steps. In this track, several other publications are presented with various frequencies mapping function for various network topologies [79–82].

Although multiband frequency mapping functions are well-addressed issue in current literature, there is still not an easy to apply and simple multiband mapping function which provide arbitrary number of pass bands mapping operations. It is always preferred to define multiband mapping function with the assigned multiband frequency specifications without use of interval steps or complex computational phases. A direct relation should be established between the intended multiband characteristic with the prototype network.

In this thesis, a novel multiband mapping function is proposed for the use of multiband filters or matching network design. The proceeding sections are organized to introduce the evaluation phases of the proposed mapping function.

3.2 Sequential Frequency Transformations for Multiband Mapping

Multiband mapping functions can be generated via employing sequential lower degree transformations such as the well-known Low Pass to Band Pass (LPtoBP) transformation [80]. If the LPtoBP transformation is applied in sequentially, it provides even number of pass bands at the each application of the LPtoBP transformation. This procedure does not provide odd number pass bands. In addition, each sequential step must be related with each other with proper mathematical equations to control the resultant multiband mapping function.

In the sequential mapping technique, to produce multiband network, the first step is constructing the proper mapping function for the concerned application

then the second steps is employing an LP network prototype to apply the multiband mapping functions on. This prototype network can be a transfer function based filter network such as Chebyshev, Elliptical, Butterworth, etc. In addition, it is possible to employ an arbitrary LP network. The third step is the application of the mapping function to the elements of the prototype LP network to transform the reactances to their multiband correspondences. Because of element mapping, the multiband network is composed of LC resonators in series/shunt configurations.

In literature there are several attempts have been done to establish concrete formulations for specific multiband operations such as dual band, quad band, etc. In this thesis, it has been also shown that to generate multiband response with odd number of pass bands special mathematical manipulations must be employed beside with sequential application of transformation. In following sections, several novel formulations are given for dual band, quad band and even for triple band mapping functions.

3.2.1 Dual Band Frequency Transformation

The dual band application of the sequential mapping scheme is illustrated in Figure (3.1), a normalized LP gain function in domain is mapped to a band pass response in w' domain then eventually mapped to real frequency domain w via two sequential LPtoBP transformation [81].

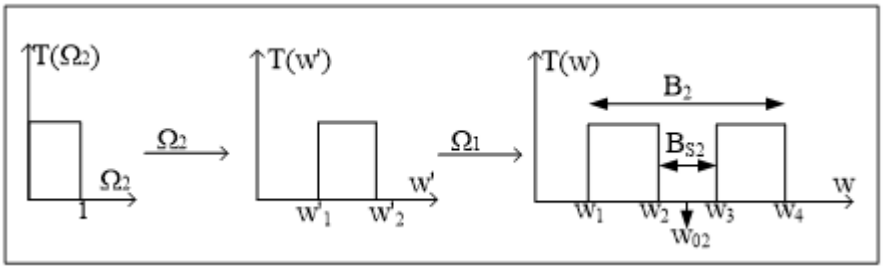

Figure 3.1: Low-pass to dual band frequency mapping scheme.

After several mathematical manipulations a direct form of low pass to dual band (LPtoDB) transformation function is established as given in (3.1)

$$\Omega_2(w) = \frac{1}{B_2 - B_{S2}} \left(\frac{w^2 - w_{02}^2}{w} \right) - \frac{B_2 B_{S2}}{B_2 - B_{S2}} \left(\frac{w}{w^2 - w_{02}^2} \right), \\ w_{02} = \sqrt{w_1 w_4} = \sqrt{w_2 w_3}, \quad B_2 = w_4 - w_1, \quad B_{S2} = w_3 - w_2 \tag{3.1}$$

Where B_2 is the total bandwidth of dual band response and represents the difference between upper cut of frequency of second band and lower cut of frequency of first band as interpreted from the Figure (3.1). The B_{S2} is the bandwidth of notch band between two pass bands as given in (3.1). The w_{02} is the geometric center frequency. The relation between the direct LPtoDB mapping function Ω_2 and the real frequency variable w is given in Figure (3.2). This is so called dual band frequency mapping diagram.

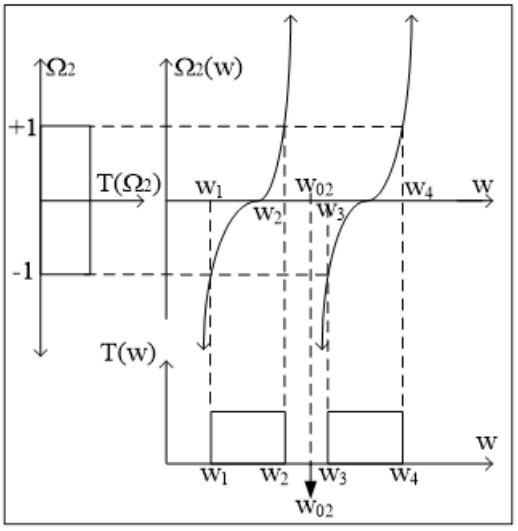

Figure 3.2: LP to DB frequency mapping diagram.

For the sake of simplicity, here an auxiliary variable Ω_{02} is defined as;

$$\Omega_{02}(w) = \left(\frac{w^2 - w_{02}^2}{w} \right) \tag{3.2}$$

By incorporating (3.2) into (3.1), the direct LPtoDB mapping function in (3.1) can be simplified as;

$$\Omega_2(w) = \frac{1}{B_2 - B_{S2}}\Omega_{02}(w) - \frac{B_2 B_{S2}}{B_2 - B_{S2}}\frac{1}{\Omega_{02}(w)} \tag{3.3}$$

After determination of cut of frequencies and by employing the LPtoDB mapping function in (3.3), any dual band mapping function can be generated for any specified application such as dual band filters or matching networks. The relation between the cut off frequencies in (3.1) restricts the independency of frequency assignment with three. Therefore any three set of those four cut off frequencies can be chosen arbitrary.

3.2.2 Quad Band Frequency Transformation

A quad band frequency mapping function can be generated by applying the LPtoBP transformation on an LP gain response in three sequential steps as illustrated in Figure (3.3)a. Therefore, each application of LPtoBP transformation produces even number of passbands. The mapping function in Figure (3.3)b suggests that LP prototype gain response is mapped to a shifted and scaled version of preserved LP response via an asymptote.

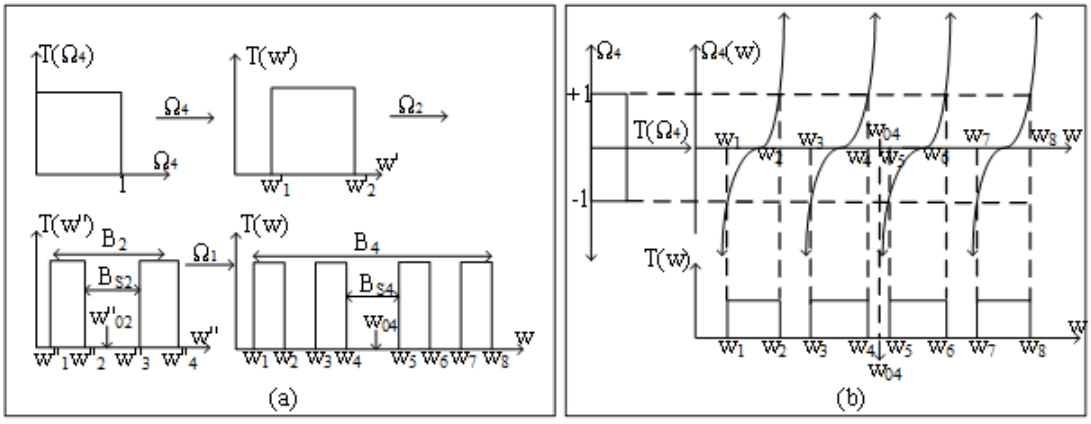

Figure 3.3: (a): Low-pass to quad-band transformation scheme; (b): Low-pass to quad-band frequency mapping diagram.

The direct form of the low pass to quad band (LPtoQB) transformation function is given as;

$$\Omega_4(w) = \frac{1}{(B_2 - B_{S2})B_4}\left(\frac{w^2 - w_{04}^2}{w}\right) - \frac{1}{(B_2 - B_{S2})B_4}\left(\frac{w}{w^2 - w_{04}^2}\right) - \frac{B_2 B_{S2}}{B_2 - B_{S2}}\frac{1}{\frac{1}{B_4}\left(\frac{w^2 - w_{04}^2}{w}\right) - B_{s4}\left(\frac{w}{w^2 - w_{04}^2}\right)}; \tag{3.4}$$

$$w_{04} = \sqrt{w_1 w_8} = \sqrt{w_2 w_7} = \sqrt{w_3 w_6} = \sqrt{w_4 w_5}$$

As a result of the sequential mapping process, there is a certain relation presents between cut off frequencies of quad band response. Here the new auxiliary variable is defined as;

$$\Omega_{04}(w) = \left(\frac{w^2 - w_{04}^2}{w}\right) \tag{3.5}$$

By incorporating the equations in (3.4) and (3.5) the simplified LPtoQB mapping function is given as;

$$\Omega_4(w) = \frac{1}{(B_2 - B_{S2})B_4}\Omega_{04}(w) - \frac{1}{(B_2 - B_{S2})B_4}\frac{1}{\Omega_{04}(w)} - \frac{B_2 B_{S2}}{B_2 - B_{S2}}\frac{1}{\frac{1}{B_4}\Omega_{04}(w) - B_{s4}\frac{1}{\Omega_{04}(w)}} \tag{3.6}$$

3.2.3 Triple Band Frequency Transformation

Even the sequential application of LPtoBP frequency transformation produces even number of pass bands as mentioned in Section 3.2.1 and Section 3.2.2, it is possible to generate a triple band mapping function by merging the different mapping functions. As a novel mathematical formulation of this thesis content, the following Low Pass to Triple Band (LPtoTB) mapping function is introduced

as;

$$\Omega_3(w) = \Omega_4(w) + \frac{B_{S4}}{(B_2 - B_{S2})}\frac{1}{\Omega_{04}(w)} = \frac{1}{(B_2 - B_{S2})B_4}\Omega_{04}(w) - \frac{B_2 B_{S2}}{B_2 - B_{S2}}\frac{1}{\frac{1}{B_4}\Omega_{04}(w) - B_{s4}\frac{1}{\Omega_{04}(w)}} \tag{3.7}$$

Here the LPtoQB mapping function Ω_4 in (3.5) and the auxiliary variable Ω_{04} in (3.4) are used to derive LPtoTB mapping function. After several mathematical manipulation steps a more elaborated equation of LPtoTB mapping function is given as;

$$\Omega_3(w) = \frac{1}{(B_2 - B_{S2})B_3}\left(\frac{w^2 - w_{03}^2}{w}\right) - \frac{1}{(B_2 - B_{S2})B_3}\left(\frac{w}{w^2 - w_{03}^2}\right) - \frac{B_2 B_{S2}}{B_2 - B_{S2}}\frac{1}{\frac{1}{B_3}\left(\frac{w^2 - w_{03}^2}{w}\right) - w_{02}^2 B_3\left(\frac{w}{w^2 - w_{03}^2}\right)} \tag{3.8}$$

To simplify the equation in (3.8), another auxiliary variable is defined as;

$$\Omega_{03}(w) = \left(\frac{w^2 - w_{03}^2}{w}\right) \tag{3.9}$$

By substituting the relation in (3.9) and (3.8), the simplified version of LPtoTB mapping function is generated as;

$$\Omega_3(w) = \frac{1}{(B_2 - B_{S2})B_3}\Omega_{03}(w) - \frac{1}{(B_2 - B_{S2})B_3}\frac{1}{\Omega_{03}(w)} - \frac{B_2 B_{S2}}{B_2 - B_{S2}}\frac{1}{\frac{1}{B_3}\Omega_{03}(w) - w_{02}^2 B_3\frac{1}{\Omega_{03}(w)}} \tag{3.10}$$

The mapping diagram for LPtoTB mapping function is given in Figure (3.4).

The LPtoTB mapping diagram in above figure also suggests a generalized version of sequential mapping function for arbitrary number of pass band is possible if an appropriate mathematical statement is achieved.

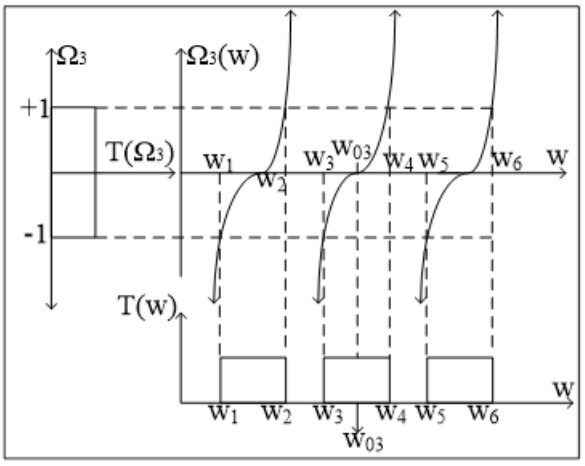

Figure 3.4: Low-pass to triple band frequency mapping diagram.

3.3 The Proposed Generalized Multiband Mapping Function

Along with the survey of sequential LPtoBP mapping similar mathematical expressions are resulted as given in (3.1), (3.6), and (3.10). All these mapping function provide a direct transformation from low pass prototype to correspondence multiband network. Therefore, there is no need for intermediate steps to produce intended multiband form. In addition, these mapping functions inherently keep the constraints of LPtoBP mapping. Therefore, they are all different version of sequential LPtoBP mapping process. The associated mapping diagrams of each mapping functions are also in similar form. Each asymptote at these mapping diagrams maps the LP gain form to a band pass form as a scaled and shifted version. The locations of these asymptotes are also determined by the corner frequencies of the multiband gain form.

Therefore to have a multiband gain form with arbitrary number of pass bands there should be a suitable multiband mapping function with a multiband mapping diagram whose asymptotes are properly placed to map the LP gain form to intended multiband characteristic.

For this propose, consider the following mapping diagram in Figure (3.5). As shown in the figure each the normalized LP gain in Ω_N domain is mapped to a

multiband gain form by through a multiband mapping diagram.

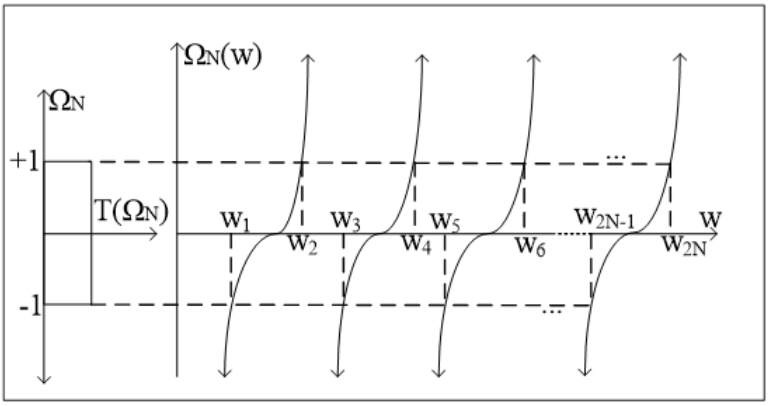

Figure 3.5: Low pass to multiband frequency mapping diagram.

After deep examination of the sequential mapping functions given in (3.1), (3.6), and (3.10), to generate such a mapping function, the following generalized multiband mapping function is introduced as;

$$\Omega_N(w) = a_1\Omega_{0N}(w) - \cfrac{1}{a_2\Omega_{0N}(w) - \cfrac{1}{a_3\Omega_{0N}(w) - \ddots - \cfrac{1}{a_N\Omega_{0N}(w)}}}; \qquad (3.11)$$
$$\Omega_{0N}(w) = \left(\frac{w^2 - w_{0N}^2}{w}\right).$$

Here the parameter N represents the assigned number of pass band of multiband mapping, and the w_{0N} parameter is the geometric center frequency as similar within the other mapping functions. The constraints for other sequential mapping functions are also valid for the generalized multiband mapping function as;

$$\begin{aligned} &w_0 = \sqrt{w_1 w_{2N}} = \sqrt{w_2 w_{2N-1}}..., \\ &w_1 < w_2 < ... < w_0 < ... < w_{2N-1} < w_{2N} \end{aligned} \qquad (3.12)$$

This mapping function maps the LP gain form to an arbitrary multiband gain form thus it is named as LPtoMB mapping function. The number of independent

corner frequencies is $N+1$ out of $2N$ corner frequencies. By selecting any $N+1$ corner frequencies, the multiband mapping function is constructed in terms of a_N parameters which are related with the derivative of the asymptotes. Also as it can be interpreted from the multiband mapping diagram, at the corner frequencies, the multiband mapping function $|\Omega_N(w)| = 1$. Therefore, by using this relation there will be number of 2N equations with N unknown parameters. By choosing any N set of $2N$ equations, the unknown a_N parameters can be calculated via employing a numeric equation solver [83].

Consider the dual band case with assigned arbitrary cut off frequencies are $w_1 = 1, w_2 = 1.5$, $w_3 = 2$ and the last corner is calculated by using the relation in (3.12) as $w_4 = 3$. The mapping function is constructed as;

$$\begin{aligned} \Omega_{02}(w) &= \left(\frac{w^2 - w_{02}^2}{w}\right), \quad w_{02} = \sqrt{w_1 w_4} \ = 1.732, \\ \Omega_2(w) &= a_1 \Omega_{02}(w) - \frac{1}{a_2 \Omega_{02}(w)} \end{aligned} \tag{3.13}$$

By setting $|\Omega_N(w)| = 1$ at the four corner frequencies and choosing the any two equations such as;

$$\left| a_1 \left(\frac{{w_1}^2 - 3}{w_1}\right) - \frac{1}{a_2 \left(\frac{{w_1}^2 - 3}{w_1}\right)} \right| = 1, \quad \left| a_1 \left(\frac{{w_3}^2 - 3}{w_3}\right) - \frac{1}{a_2 \left(\frac{{w_3}^2 - 3}{w_3}\right)} \right| = 1 \tag{3.14}$$

The unknown parameters are found as $a_1 = 0.667$, $a_2 = 1.5$. The dual band mapping function is derived as;

$$\Omega_2(w) = 0.667 \Omega_{02}(w) - \frac{1}{1.5 \Omega_{02}(w)} \tag{3.15}$$

After the dual band mapping function is generated it is applied on an 11^{th} degree equal ripple Chebyshev LP prototype [84] and the dual band gain response is achieved as given in Figure (3.6).

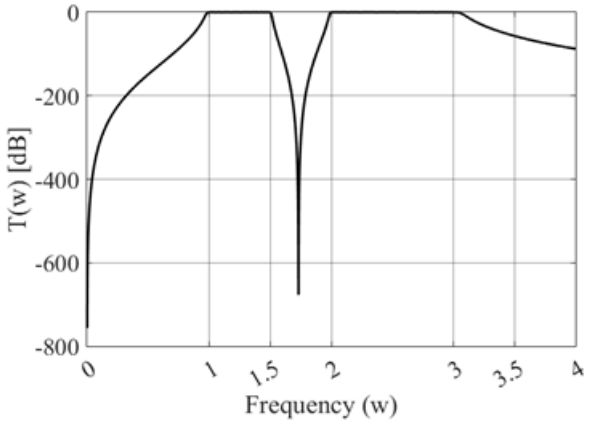

Figure 3.6: Gain response of dual band characteristic produced with LP to MB.

For the triple band mapping function, here the arbitrary cut off frequencies are assigned as; $w_1 = 0.85, w_2 = 1.15, w_6 = 3, w_3 = 1.5$ and the left corner frequencies are found as $w_4 = 1.7, w_5 = 2.2174$ by using the equation in (3.12). The mapping function is constructed with unknown the a_N parameters as;

$$\begin{aligned} \Omega_{03}(w) &= \left(\frac{w^2 - w_{03}^2}{w}\right), \qquad w_{03} = \sqrt{w_1 w_6} \ = 1.5969 \\ \Omega_3(w) &= a_1\Omega_{03}(w) - \frac{1}{a_2\Omega_{03}(w) - \dfrac{1}{a_3\Omega_{03}(w)}} \end{aligned} \tag{3.16}$$

To calculate the unknown parameters, the same routine is performed as follows;

$$|\Omega_3(w)| = \left| a_1\Omega_{03}(w) - \frac{1}{a_2\Omega_{03}(w) - \dfrac{1}{a_3\Omega_{03}(w)}} \right|_{w=\{w_1,w_2,w_3,w_4,w_5,w_6\}} = 1 \tag{3.17}$$

By employing a numeric solver the unknown parameters are found as; $a_1 = 0.7797$, $a_2 = 0.7455$, $a_3 = 3.7486$. The triple band mapping function is achieved as;

$$\Omega_3(w) = 0.7797\Omega_{03}(w) - \frac{1}{0.7455\Omega_{03}(w) - \dfrac{1}{3.7486\Omega_{03}(w)}} \tag{3.18}$$

This mapping function is also applied on a 9th degree equal ripple Chebyshev LP prototype [84] and the triple band gain characteristic is given in Figure (3.7).

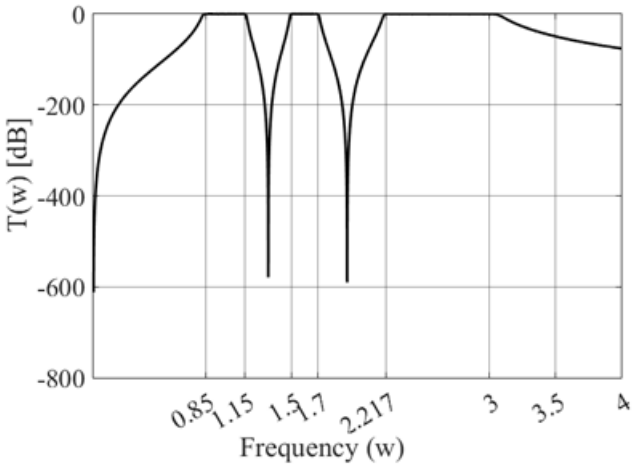

Figure 3.7: Gain response of triple band characteristic produced with LP to MB.

In this method the selectivity of the multiband filter is inherently depend on the chosen LP prototype network and also assigned cut-off frequencies of the multiband response. Higher degree LP prototype will provide more selective multiband filters with same cut-off frequencies. The cut-off frequencies of the multiband filter can be chosen arbitrarily under the constraint in (3.12). If a lower degree LP prototype is chosen, and the pass-bands are placed closely with each other, this may cause signal cross-talk due to limited attenuation between pass-bands [80].

3.4 Determination of Prototype Network

The prototype network to be applied on should be normalized to obtain desired multiband response in this procedure. The band characteristic of the prototype network is preserved as previously stated. The prototype network in this context chosen as low pass form. This can be a transfer function based filters such as low pass Chebyshev, Butterworth, Elliptical etc. or an arbitrary low pass network.

Also as a sub-track of this thesis, band pass prototype networks have been incorporated for dual band network design problem. Through the following sections, the prototype networks are investigated.

3.4.1 Low Pass Prototype Based Approach

Normalized low pass networks can be generated in two ways. First, one can select a low pass Chebyshev, Elliptical, Butterworth etc. transfer function with assigned complexity then apply the determined multiband mapping function on to generate multiband network. Second, an arbitrary low pass network can be used. Such a network can be generated with RFT methods easily.

3.4.1.1 Employment of Transfer Function Based Low Pass Prototype

The transfer function of filter is a frequency dependent expression. It describes the power transfer characteristic between input and output port of the filter. By incorporating the multiband frequency mapping function as a new frequency mapping function in the transfer function , it is possible to produce multiband transfer function $T(\Omega_N) \rightarrow T(w)$ as illustrated in Figure (3.8).

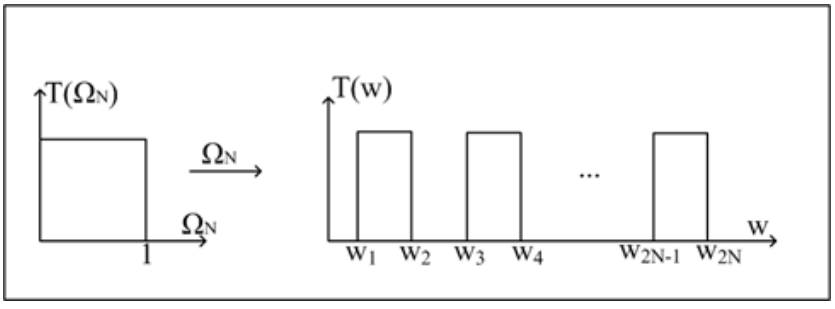

Figure 3.8: LP to MB transformation scheme.

If the LP prototype filter function is a Chebyshev equal ripple form the application of multiband mapping is achieved as;

$$T(\Omega_N) = \frac{1}{1 + \varepsilon^2 {T_n}^2(\Omega_N)} \tag{3.19}$$

Where $T_n(\Omega_N)$ is the Chebyshev polynomial of order n, the Ω_N is the multiband mapping function in (3.11).

If a Butterworth LP prototype is chosen then the multiband transfer function is derived as;

$$T(\Omega_N) = \frac{1}{1 + \varepsilon^2 \Omega_N^2} \tag{3.20}$$

Similarly, if an Elliptical LP prototype is taken then the multiband transfer function is stated as;

$$T(\Omega_N) = \frac{1}{1 + \varepsilon^2 {R_n}^2(\Omega_N)} \tag{3.21}$$

Where the R_n parameter is elliptical rational function of order n.

3.4.1.2 Generation of Low Pass Prototype with RFT

The parametric representation of lossless two-port network is investigated in Chapter 2. By using this representation and employing Real Frequency Parametric Approach in Section 2.2.1 or SRFT in Section 2.2.2 from the perspective of matching network design for matched terminals, it is possible to generate low pass network with normalized response. In this case the TPG function in (2.11) to be optimized is written as;

$$TPG\left(\Omega_N\right) = \frac{4R\left(\Omega_N\right)}{\left(R\left(\Omega_N\right)\right)^2 + \left(X\left(\Omega_N\right)\right)^2} \tag{3.22}$$

Same way the TPG function in (2.17) is written as;

$$TPG\left(\Omega_N\right) = \left|S_{21}\left(\Omega_N\right)\right|^2 \tag{3.23}$$

The RFT routine is followed as summarized in Chapter 2.

3.4.2 Band Pass Prototype Based Approach

Instead of using a low pass prototype network and applying two sequential LPtoBP to produce a dual band characteristic, one can use a normalized band pass prototype gain form to map dual band response via a single LPtoBP transformation. For this reason, first the parametric form of BP network has to be defined in terms of either parametric representation of driving point impedance or scattering polynomials. This approach is used only for dual band network design case, however it can be extended other multiband mapping function as well. SRFT method is employed to construct parametric form of normalized band pass prototype network.

3.4.2.1 A Parametric Study for Generation of Band Pass Prototype

A band pass prototype network can be synthesized as cascaded configuration of low pass and high pass network with unity terminations [80]. This can be approached as a two cascaded resistively terminated matching application. SRFT is one of the most effective method for cascaded matching network design applications as mentioned in Chapter 2. To establish parametric representation of BP prototype network, the LP part and HP part networks are separately initiated in SRFT routine. The following algorithm is presented for the unity terminated LP network part:

- The coefficients of the $h(p)$ polynomial is arbitrarily initiated.
- For LP case, there should be no zero at DC and finite frequencies thus $f(p) = 1$.
- The strictly Hurwitz polynomial $g(p)$is calculated via Hurwitz factorization as mentioned in Chapter 2.
- The TPG function in (2.17) is optimized for unity termination over the normalized frequency $w = [0 \quad 1]$ by using the objective function (2.19).

The optimization routine results with the coefficients of $h(p)$ polynomial. The $f(p) = 1$ and the strictly Hurwitz polynomial $g(p)$ is generated by employing Hurwitz factorization as mentioned before. For the HP network part the only difference is the $f(p) = p^k$ where defines the number of transmission zeros at DC. The same steps are also followed but the TPG is optimized over normalized $w = [w_1 \quad \infty]$ where $w_1 < 1$. The unity terminated normalized LP and HP network parts are united in cascaded configuration as illustrated in Figure (3.9).

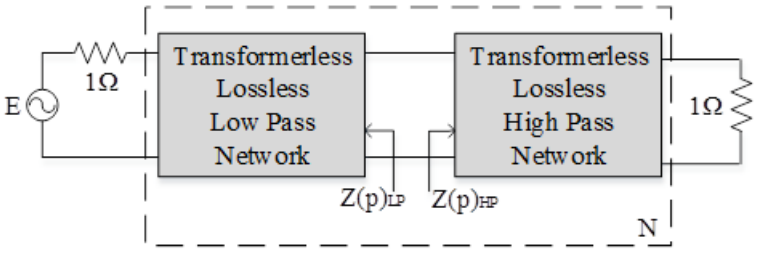

Figure 3.9: Normalized BP prototype network.

The scattering transfer matrix of the BP network can be given as [8];

$$T(p) = \frac{1}{f(p)} \begin{vmatrix} \mu g(-p) & h(p) \\ \mu h(-p) & g(p) \end{vmatrix}, \quad \sigma = \frac{f(-p)}{f(p)} = \pm 1 \tag{3.24}$$

Here the σ parameter is a unimodular constant. The scattering transfer matrix of the LP and HP parts are given as;

$$T_l(p) = \frac{1}{f_l(p)} \begin{vmatrix} \mu_l g_l(-p) & h_l(p) \\ \mu_l h_l(-p) & g_l(p) \end{vmatrix}, \quad T_h(p) = \frac{1}{f_h(p)} \begin{vmatrix} \mu_h g_h(-p) & h_h(p) \\ \mu_h h_h(-p) & g_h(p) \end{vmatrix} \tag{3.25}$$

Here $T_l(p)$ and $T_h(p)$ represent the LP and the HP parts respectively. Therefore the following expression is given for the cascaded network as;

$$T(p) = T_l(p)T_h(p) \tag{3.26}$$

The scattering polynomials of the BP network is derived as;

$$\begin{aligned} g(p) &= g_l(p)g_h(p) + \mu h_l(-p)h_h(p) \\ h(p) &= h_l(p)g_h(p) + \mu g_l(-p)h_h(p) \\ f(p) &= f_l(p)g_h(p), \quad \mu = \mu_l\mu_h \end{aligned} \tag{3.27}$$

After the construction of the LP and HP parts alone, the scattering polynomials of the cascaded structure are re-optimized over normalized frequency $w = [w_1 \quad 1]$. The outputs of the optimization are the optimized coefficients of the $h_l(p)$ and $h_h(p)$ polynomials. By applying SRFT routine the $g_l(p)$ and $g_h(p)$ polynomials are calculated, thus the prototype BP network parametrically is defined. By employing Darlington sense synthesis routine the prototype network can be synthesized [8].

3.5 Synthesis of Transformed Multiband Network

After the multiband mapping function is constructed via the given instruction in Section 3.3, the reactance mapping of the prototype network is performed by application of the proposed generalized mapping function in (3.11) onto each element of the prototype network. Each reactive element is mapped to its multiband correspondence by employing the multiband mapping function as a new frequency variable. Then one-port synthesis of the each reactive element is obtained. Since the prototype network is assumed to be lossless, there exists only capacitors and inductors as frequency dependent variable impedance.

For inductors, the transformed impedance is obtained as;

$$Z_L(\Omega_N(w)) = j\Omega_N(w)L \tag{3.28}$$

For the capacitors, the transformed admittance is given as;

$$Y_C(\Omega_N(w)) = j\Omega_N(w)C \tag{3.29}$$

Where, $\Omega_N(w)$ is given in (3.11). One-port synthesis of the reactances can be performed via well-known network synthesis routine [8]. After the each elements of the prototype network are mapped to their multiband correspond aces and synthesized, then the multiband network can be obtained by cascading the transformed reactances as same configuration in the prototype network. For the dual band mapping function given below;

$$\Omega_2(w) = a_1\left(\frac{w^2 - w_{02}^2}{w}\right) - \frac{1}{a_2\left(\frac{w^2 - w_{02}^2}{w}\right)} \tag{3.30}$$

The dual band transformed impedance of each inductors derived as;

$$\begin{aligned}
&Z_L(\Omega_2(w)) = j\Omega_2(w)L \\
&= ja_1Lw + \frac{1}{jw\frac{1}{a_1Lw_{02}^2}} + \frac{1}{jw\frac{a_2}{L} + \frac{1}{jw\frac{L}{a_2w_{02}^2}}} \\
&= jwL_1 + \frac{1}{jwC_1} + \frac{1}{jwC_2 + \frac{1}{jwL_2}}; \\
&L_1 = a_1L, \quad C_1 = \frac{1}{a_1Lw_{02}^2}, \quad C_2 = \frac{a_2}{L}, \quad L_2 = \frac{L}{a_2w_{02}^2}
\end{aligned} \tag{3.31}$$

In similar way, the dual band transformed admittance of the capacitance is derived as;

$$\begin{aligned} & Y_C(\Omega_2(w)) = j\Omega_2(w)C \\ & = ja_1Cw + \frac{1}{jw\dfrac{1}{a_1Cw_{02}^2}} + \frac{1}{jw\dfrac{a_2}{C} + \dfrac{1}{jw\dfrac{C}{a_2w_{02}^2}}} \\ & = jwC_1 + \frac{1}{jwL_1} + \frac{1}{jwL_2 + \dfrac{1}{jwC_2}}; \\ & C_1 = a_1C, \quad L_1 = \frac{1}{a_1Cw_{02}^2}, \quad L_2 = \frac{a_2}{C}, \quad C_2 = \frac{C}{a_2w_{02}^2} \end{aligned} \tag{3.32}$$

One-port synthesis of the dual band transformed impedance in (3.31) and admittance in (3.32) are given in Figure (3.10)a and in Figure (3.10)b respectively.

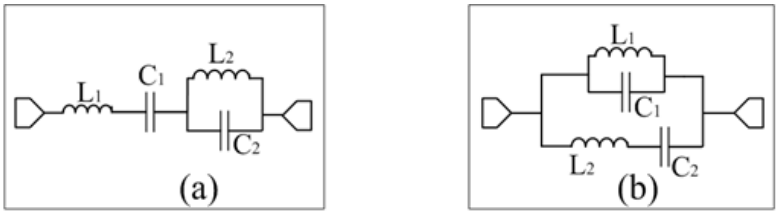

Figure 3.10: (a) Transformed inductor for dual band mapping, (b) transformed capacitor for dual band mapping.

For triple band mapping function as given;

$$\Omega_3(w) = a_1\left(\frac{w^2 - w_{03}^2}{w}\right) - \frac{1}{a_2\left(\dfrac{w^2 - w_{03}^2}{w}\right) - \dfrac{1}{a_3\left(\dfrac{w^2 - w_{03}^2}{w}\right)}} \tag{3.33}$$

The triple band element mapping for each inductor is performed as;

$$
\begin{aligned}
&Z_L(\Omega_3(w)) = j\Omega_3(w)L \\
&= jwa_1L + \frac{1}{jw\dfrac{1}{a_1Lw_{03}^2}} + \frac{1}{jw\dfrac{a_2}{L} + \dfrac{1}{jw\dfrac{L}{a_2w_{03}^2}} + \dfrac{1}{jwa_3L + \dfrac{1}{jw\dfrac{1}{a_3Lw_{03}^2}}}} \\
&= jwL_1 + \frac{1}{jwC_1} + \frac{1}{jwC_2 + \dfrac{1}{jwL_2} + \dfrac{1}{jwL_3 + \dfrac{1}{jwC_3}}}; \\
&L_1 = a_1L, \quad C_1 = \frac{1}{a_1Lw_{03}^2}, \quad L_2 = \frac{L}{a_2w_{03}^2}, \quad C_2 = \frac{a_2}{L}, \\
&L_3 = a_3L, \quad C_3 = \frac{1}{a_3Lw_{03}^2}
\end{aligned}
\tag{3.34}
$$

The triple band element mapping for each capacitor is also given as;

$$
\begin{aligned}
&Y_C(\Omega_3(w)) = j\Omega_3(w)C \\
&= jwa_1C + \frac{1}{jw\dfrac{1}{a_1Cw_{03}^2}} + \frac{1}{jw\dfrac{a_2}{C} + \dfrac{1}{jw\dfrac{C}{a_2w_{03}^2}} + \dfrac{1}{jwa_3C + \dfrac{1}{jw\dfrac{1}{a_3Cw_{03}^2}}}} \\
&= jwC_1 + \frac{1}{jwL_1} + \frac{1}{jwL_2 + \dfrac{1}{jwC_2} + \dfrac{1}{jwC_3 + \dfrac{1}{jwL_3}}}; \\
&C_1 = a_1C, \quad L_1 = \frac{1}{a_1Cw_{03}^2}, \quad C_2 = \frac{C}{a_2w_{03}^2}, \quad L_2 = \frac{a_2}{C}, \\
&C_3 = a_3C, \quad L_3 = \frac{1}{a_3Cw_{03}^2}
\end{aligned}
\tag{3.35}
$$

One-port synthesis of the expressions in (3.33) and in (3.34) are given in Figure (3.11)a and in Figure (3.11)b respectively.

Therefore the multiband mapping function directly determines the topology of the multiband network and element values.

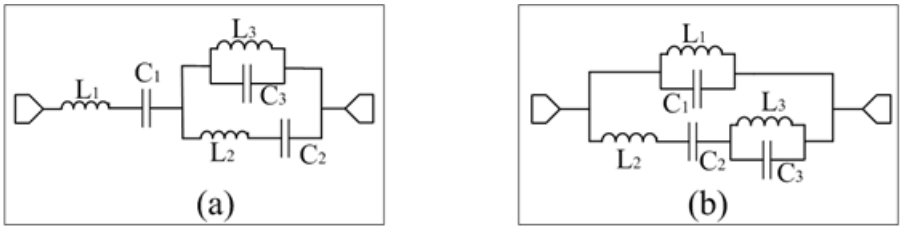

Figure 3.11: (a) Transformed inductor for triple band mapping, (b) transformed capacitor for triple band mapping.

3.6 Multiband Filter Design Applications

Multiband filters can be designed with the proposed mapping functions. The required steps to be employed are introduced in Section 3.3 and Section 3.4. In this section, several filter design examples are presented to validate the proposed mapping functions and the synthesis routine of the multiband networks.

3.6.1 Dual Band Filter Design

A dual band filter is aimed to design with the proposed multiband mapping function. The three normalized cut off frequencies are assigned as; $w_1 = 0.8$, $w_2 = 1.1$, and $w_4 = 2.5$, the last cut off frequency is calculated by using (3.12) as $w_3 = 1.8182$,. The mapping function is established by using (3.11) as;

$$\begin{aligned} \Omega_{02}(w) &= \left(\frac{w^2 - w_{02}^2}{w}\right), \quad w_{02} = \sqrt{w_1 w_4} \ = 1.4142, \\ \Omega_2(w) &= a_1\Omega_{02}(w) - \frac{1}{a_2\Omega_{02}(w)} \end{aligned} \tag{3.36}$$

Then the unknown parameters are found by setting $|\Omega_N(w)| = 1$ at the four corner frequencies as previously mentioned in Section 3.3. The mapping function is obtained as;

$$\Omega_2(w) = 1.0185\Omega_{02}(w) - \frac{1}{0.8042\Omega_{02}(w)} \tag{3.37}$$

3rd degree equal ripple Chebsyev prototype network is chosen to apply the mapping function in (3.37). The TPG response of the resulted dual band filter is given in Figure (3.12).

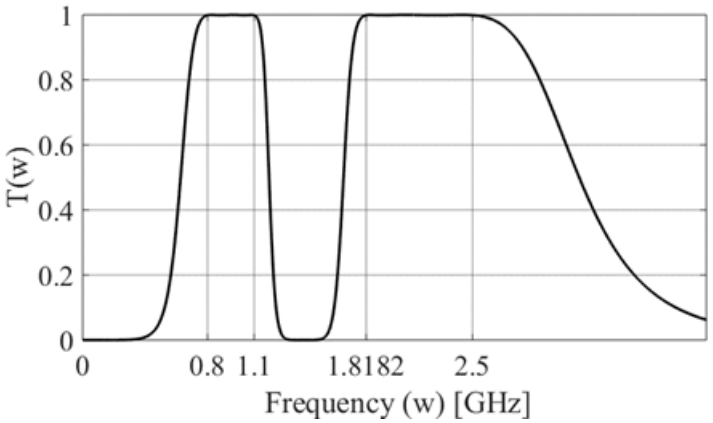

Figure 3.12: Gain response of dual band characteristic produced with LP to MB.

The de-normalized LP prototype network is given as in Figure (3.13).

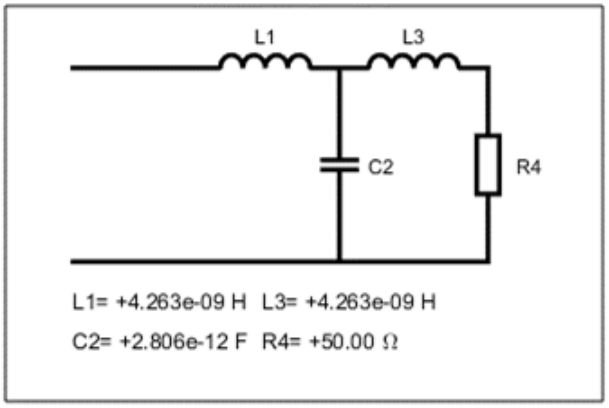

Figure 3.13: LP prototype network for dual band mapping.

The reactance mappings are performed by using the explicit formulations in (3.31) and in (3.32). The synthesized dual band filter is obtained as in Figure (3.14). As it can be seen in the figure, the number of resonator is related with the degree of the mapping.

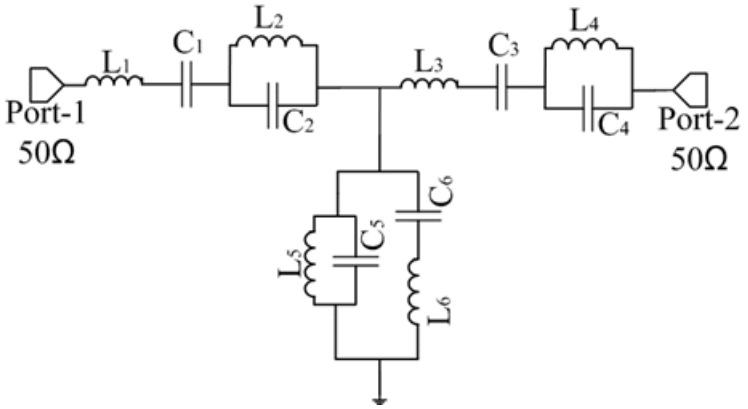

Figure 3.14: Dual Band Filter Network (L1=L3=4.3419nH, L2=L4=2.6506nH, L5=4.4315nH, L6=7.2594nH, C1=C3=2.9169pF, C2=C4=4.7783pF, C5=2.858pF, C6=1.7447pF).

3.6.2 Triple Band Filter Design

In this design, a triple band filter is concerned. The number of independent cut off frequencies is four according to the given explanation in Section 3.3. Here these cut off frequencies are determined as; $w_1 = 0.3, w_2 = 0.5, w_6 = 1.8, w_3 = 0.66$ and the remaining corner frequencies are calculated as $w_4 = 0.8182, w_5 = 1.08$ by using geometric center relation in (3.12). Then the triple band mapping function is obtained with unknown the a_N parameters as;

$$\begin{aligned} \Omega_{03}(w) &= \left(\frac{w^2 - w_{03}^2}{w}\right), \qquad w_{03} = \sqrt{w_1 w_6} \ = 0.7348 \\ \Omega_3(w) &= a_1\Omega_{03}(w) - \cfrac{1}{a_2\Omega_{03}(w) - \cfrac{1}{a_3\Omega_{03}(w)}} \end{aligned} \tag{3.38}$$

The unknown parameters are determined by setting $|\Omega_N(w)| = 1$ at the six corner frequencies as previously mentioned in Section 3.3. The resulted triple band mapping function is given as;

$$\Omega_3(w) = 0.9275\Omega_{03}(w) - \cfrac{1}{1.8065\Omega_{03}(w) - \cfrac{1}{4.3369\Omega_{03}(w)}} \tag{3.39}$$

This mapping function is applied on a normalized 3rd degree equal ripple Chebsyev prototype network The TPG response of the resulted triple band filter is given in Figure (3.15).

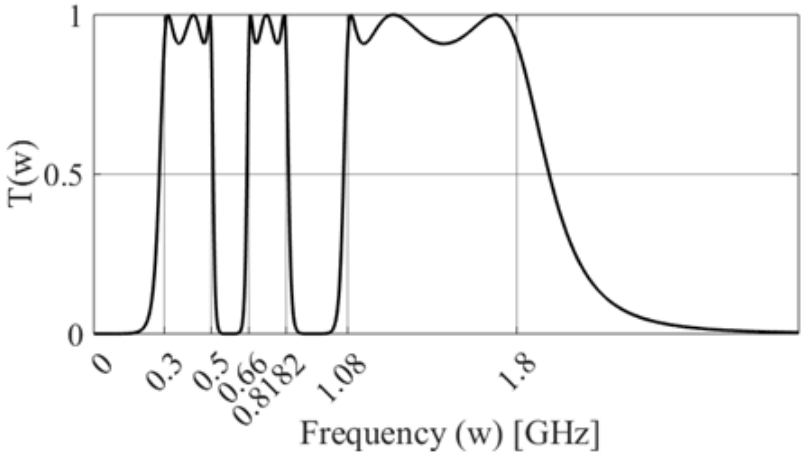

Figure 3.15: Gain response of triple band characteristic produced with LP to MB.

The de-normalized LP prototype network is given as in Figure (3.16);

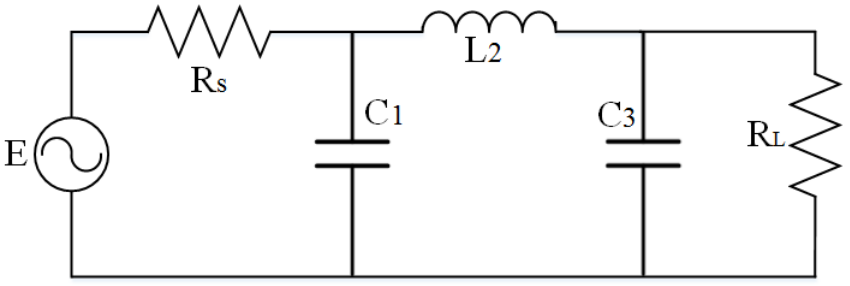

Figure 3.16: LP prototype network for triple band mapping (Rs = 50Ω, C1 = C3 = 4.794pF, L2 = 8.874nH, RL = 50Ω).

The reactance mappings are also performed by using the explicit formulations in (3.34) and in (3.35). The synthesized triple band filter is given as in Figure (3.17);

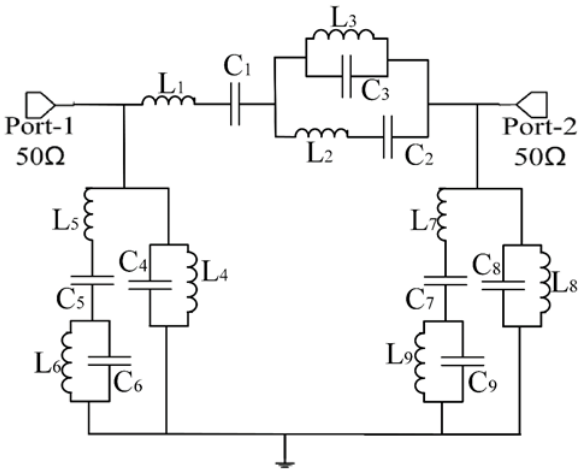

Figure 3.17: Triple Band Filter Network (L1=8.23nH, L2=38.49nH, L3=9.1nH, L4=L8=10.55nH, L5=L7=9.55nH, L6=L9=2.26nH, C1=5.699pF, C2=1.219pF, C3 = 5.157pF, C4 = C8=4.45pF, C5 = C7 = 4.91pF, C6 = C9 = 20.79pF).

3.7 Incorporation of Frequency Mapping with RFT

In the design of multiband matching network with multiband mapping functions, RFT methods are utilized. An arbitrary LP prototype network is initiated through RFT routine and optimized under the multiband mapping functions. The result of the optimization is the driving point impedance or scattering polynomials of a new LP prototype network. This network is aimed to be best LP prototype network to produce multiband TPG characteristic for the matching problem after the assigned multiband mapping function applied on.

Therefore the course of multiband matching network design is simplified only to an optimization problem of an arbitrary LP network instead of explicit determination of a multiband network and its optimization jungle. Here is the SRFT is used for the sake of better convergence in optimization [9]. Here the single matching problem is concerned without any loss of generality as illustrated in Figure (3.18).

Since the lossless two-port is need to be LP then polynomial $f(p)$ is assigned as $f(p) = 1$. The coefficients of the $h(p)$ polynomial is arbitrarily initiated then strictly Hurwitz polynomial $g(p)$ is generated by employing Hurwitz factorization.

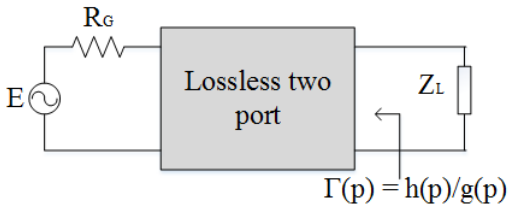

Figure 3.18: Single matching problem.

The coefficients of the $h(p)$ polynomial is optimized under the defined multiband mapping function to maximize the multiband TPG of the network as given;

$$TPG(\Omega_N) = \frac{(1-|S_G|^2)|S_{21}|^2(1-|S_L|^2)}{|1-S_1S_G|^2|1-S_2S_L|^2} \tag{3.40}$$

By employing any unconstrained optimization routine the coefficient of the $h(p)$ polynomial is iterated to minimize the objective function defined as;

$$\delta = \sum_{j=0}^{N_j} [TPG(\Omega_{N,j}, h_i) - T_0(\Omega_{N,j})]^2 \tag{3.41}$$

Here the target gain $T_0(\Omega_N)$ is chosen as ideal multiband gain form as illustrated in Figure (2.2).

3.7.1 The Design Algorithm

The outlined procedure is given in an algorithmic order as follows,

- Construct the multiband mapping function as introduced in Section 3.3.
- Generate the arbitrary LP network by employing SRFT routine as given in Section 2.2.2.
- Arbitrarily initiate the coefficients of the polynomial and include in an optimization routine to minimize the objective function given in (3.40).

- The TPG function in 2.17 is optimized for unity termination over the normalized frequency $w = [0 \quad 1]$ by using the objective function 2.19.
- The output of the optimization is used to obtain scattering polynomial representation of the optimized LP prototype network. By using these polynomials synthesize the LP network [8].
- Employ the multiband reactance mapping on the each reactive component of the optimized LP network to generate multiband matching network.

This algorithm can be easily implemented in software. In the following sections, several matching examples are presented as an application of this algorithm.

3.8 Multiband Matching Network Design Examples

The integration of the multiband frequency mapping technique and the RFT method has been resolved. Therefore, in this section several multiband matching network designs are presented.

3.8.1 Dual Band Matching Network Design

In this section, a multiband Sierpinski antenna [85] is taken as complex load of single matching problem and performed dual band matching to a resistive 50Ω generator. The Sierpinski antenna load and its simulated reflectance characteristic are given in Figure (3.19) and in Figure (3.20) respectively.

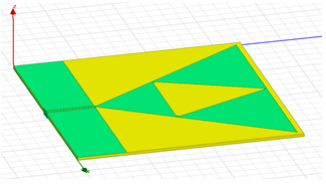

Figure 3.19: Triple band Sierpinski antenna.

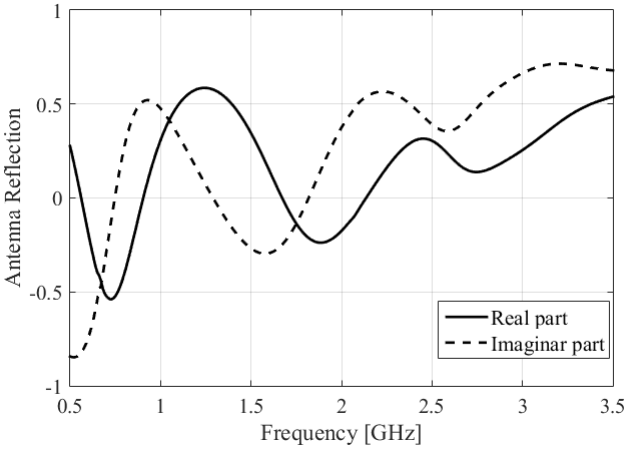

Figure 3.20: Simulated reflection coefficients of Sierpinski antenna.

The algorithm in Section 3.7.1 is employed. Therefore, the dual band mapping function is generated with the normalized assigned cut off frequencies as; $w_1 = 1.596$, $w_2 = 1.881$ and $w_4 = 2.735$ the last cut off frequency is calculated by using (3.12) as $w_3 = 2.32$. The mapping function is established by using (3.11) as;

$$\begin{aligned} \Omega_{02}(w) &= \left(\frac{w^2 - w_{02}^2}{w}\right), \quad w_{02} = \sqrt{w_1 w_4} \ = 2.089, \\ \Omega_2(w) &= a_1\Omega_{02}(w) - \frac{1}{a_2\Omega_{02}(w)} \end{aligned} \tag{3.42}$$

Then the unknown parameters are found by setting $|\Omega_N(w)| = 1$ at the four corner frequencies as previously mentioned in Section 3.3. The mapping function is obtained as; and choosing the any two equations such as;

$$\Omega_2(w) = 1.43\Omega_{02}(w) - \frac{1}{1.397\Omega_{02}(w)} \tag{3.43}$$

The second step of the algorithm is initiated with 3rd degree arbitrary LP function produced with SRFT routine. The coefficients of the $h(p)$ polynomial of the LP prototype network are optimized by using the dual band mapping function (3.43) in optimization. The scattering polynomial of the optimized LP prototype network is achieved as;

$$
\begin{aligned}
h(p) &= -0.0071p^3 - 0.3243p^2 + 0.0929p \\
g(p) &= 0.0071p^3 + 0.344p^2 + 0.8347p + 1
\end{aligned}
\tag{3.44}
$$

Once the scattering polynomials are obtained then the dual band matching network is generated via element mapping as mentioned in Section 3.5. The resulted network is given in Figure (3.21).

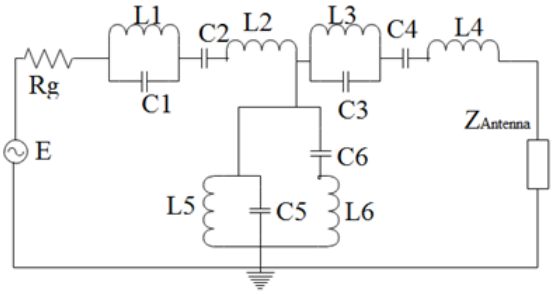

Figure 3.21: Transformed dual band matching network; (Rg=50Ω, L1=0.028nH, L2=0.24nH, L3=1.18nH, L4=10.25nH, L5= 1.7302nH, L6= 15.046nH, C1=207.6pF, C2=23.88pF, C3=4.9pF, C4=0.57pF, C5= 3.35pF, C6= 0.385pF).

The TPG of the dual band matching network is given in Figure (3.22).

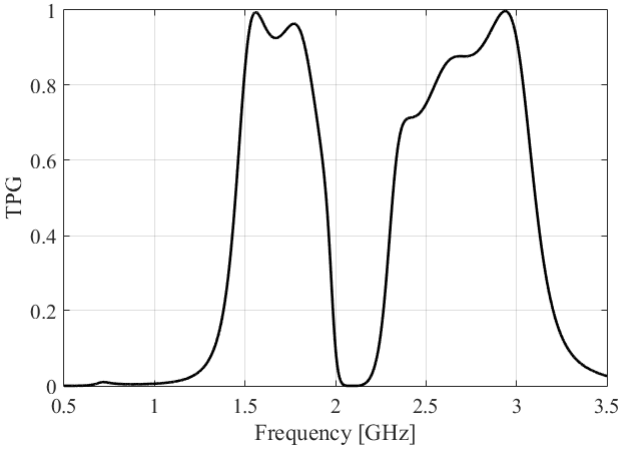

Figure 3.22: TPG response of synthesized dual-band matching network.

The return loss characteristics of matched and unmatched case are given in Figure (3.23).

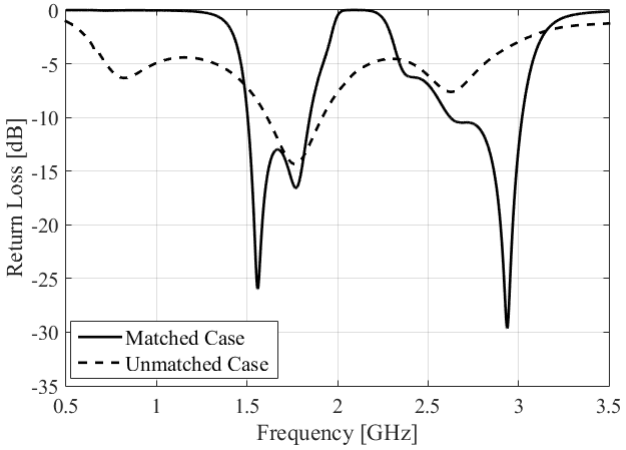

Figure 3.23: Return Loss characteristic of matched and unmatched antenna.

As it can be interpreted from the figures there are certain improvement at the return loss characteristic of the antenna at the assigned pass bands.

3.8.2 Quad Band Matching Network Design

A quad band matching network design for a UWB PIFA antenna is performed in this section. The single matching problem is concerned. It is aimed to design a quad band matching network between resistive 50Ω generator and the PIFA antenna [86]. The layout of the antenna is given in Figure (3.24).

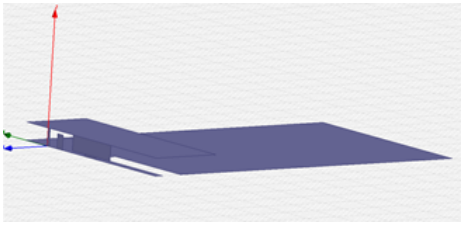

Figure 3.24: PIFA antenna.

The antenna has a UWB characteristic however, in this design, several pass band of the antenna will be suppressed by the matching network. The algorithm in Section 3.7.1 is followed. In the design specifications, five cut off frequencies are assigned as $w_1 = 0.95$, $w_2 = 1.05$, $w_3 = 1.2626$, $w_4 = 1.3$, and $w_8 = 2.1$, the

remaining cut off frequencies are calculated as $w_5 = 1.5346$, $w_6 = 1.58$, $w_7 = 1.9$ then the quad mapping function is derived by employing (3.11) as;

$$\begin{aligned} \Omega_{04}(w) &= \left(\frac{w^2 - w_{04}^2}{w}\right), \quad w_{04} = \sqrt{w_1 w_8} \ = 1.4134, \\ \Omega_4(w) &= a_1\Omega_{04}(w) - \cfrac{1}{a_2\Omega_{04}(w) - \cfrac{1}{a_3\Omega_{04}(w) - \cfrac{1}{a_4\Omega_{04}(w)}}} \end{aligned} \tag{3.45}$$

The unknown parameters are calculated and the resulted mapping function is generated as;

$$\Omega_4(w) = 2.6119\Omega_{04}(w) - \cfrac{1}{0.5056\Omega_{04}(w) - \cfrac{1}{11.3823\Omega_{04}(w) - \cfrac{1}{0.9137\Omega_{04}(w)}}} \tag{3.46}$$

A second degree arbitrary LP prototype network is initiated in SRFT routine and optimized to match those four pass bands under the quad band mapping function. The scattering polynomials of the optimized LP prototype network are achieved as;

$$\begin{aligned} h(p) &= -0.0599p^2 + 0.0432p; \\ g(p) &= 0.0599p^2 + 0.3488p + 1; \end{aligned} \tag{3.47}$$

The synthesis of the network function is performed as previous examples. The resulted quad band matching network is given in Figure (3.25).

The TPG characteristic of the quad band matching network and the matched and unmatched case return loss performances are presented in Figure (3.26) and in Figure (3.27) respectively.

As it can be seen in the figures, the quad-band matching response for the PIFA antenna has been achieved. The proposed method is applied to improve the return loss performance over the specified bands and also suppressing the determined notch bands.

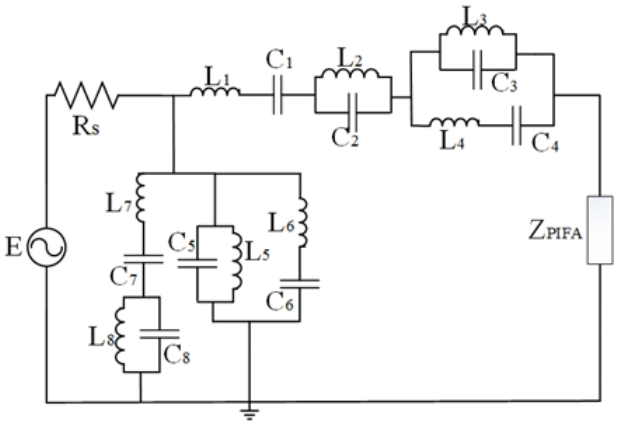

Figure 3.25: Synthesized quad-band matching network; (Rs = 50Ω, L1 = 8.16nH, L2 = 1.074nH, L3 = 1.85nH, L4 = 14.07nH, L5 = 5nH, L6 = 38nH, L7 = 22nH, L8=2.9nH, C1 = 1.55pF, C2=11.8pF, C3 = 6.85pF, C4 = 0.9pF, C5 = 2.54pF, C6 = 0.335pF, C7 = 0.577pF, C8 = 4.4pF).

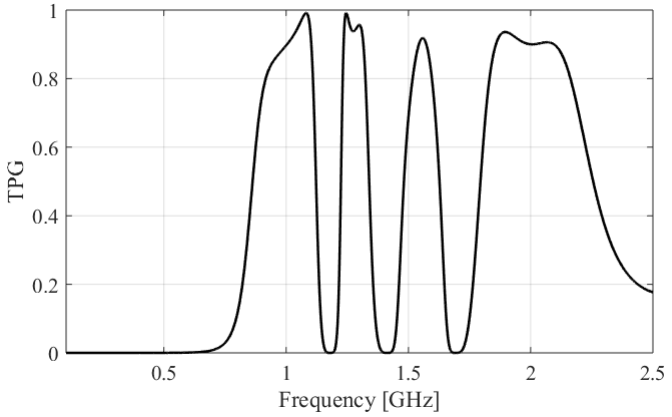

Figure 3.26: TPG response of synthesized quad-band matching network.

By using the obtained results of the proposed mapping functions it is possible to design matching networks over an arbitrary number of pass bands.

The integration of the proposed method with RFT methods provide a strong analytical basis in addition to that of numerical advantages.

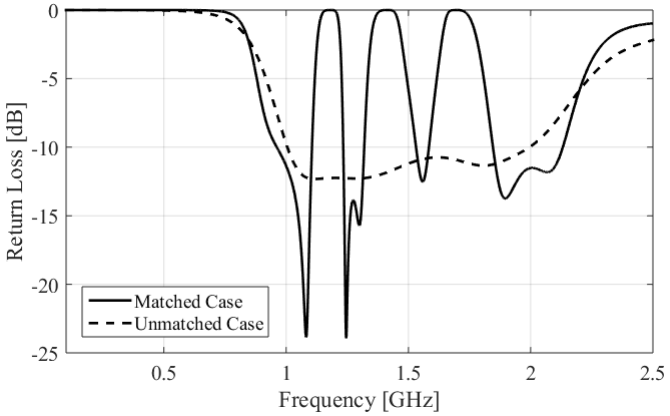

Figure 3.27: Return loss characteristic of matched and unmatched PIFA.

3.9 Concluding Remarks

In this chapter of the thesis, a generalized mapping function, which is based on sequential LPtoBP mapping is proposed. This function is evaluated by deep investigation of the sequential mapping functions. The mapping function is incorporated in multiband filter and matching network design applications. Several examples are presented in this track. It has been shown that, this method provides a strong analytical tool to design and synthesis of the multiband networks.

The given procedure for filter and matching network cases are clear and proved with numerical examples and simulations. By employing this method, multiband network with arbitrary number of pass bands can be designed, optimized and synthesized.

One disadvantage of this method is, the cut off frequencies have to distribute around a geometric center frequency. Therefore the number of independent cut off frequency is restricted by $N+1$ where N is the number of pass band. Moreover when the number of pass band is increased, the multiband network is become unpractical for lumped network realizations. However different network topologies can be also synthesized [39, 77] such as; distributed, cavity, etc.

In the following section the second objective of the thesis is elaborated for more practical multiband matching network realizations.

Chapter 4

Multiband Matching with Synthesis Approach

4.1 Introduction

In the design of multiband matching networks, second objective for analytical solution incorporates explicit network functions in terms of either impedance functions or scattering transfer matrixes.

The parametric representation of impedance of a lossless two-port network is well established [46, 57] in literature. An impedance function can be defined in terms of its transmission zeros and zeros of the denominator polynomial.

As mentioned in Section 2.1, a lossless two-port multiband network has to acquire FTZs (Finite Transmission Zeros) to control the attenuation characteristic of TPG at the specified frequencies. FTZs can be synthesized as LC resonance sections in series or shunt configuration at series or shunt arm. A well-known extraction of FTZs is known as Brune sections [65]. However in the synthesis of Brune sections, generally a negative unrealizable network element occurs [65, 87]. It is possible to eliminate these negative elements by using coupled coil equivalencies of Brune sections. However, couple coils are not easy to implement at high frequencies. Several equivalent models are proposed to realize these coupled coils via microstrip lines. However they require several complex modeling steps [88–90].

Multiband realizable network synthesis in ladder form without coupled coils is always most preferred way to overcome the synthesis issue of FTZs. However this

problem has not been completely resolved in literature especially for matching networks.

In this chapter of the thesis, theoretical background of the multiband network synthesis is elaborated. Several research attempts are introduced for the coupled coil free synthesis of multiband networks such as network transformations. As a semi-analytical solution, an integrated parametric design technique is proposed for the design and synthesis of multiband realizable ladder networks consisting of FTZs. The proposed representation of multiband network provides a construction algorithm of the driving point impedance of multiband ladders which allows to achieve multiband ladders without coupled coils.

4.2 Parametric Characterization of Multiband Matching Network

Referring to the general multiband transducer power gain response in Figure (2.2), in a multiband matching problem, the impedance function of the lossless two-port must possess FTZs at the stopbands to provide matching over multiple pass bands. Considering the single matching problem illustrated in Figure (2.3) the back-end driving point impedance of the matching network can be fully defined in terms of the roots of the denominator polynomial and the $f(p)$ polynomial which defines the transmission zeros of the network. For the practical multiband matching problem, the $f(p)$ polynomial is defined as;

$$f(p) = p^{n_{dc}} \prod_{r=1}^{n_w} (p^2 + w_r^2) \tag{4.1}$$

Here the n_{dc} and n_w are the number of transmission zeros at DC and finite frequencies. The number of transmission zeros are infinity is derived as;

$$n_\infty = n - n_{dc} - 2n_w \tag{4.2}$$

Where n is the degree of denominator polynomial of impedance function in (2.4). The outlined definition for multiband networks fully characterizes the network and provides the driving point impedance of lossless two-port. However it does not provide a projection on the synthesis of the impedance.

4.3 Synthesis of Multiband Ladder Network

Once the proper driving point impedance function is formed then the element extraction from impedance can be performed by employing one of the well-known technique which is called zero shifting technique [91]. Each transmission zero corresponds to a network structure.

Each transmission zeros at DC is extracted as either a capacitor on series arm or a shunt inductor as illustrated in Figure (4.1).

Figure 4.1: Transmision zero extraction at w=0.

Each transmission zeros at infinity is extracted as either an inductor on series arm or a shunt capacitor as illustrated in Figure (4.2).

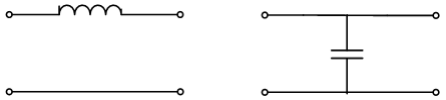

Figure 4.2: Transmision zero extraction at w= ∞.

Transmission zeros at finite frequencies are extracted as a partial series/shunt reactive component and a series/shunt resonator in series or shunt configuration [65]. Also one of the well-known extractions is called Brune section as shown in Figure (4.3).

Brune section extraction is well elaborated in classical network synthesis literature [65]. The extraction cycle of FTZs may inherently result in a negative valued

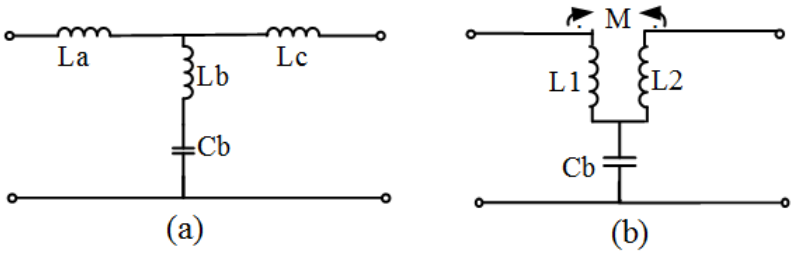

Figure 4.3: Transmision zero extraction at FTZs.

inductor La or Lc in the ladder realization of in Figure (4.3)a. For a physically realizable circuit, such negative valued non-realizable elements in a ladder realization can be eliminated by use of the coupled coil equivalence shown in Figure (4.3)b. Realization with coupled coils is however possible only at low frequencies and for high frequency applications in general a coupled coil free realization is preferred. On the other hand, the distributed implementation of Brune sections is possible with several approximate structures such as Ikono loop [89].

Moreover, proper usage of network transformations, such as Norton transformations are employed to eliminate unrealizable elements for several applications [92].

In the following example, a triple band matching network in ladder topology design is presented. A successive application of Norton transformation is performed to obtain ladder network topology with all positive valued network elements.

4.3.1 Application of Norton Transformation for Multiband Matching Ladders

In the design of multiband matching network, the triple band Sierpinski antenna in Figure (3.19) is chosen as complex load to be matched.

The antenna load data is already provided in Figure (3.20). The unmatched return loss characteristic of the antenna suggests that the antenna has triple band characteristic without using any matching circuitry. The aim of the matching network design is, improving the power transfer capability of the antenna over its

predetermined bands. Therefore the location of finite transmission zeros in the matching network is assigned according to the unmatched return loss characteristic of the antenna. Using only finite transmission zeros at the stop bands of the antenna may provide desired improvements in triple band TPG characteristic.

This is naturally a single matching problem. Therefore, RFT Parametric Approach is utilized. Here, four finite transmission zeros are assigned to construct the $f(p)$ polynomial in (2.10). These are the normalized frequencies $w_1 = 0.1$, $w_2 = 1.2$, $w_3 = 2.3$, and $w_4 = 4.5$ corresponding to 0.1GHz, 1.2GHz, 2.3GHz and 4.5GHz respectively. An eight-degree back-end driving-point impedance is optimized over the frequency bands of GSM900, GSM1800 and 4G-LTE, which are around 900MHz, 1800MHz and 2600MHZ respectively.

The back-end driving point impedance $Z(p) = a(p)/b(p)$ of the matching network is then generated by optimization. The output of the optimization is the poles of the impedance function. The coefficients of the generated numerator and denominator polynomials of the impedance are as given in (4.3).

$$\begin{aligned} a(p) &= 1.0952p^8 + 0.0438p^7 + 31.6489p^6 + 0.6259p^5 + 174.6918p^4 \\ &\quad + 1.8199p^3 + 199.9627p^2 + 0.2539p + 1.6143 \\ b(p) &= p^8 + 6.8842p^7 + 25.3579p^6 + 67.2876p^5 + 131.1482p^4 \\ &\quad + 171.7883p^3 + 133.3896p^2 + 47.5184p + 1.6143 \end{aligned} \tag{4.3}$$

The triple band TPG characteristic of the matching network is given in Figure (4.4). The return loss performances of matched and unmatched cases of the antenna is given in Figure (4.5).

The resultant impedance is synthesized by employing classical transmission zero extraction routine [65]. The triple band matching with normalized element values is presented in Figure (4.6).

As it can be seen in the matching network in Figure (4.6), the negative valued inductances are occurs as a result of Brune section extractions [65]. It is possible

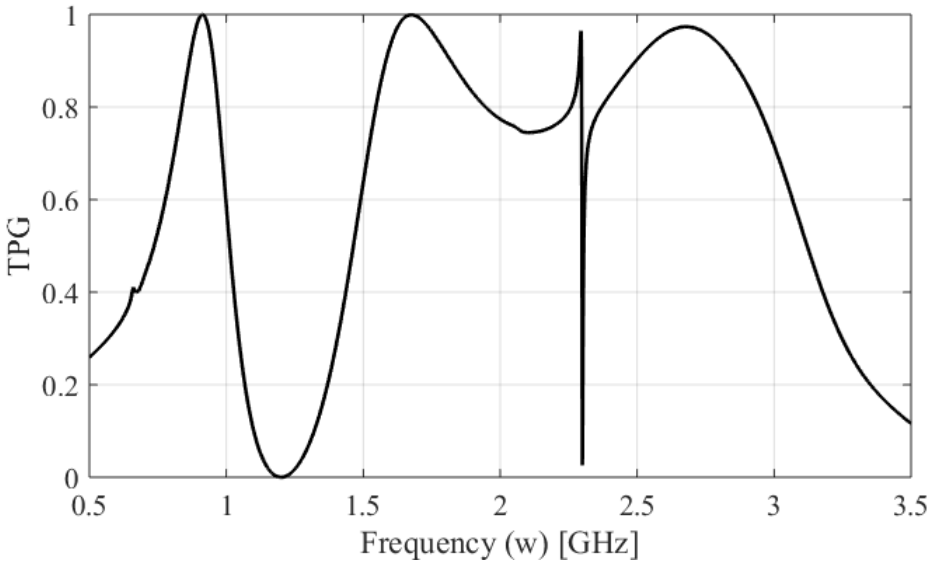

Figure 4.4: TPG response of the triple band matching network.

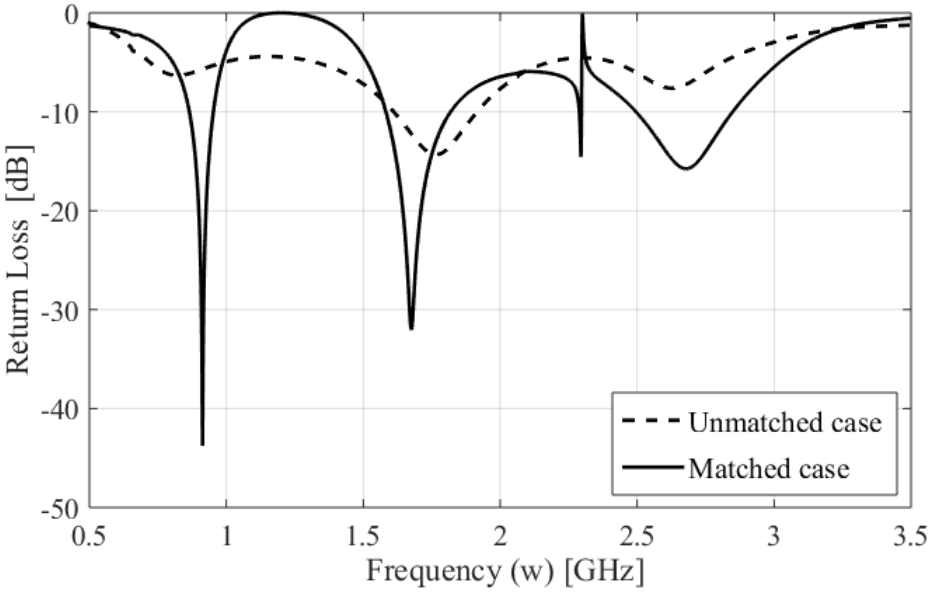

Figure 4.5: Return loss responses of the matched and unmatched cases of the antenna.

to use coupled coil equivalences of the Brune sections in Figure (4.3)b and remove the negative inductors as presented in Figure (4.7). However, as mentioned before, it is not easy to implement such transformers.

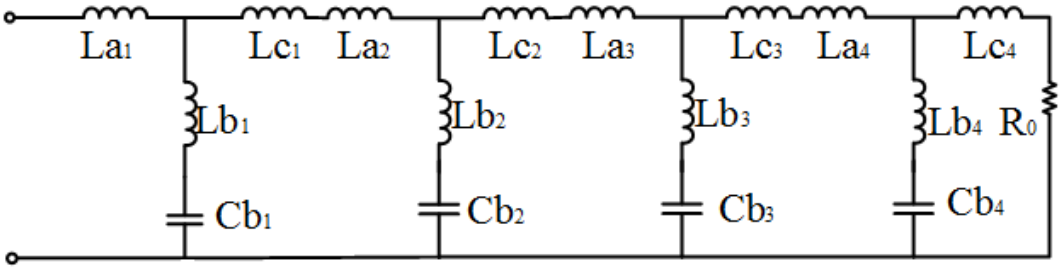

Figure 4.6: The normalized matching network of triple band antenna (La1 = 0.8H, Lb1 = 3.5H, Cb1 = 28.44F, Lc1 = -0.65H, La2 = -0.076H, Lb2 = 1.03H, Cb2 = 0.677F, Lc2 = 82mH, La3 = -0.2H, Lb3 = 44.2H, Cb3 = 4.3mF, Lc3 = 0.2mH, La4 = -12mH, Lb4 = 0.16H, Cb4 = 0.3F, Lc4 = 13mH, R0 = 1Ω).

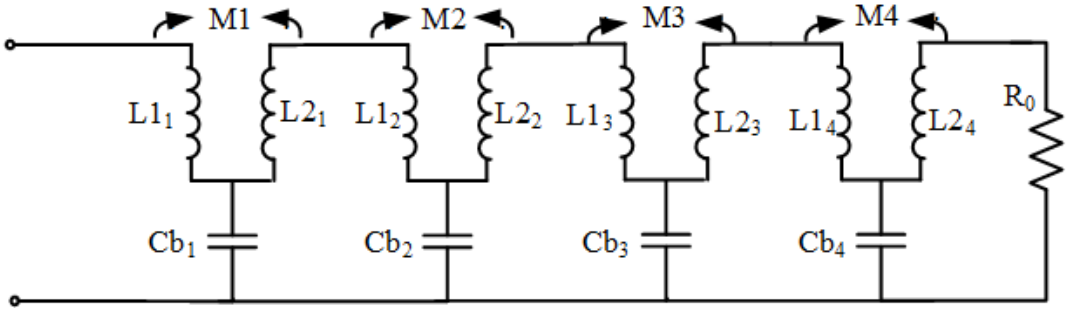

Figure 4.7: Coupled coil equivalent of the triple band denormalized matching network (L11 = 6.39nH, L21 = 27.98nH, Cb1 = 90.53pF, M1 = 27.9nH, L12 = 6.9nH, L22 = 8.8nH, Cb2 = 2.158pF, M2 = 7.8nH, L13 = 6.39nH, L23 = 27.98nH, Cb3 = 0.014pF, M3 = 399.2nH, L14 = 6.39nH, L24 = 27.98nH, Cb4 = 0.994pF, M4 = 1.2nH, R0 = 50Ω).

Another way to remove the negative elements is, using several successive application of Norton Transformations [15] on network elements in Figure (4.6). The resultant simplified matching network is achieved in ladder form as given in Figure (4.8).

For the elimination of negative valued elements in a ladder network, several alternative trial error based approaches are available in the literature. In [87] it has been suggested that, before extraction of FTZs, a partial L/C component should be extracted. This may yield all positive valued network elements.Another approach in [93] states that, changing the extraction order of transmission zeros may result with realizable ladder networks.

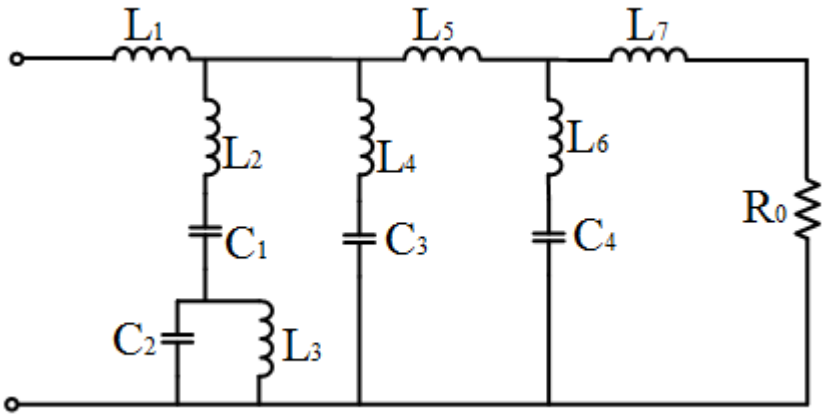

Figure 4.8: Alternative synthesize of matching network. (L1 = 0.5868nH, L2 = 6.313nH, L3 = 20.4nH, L4 = 352nH, L5 = 0.5627nH, L6 = 1.258nH, L7 = 0.1035nH, C1 = 92.7pF, C2 = 3.74pF, C3 = 0.014pF, C4 = 0.984pF, R0 = 50Ω).

All these methods are based on trial-error adjustment and do not ensure coupled coil free realizations. In the following section, a parametric approach is proposed for eliminating negative elements and obtaining transformer-less network.

4.4 A Parametric Approach for Transformer-less Network Synthesis

In this section, a parametric design procedure is proposed to synthesize driving point impedance with realizable circuit elements without transformers. By employing the proposed technique, the negative elements are eliminated by the cascading Brune sections while extracting FTZs. The driving point impedance of lossless two-port is composed of a Foster part and a minimum impedance part. The constructed impedance is optimized by employing Real Frequency Technique (RFT) routine while keeping Foster part out of the optimization. The synthesis procedure of the optimized impedance starts with extraction of dummy Foster reactance then the minimum impedance part. It has been shown that the negative elements of Brune sections are eliminated by the positive values parts of the neighboring Brune sections.

A given non-minimum impedance can be separated as Foster part and a minimum impedance part as in (4.4). The minimum part and Foster part impedances are given in (4.5) and in (4.6) respectively.

$$Z(p) = \frac{n(p)}{d(p)} = Z_{Foster}(p) + Z_{\min}(p) \tag{4.4}$$

$$Z_{Foster}(p) = k_\infty p + \frac{k_0}{p} + \sum_{i=1}^{N_w} \frac{k_i p}{p^2 + w_i^2} \tag{4.5}$$

$$Z_{\min}(p) = \frac{a(p)}{b(p)} = \frac{a_k p^k + a_{k-1} p^{k-1} + ... + a_1 p + a_0}{b_l p^l + b_{l-1} p^{l-1} + ... + b_1 p + b_0} \tag{4.6}$$

In the above equations,k_∞ is the residue of the pole at infinity k_0 is the residue of the pole at zero and k_i is the residues at the complex conjugate poles located at $p = jw_i$. All the residues k_∞, k_0 and k_i of must be real and non-negative [8]. If Foster function describes an impedance function of a inductor then the values of inductor is $L = k_\infty$. Then the resultant non-minimum impedance can be defined parametrically as;

$$\begin{aligned} Z(p) = \frac{n(p)}{d(p)} &= pk_\infty + \frac{a(p)}{b(p)} = \frac{pk_\infty b(p) + a(p)}{b(p)} \\ &= \frac{n_n p^n + n_{n-1} p^{n-1} + ... + n_1 p + n_0}{d_m p^m + d_{m-1} p^{m-1} + ... + d_1 p + d_0} \end{aligned} \tag{4.7}$$

The minimum impedance part of the impedance is well defined in literature [94]. If the topology of the network is determined then the minimum impedance can be generated.

The synthesis is obtained in two parts. First the Foster reactance part is extracted then the minimum part is extracted. The extraction of Foster reactance is utilized by extracting a zero at infinity as;

$$L = k_\infty = \frac{n_n}{d_m} \tag{4.8}$$

The remainder minimum part impedance is generated as;

$$Z_{\min}(p) = \frac{a_k(p)}{b_l(p)} = \frac{a(p) - pk_\infty b(p)}{b(p)} \tag{4.9}$$

Once minimum driving point impedance of a lossless network is obtained, a ladder realization can be obtained by employing classical Darlington sense synthesis. The FTZs can be extracted as Brune section [65].

As mentioned before the extraction cycle of FTZs as Brune section is inherently result in a negative valued inductor La or Lc in the ladder realization of Figure (4.3). From practical observations the proposed procedure also enforces the La to be the negative and Lc to be positive.

In the outlined procedure, such negative valued non-realizable elements in a ladder realization are omitted by positive valued inductor of cascading section. The first negative inductor of the Brune section is eliminated by the dummy Foster reactance part as illustrated in Figure (4.9).

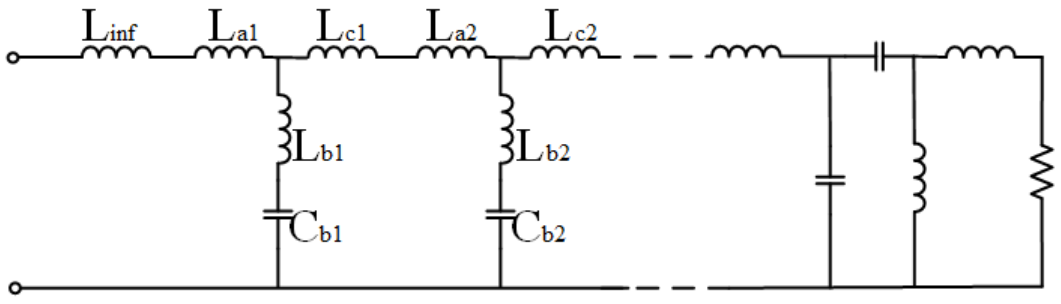

Figure 4.9: Synthesis of the non-minimum impedance.

Each adjacent inductor at series arm is summed with the following inductor. The results of summations are supposed to be positive as it is claimed. From practical observations, the L_{inf} should be chosen as bigger than absolute value of the summation of the negative inductors of the minimum part impedance (i.e.$L_{\text{inf}} > |L_{a1} + L_{a2} + ...|$). The following example is obtained by using this method.

A sixth degree driving point impedance function is generated by following the procedure in [8]. The impedance function is formed with three normalized FTZs at $w_1 = 1.2$, $w_2 = 1.5$ and $w_3 = 2$. A dummy Foster reactance $L_{\text{inf}} = 1.9227$ is introduced to the generated impedance. As mentioned in Section 2.2.1, the impedance function is optimized over normalized frequencies $[\ 0 \quad 1\ ]$ in RFT routine. The coefficients of numerator and denominator polynomials of the resultant impedance function are given as in Table (4.1).

n(p)	**d(p)**
1.9227	0
2.4193	1.0000
5.7703	1.2580
4.8692	2.6030
5.2819	2.0283
2.7092	1.8430
1.4346	0.7526
0.2877	0.2877

Table 4.1: The coefficients of the impedance numerator and denominator polynomials.

As given in Table (4.1), the degree of numerator and the denominator differs by one. It is an obvious result of the construction routine of the non-minimum impedance function mentioned in above. The transducer power gain response of the designed LP filter is given in Figure (4.10).

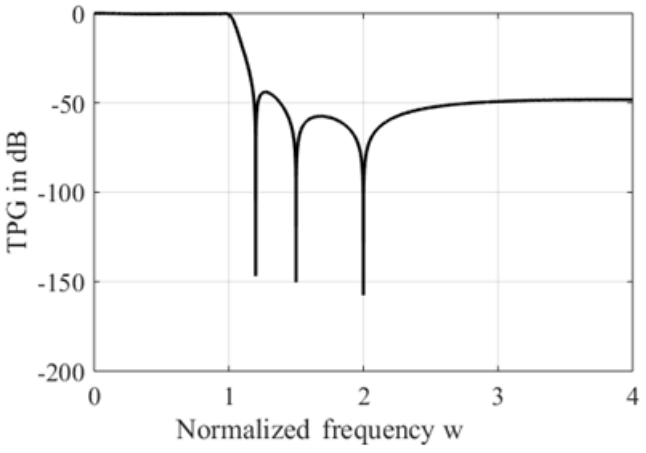

Figure 4.10: TPG response of the designed LP filter with three FTZs.

The impedance is synthesized by following the procedure described above. The resultant network is given in Figure (4.11).

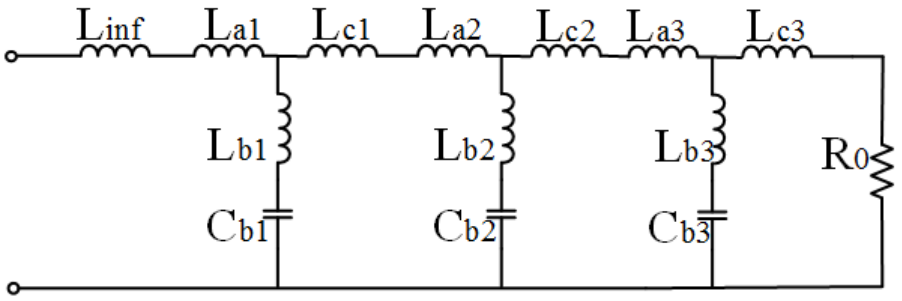

Figure 4.11: Synthesis of the impedance of the normalized LP filter with three FTZs (Linf = 1.9227H, La1 =-0.754522H, Lb1 = 1.22308H, Cb1 = 0.567785F, Lc1 = 1.96954H, La2 =-0.347927H, Lb2 = 0.431688H, Cb2 = 1.02955F, Lc2 = 1.79317H, La3 = -0.172111H, Lb3 = 0.245385H, Cb3 = 1.01881F, Lc3 = 0.57638H, R0 = 1Ω).

As it can be seen in the figure, $Linf + La1 > 0$, $Lc1 + La2 > 0$, $Lc2 + La3 > 0$. Thus the network is composed of only realizable positive valued components.

Beside of obtaining positive realizable ladder network topology, this method also yields freedom of choosing FTZs locations on filter response. Thus the stop band characteristic of filter can be controlled in comparison with classical transfer function based LP filter design tools [95].

4.5 Concluding Remarks

The synthesis based characterization and design of multiband network offers advantages in analytical way to control the characteristic of the response. It has been observed that, the practical realization with ladder form with all positive element values can be achieved by proper application of circuit transformations such as that of Norton transformations and partial extraction approaches, and modifying the extraction order in a synthesis approach.

An improvement in the extraction and the characterization of multiband network can be achieved by following the parametric characterization approach as proposed and discussed in this chapter. A better control and systematic cancellation of negative valued elements for the purpose of ladder type topologies are achieved.

In the literature, several alternative techniques are proposed to handle this issue by establishing and introducing some additional constraints on the Brune function to be synthesized.

In this track; Darlington, gave sufficient conditions for physical realizability of the above-mentioned circuits without mutual induction [96]. Fujisawa [97], Watanabe [98], Nish [99], Meinguet and Belevitch [100] studied on realizable two-port network functions. Ozaki and Ishii gave realization condition on distributed networks [101]. Yang and Yao etc. [102] applied this conditions on distributed matching network. They use numeric iteration methods to generate the impedance function to satisfy the conditions. Yildiz, Aksen and Yarman [103] applied Fujisawa conditions on lumped matching network design. They use also numeric search routines to satisfy the conditions.

T. Fujisawa established several constraints on the driving point impedance/admittance of lossless two-ports which include FTZs, to obtain as realizable low-pass ladders [97]. Once his constraints are satisfied then driving point impedance can be extracted as a mid-series or mid shunt LP ladders without negative elements so mutual inductance.

As a future work, Fujisawa's constraints can be implemented for arbitrary impedance or admittance functions through a parametric design algorithm. This may provide multiband matching ladders without coupled coils via proper integration of real frequency techniques.

Chapter 5

Practical Designs and Implementations

In this chapter several multiband RF networks are demonstrated. The implemented networks are designed by employing the two objectives of the thesis. The multiband network design problem is investigated from analytical point of view through the thesis. Therefore, the proposed approaches can be applicable for both filter and matching network designs. The following multiband network implementations are given to validate the efficiency of the proposed theoretical contributions on multiband network design.

5.1 Dual Band Filter Design and Implementation

A dual band filter design and realization is presented for the commercial bands of GSM900 and GSM1800/UMTS applications. The parameters of DB mapping function are chosen to cover these two bands. First pass-band is 0.85GHz-1.15GHz and second band is 1.7GHz-2.3GHz.

If we apply the new MB mapping function for the assigned band characteristic then the mapping function is derived as;

$$\begin{aligned} \Omega_{02}(w) &= \left(\frac{w^2 - w_{02}^2}{w}\right), \quad w_{02} = \sqrt{w_1 w_4} \ = 1.398 \\ |\Omega_2(w)| &= \left| a_1 \Omega_{02}(w) - \frac{1}{a_2 \Omega_{02}(w)} \right|_{w=\{w_1,w_2,w_3,w_4\}} = 1 \end{aligned} \tag{5.1}$$

The two sets of equations are solved and the unknown parameters are calculated as $a_1 = 1.111$, $a_2 = 1.285$.

Eventually the mapping function is derived as;

$$\Omega_2(w) = 1.111\Omega_{02}(w) - \frac{1}{1.285\Omega_{02}(w)} \tag{5.2}$$

The prototype network is generated by following the procedure in Section 3.4.1.2. Therefore the optimized impedance of LP prototype is given as;

$$Z(p) = \frac{1.0767\mathrm{p}^3 + 2.5372\mathrm{p}^2 + 2.1118\mathrm{p} + 1}{1.2284\mathrm{p}^4 + 2.8947\mathrm{p}^3 + 3.0474\mathrm{p}^2 + 2.6444\mathrm{p} + 1} \tag{5.3}$$

The synthesis of the impedance of LP prototype is given in Figure (5.1) as;

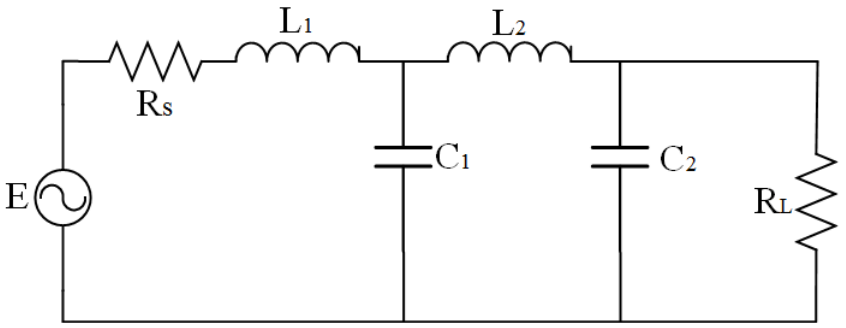

Figure 5.1: Optimized LP prototype network (L1 = 9.079nH, L2 = 11.96nH, C1 = 5.371pF, C2 = 1.351pF, Rs = RL = 50Ω).

Since the LP prototype network is synthesized then DB filter can be achieved by using the given dual band transformed resonator sections in Section 3.5. The resulted DB filter network is given in Figure (5.2).

The TPG response of the DB filter is given in Figure (5.3).

Since all lumped realization would not be practical due to the parasitics and losses of commercially passive elements, for the realization of the filter, mixed element implementation is considered. The DB filter in Figure (5.1) is performed

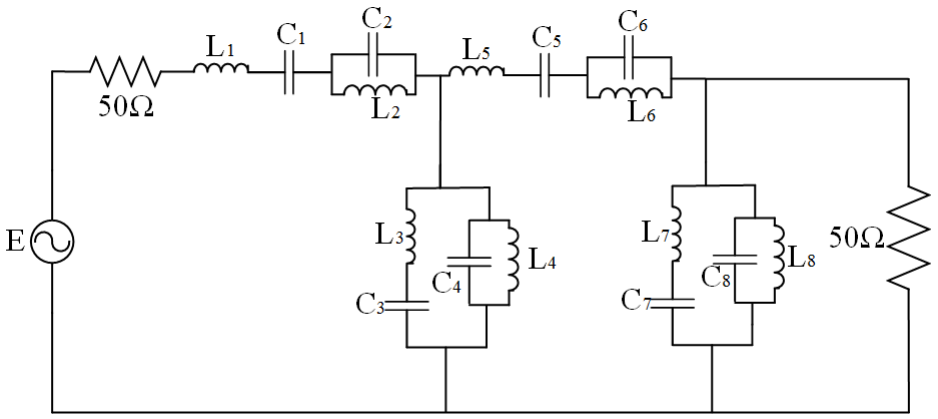

Figure 5.2: Transformed dual band filter network (L1 = 10.09nH, C1 = 1.284pF, L2 = 4.115nH, C2 = 3.149pF, L3 = 5.32nH, C3 = 2.435pF, L4 = 2.171nH, C4 = 5.968pF, L5 = 13.29nH, C5 = 0.975pF, L6 = 5.423nH, C6 = 2.389pF, L7 = 21.16nH, C7 = 0.612pF, L8 = 8.633nH, C8 = 1.501pF).

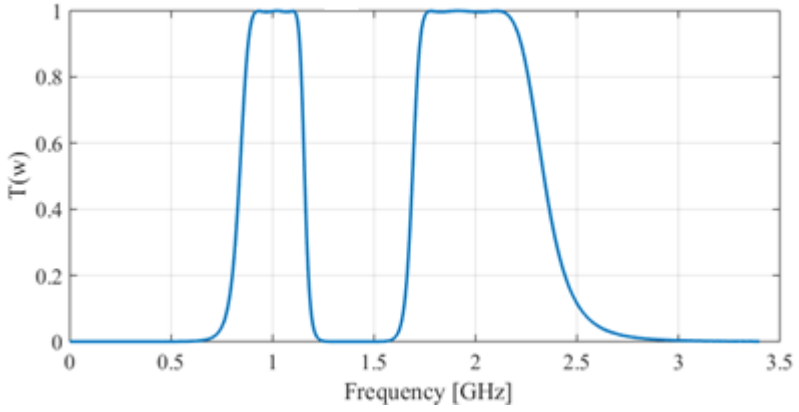

Figure 5.3: TPG response of designed DB filter.

by using microstrip equivalences of some network elements. Some lumped resonator elements are transformed into distributed correspondences (i.e. inductors are into serial transmission lines; shunt capacitors are into open stubs) [15]. The performance results are obtained as close as possible to ideal lumped circuit via tuning the converted element parameters and finally optimizing the overall performance. The microstrip implementation of the DB filter is demonstrated in Figure (5.4). The filter is printed on FR4 substrate. Its relative permittivity is 4.4 and thickness is 1.6mm.

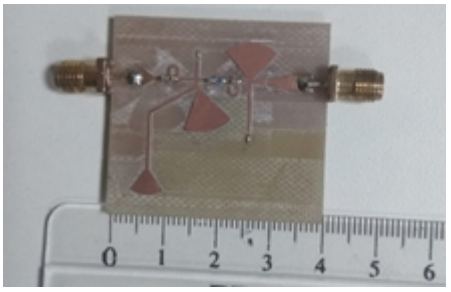

Figure 5.4: Implemented microstrip DB filter.

The performance of the implemented filter is measured by using Rohde&Schwarz ZVB14 network analyzer.

Comparison of TPG and return loss responses of the lumped model, distributed model and implemented filter are given in Figure (5.5) and Figure (5.6) respectively.

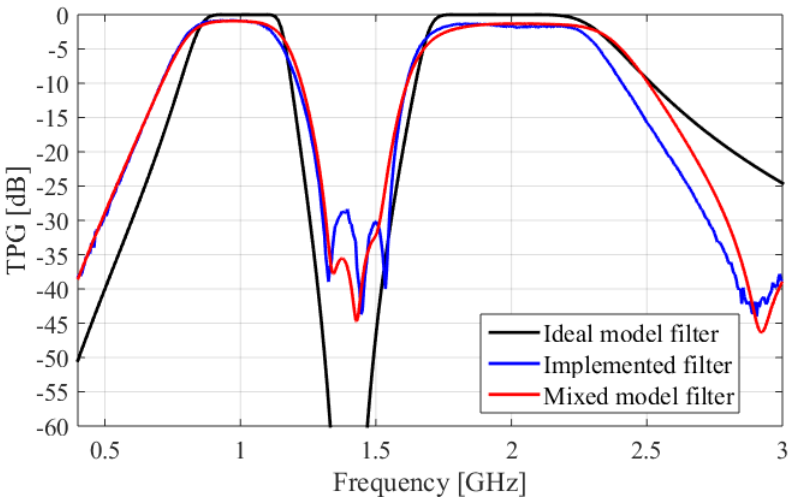

Figure 5.5: TPG response of the dual band filter.

As seen in the figures, performances of the designed and the realized filters are consistent with each other.

In this application, a DB filter design and implementation is presented. Real frequency design approach is incorporated with DB filter design problem using the generated DB mapping function. The approach is based on the employment

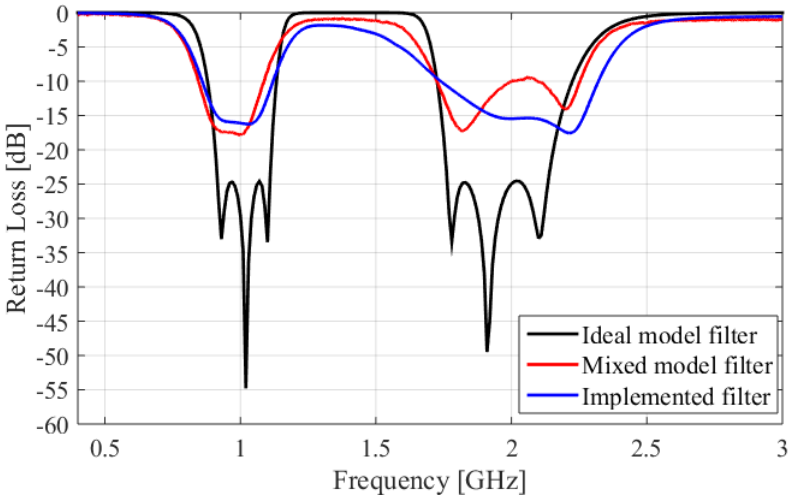

Figure 5.6: Return Loss response of the dual band filter.

of the proposed frequency mapping technique in Chapter 3. The prototype LP network is designed with parametric representation of back-end impedance function as mentioned in Section 3.4.1.2. This give us more freedom of determination of filter complexity and band characteristic. The impedance of the prototype LP filter is optimized in RFT routine under the DB mapping function. The optimized LP prototype is used to achieve DB filter by applying using dual band reactance mapping presented in Section 3.5. The DB filter design is devoted for GSM900 and GSM1800/UMTS bands. The band characteristic is chosen to cover these two bands. Hence DB mapping function is constructed under this definition. Implementation of designed filter is made with microstrip elements. Lumped model of designed filter is transformed in distributed domain. Measurement results are presented. There is a good match between simulation and the measurement results.

The presented results show that the dual band filter design can be succeeded by employing the proposed mapping functions and Real Frequency Technique. The shift between the response of the ideal dual band filter and the implemented filter is due to conversion approximations from lumped to distributed elements, dielectric losses, assembly imperfections and measurement inaccuracy.

To compare the results obtained from the implemented filter with the several different studies, the following table is given.

Reference	**Topology**	**Number of resonator**	**Pass band RL[dB]**	**Pass band IL[dB]**
[77]	Cavity	12	-20	<1
This study	Lumped	8	-15	<1.5
[73]	Stripline	8	-15	5<
[72]	Microstrip	8	-20	3<

Table 5.1: Comparison of the dual band filter with other studies.

As it can be seen form the table, the proposed approach provide lumped realizations. Therefore the size of the circuit board is much less than other implementations. The complexity and the performance of the filter is in a comparable range.

5.2 Dual Band Stop Filter Design and Implementation

A Dual Band Stop (DBS) frequency transformation is proposed in Appendix A. The presented mapping function is employed for a dual band stop filter application [104].

The aim of the design is suppressing the GSM900 and GSM1800/UMTS bands. Therefore, the first notch band is between 0.7GHz-1.1GHz and the second notch band is between 1.655GHz-2.6GHz. The DBS mapping function is derived by using (A.3) as;

$$\Omega(w) = \frac{1}{0.7432\left(\frac{w^2-1.82}{w}\right) - \frac{1}{1.277\left(\frac{w^2-1.82}{w}\right)}} \tag{5.4}$$

The generated mapping function is applied on a third degree LP Chebyshev filter prototype network given in Figure (5.7).

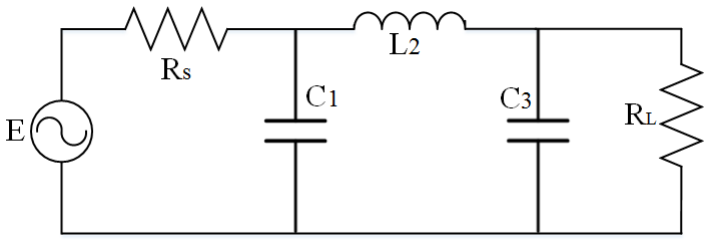

Figure 5.7: The LP prototype network (Rs = 50Ω, C1 = C3 = 2.71066pF, L2 = 8.7787nH, RL = 50Ω).

The next step of the design is applying the mapping function in (5.4) to transform the each reactive elements of the LP prototype network to their corresponding resonator equivalencies.

The explicit resonator blocks of DBS mapped inductor and capacitor are already given in Appendix A. Thus the DBS filter network is achieved by employing these resonator blocks, as given in Figure (5.8). The TPG performance of the DBS filter is given in Figure (5.9).

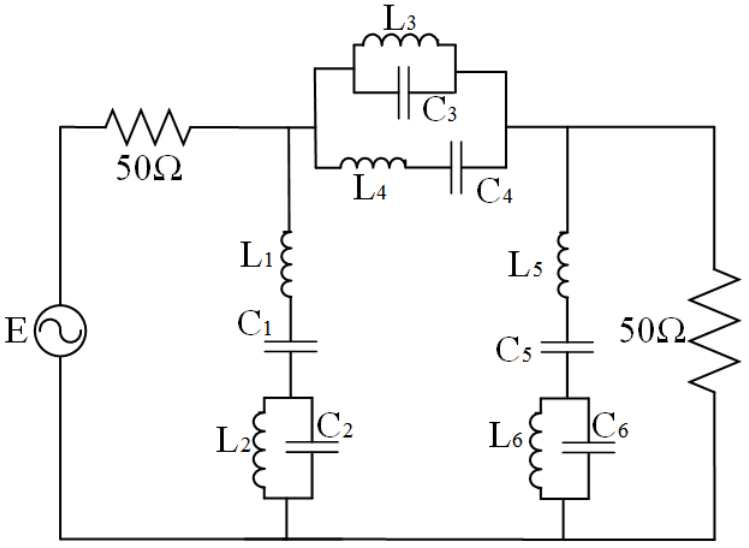

Figure 5.8: The DBS filter (L1=6.945nH, L2=4.021nH, L3=6.49nH, L4=11.21nH, L5=6.945nH, L6=4.021nH, C1=2.004pF, C2=3.46pF, C3=2.145pF, C4=1.242pF, C5=2.004pF, C6=3.46pF).

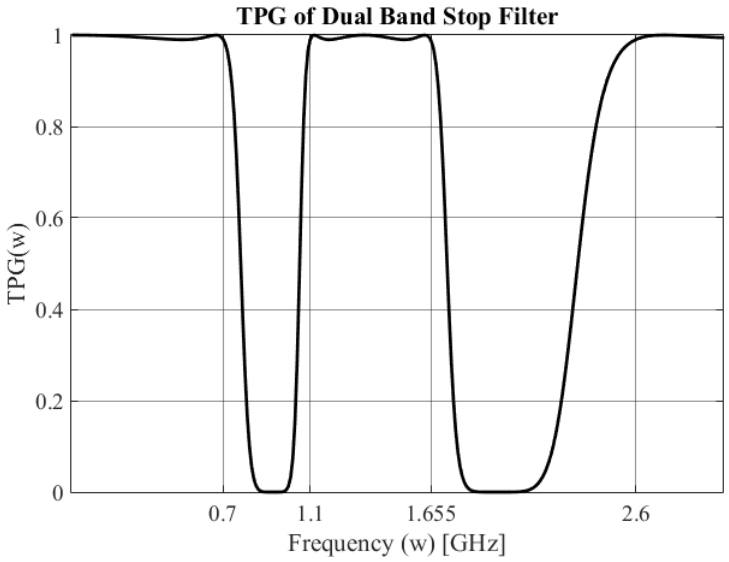

Figure 5.9: Gain performance of the designed DBS filter.

The application of the DBS filter in Figure (5.8) is performed by successive transformation of several lumped elements to their approximate microstrip correspondences [15]. Several lumped elements are provided from commercially available libraries. Therefore, the application of the DBS filter is in mixed element topology. After several fine-tuning steps of the network elements to approach the ideal response of the theoretical filter, the filter layout is obtained as given in Figure (5.10). FR4 substrate is chosen to print the filter on. The substrate dielectric permittivity is 4.6 and the thickness is 1.6mm.

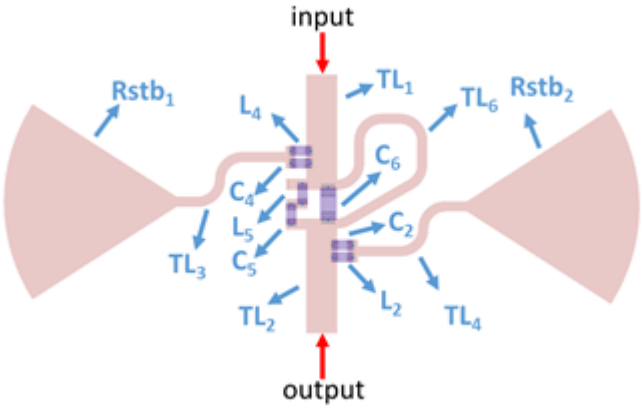

Figure 5.10: The mixed implementation layout of the DBS filter [104].

The element values used in the circuit are given on Table (5.2).

Component Name	**Values**
L2, L4	4.7nH, Johansontechnology JTI402
C2, C4	3.0pF, ATC 600L3R0
C5	1.2pF, ATC 600L1R2
L5	10nH, Johansontechnology JTI402
C6	1.6pF, ATC 600S1R6
TL1, L2	Transmission line W=1.5mm; L=5.7mm
TL3,TL4	Transmission line W=0.5mm; L=6.7mm
Rstb1, Rstb2	Radial stub, Wi=0.5mm, L=6.96mm, Angle=75 deg
TL6	Transmission line W=0.5mm; L=13.5mm
PCB	FR4, 1.6mm, ε_r=4.6, Loss tan=0.02
L2, L4	4.7nH, Johansontechnology JTI402

Table 5.2: Component values of the prototyped filter.

Manufactured mixed element prototype of the filter is given in Figure (5.11).

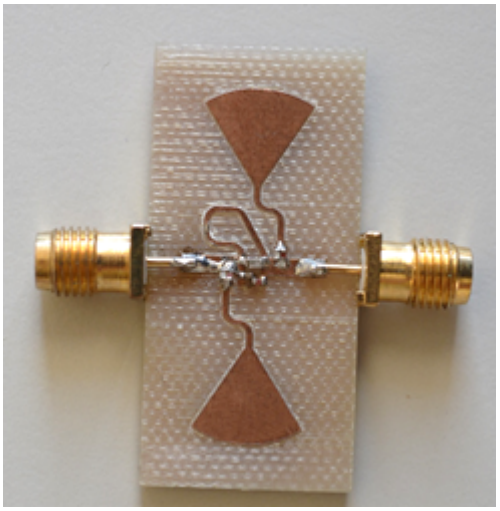

Figure 5.11: Manufactured mixed element prototype of the DBS filter.

The implemented filter is measured with Rohde&Schwarz ZVB14 network analyzer. The measured TPG and return loss responses of the implemented filter, its mixed model in Figure (5.10) and ideal filter in Figure (5.8) are given in Figure (5.12) and Figure (5.13) respectively.

The performances of the ideal filter, its mixed model and implemented filter are consistent with each-other. The difference between ideal and mixed model is due

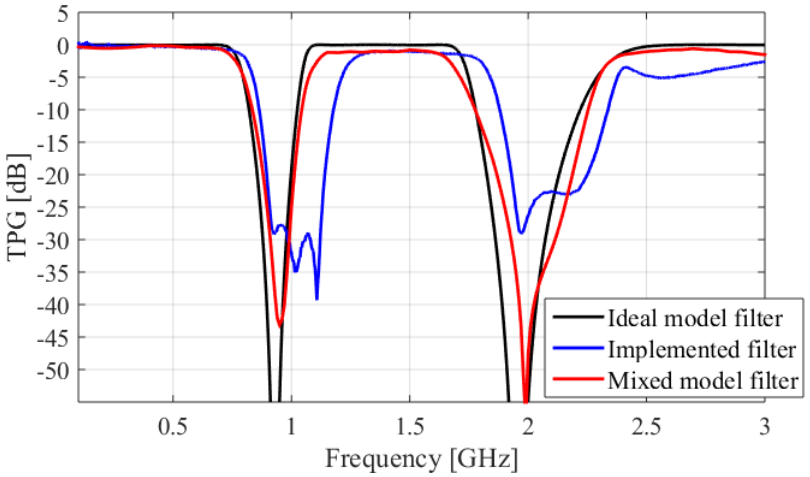

Figure 5.12: TPG responses results of the ideal lumped element filter, its mixed element model and the manufactured prototype of the DBS filter.

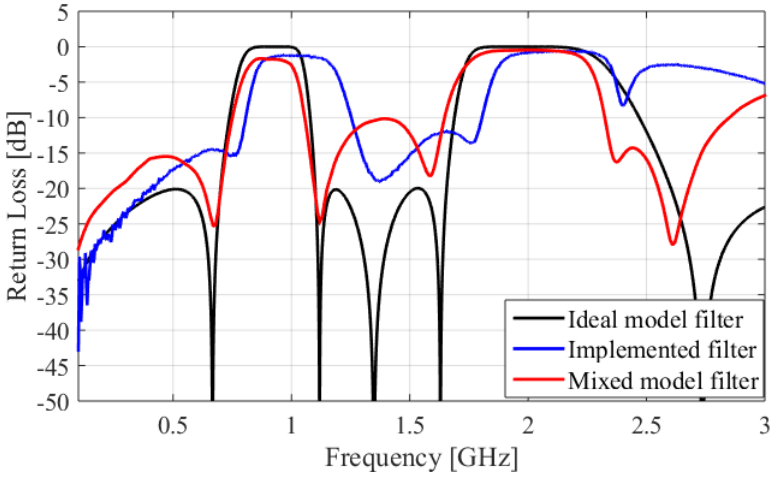

Figure 5.13: Return loss responses results of the ideal lumped element filter, its mixed element model and the manufactured prototype of the DBS filter.

to approximations when performing conversions of the ideal lumped elements to their microstrip correspondences. In addition, the lumped elements in mixed model are determined as most compatible, commercially available counterparts. This also contributes the difference between the performances of ideal and mixed models. The shift between the mixed model and the implemented filter is caused by the component tolerances, measurement inaccuracies, also assembly imperfections.

In this implementation example, the proposed DBS mapping function in Appendix A.1 is verified. After assignment of the corner frequencies of the DBS filter, the DBS mapping function is determined by using the formula given in Appendix A.1. The DBS mapping function is applied on an 3rd degree equiripple Chebyshev filter. The elements of the LP prototype filter is transformed to their DBS correspondences resonator blocks which are already provided in Appendix A.1. The lumped model of the DBS filter is achieved by replacing the elements of the LP prototype with the explicit resonator blocks counterparts. The element values are also calculated by using the given formulations in Appendix A.1. The implementation of filter is performed by using the its compatible possible mixed model. The filter is printed on FR4 substrate and measurement results are provided.

The following table is given to compare the results obtained from this implementation with the several other studies.

Reference	**Topology**	**Number of resonator**	**Pass band RL[dB]**	**Pass band IL[dB]**
[105]	Cavity	4	<-20	<1
This study	Lumped	6	<-20	<5
[106]	Microstrip	4	<-20	<2
[107]	Cavity	8	<-20	<2

Table 5.3: Comparison of the dual band stop filter with other studies.

This table suggests that, the performance of the filter is acceptable. The insertion loss performance of the implemented filter above 2.4GHz is high due to dielectric losses since the circuit is printed on FR4 substrate.

5.3 Triple Band Filter Design and Implementation

A triple band filter design is performed in this section. The proposed procedure in Section 3.3 is employed. Due to independency constraint on the number of arbitrary selectable corner frequencies, only four corner frequencies are allowed to be chosen arbitrarily. These normalized corner frequencies are assigned as; $w_1 = 0.45$, $w_2 = 0.75$, $w_3 = 0.99$, $w_6 = 2.7$ the left corners are calculated by using

(3.12) and found as; $w_4 = 1.2273$, $w_5 = 1.62$. The unknown a_N parameters of the mapping function are achieved by solving the any three set of those six equation as below;

$$\Omega_{03}(w) = \left(\frac{w^2 - w_{03}^2}{w}\right), \quad w_{03} = \sqrt{w_1 w_6} \; = 1.1023$$
$$|\Omega_3(w)| = \left| a_1\Omega_{03}(w) - \frac{1}{a_2\Omega_{03}(w) - \frac{1}{a_3\Omega_{03}(w)}} \right|_{w=\{w_1,w_2,w_3,w_4,w_5,w_6\}} = 1 \tag{5.5}$$

The unknown parameters are calculated as; $a_1 = 0.6183$, $a_2 = 1.2043$, $a_3 = 2.8913$. Therfore the triple band mapping function is constructed as;

$$\Omega_3(w) = 0.6183\Omega_{03}(w) - \frac{1}{1.2043\Omega_{03}(w) - \frac{1}{2.8913\Omega_{03}(w)}} \tag{5.6}$$

The next step of the design is choosing an low pass prototype network. Here a 3rd degree LP Chebyshev prototype filter is taken as given in Figure (5.14).

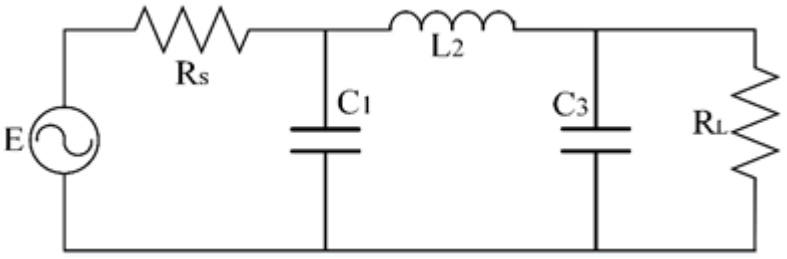

Figure 5.14: 3rd degree equal ripple Chebyshev LP prototype network (Rs=50Ω, C1=15.98pF, L2=29.58nH, C3=15.98pF, RL=50Ω).

Since the triple band mapping function and the LP prototype network are determined, the next step of the design is, applying the mapping function in (5.6) to each reactive component of the LP prototype network.on the each reactive component of the LP prototype network and performing required element mappings. The explicit triple band mapping of reactances are already given in Section 3.5. Thus the triple band filter is synthesized by replacing the reactive components of

the LP prototype network with their corresponding resonator blocks. The finalized lumped model of the triple band band filter is given in Figure (5.15). The TPG characteristic of the filter is presented in Figure (5.16).

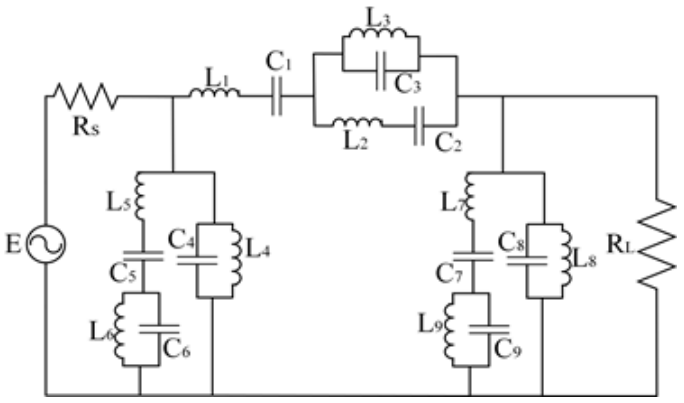

Figure 5.15: Transformed triple band filter network (L1=5.5nH, L2=25.674nH, L3=6.07nH, L4=7.024nH, L5=6.36nH, L6=1.5nH, L7=6.36nH, L8 = 7.024nH, L9 = 1.5nH, C1 = 3.8pF, C2 = 0.812pF, C3 = 3.44pF, C4 = 2.97pF, C5=3.28pF, C6=13.96pF, C7=3.28pF, C8=2.97pF, C9=13.96pF, RL=Rs=50Ω).

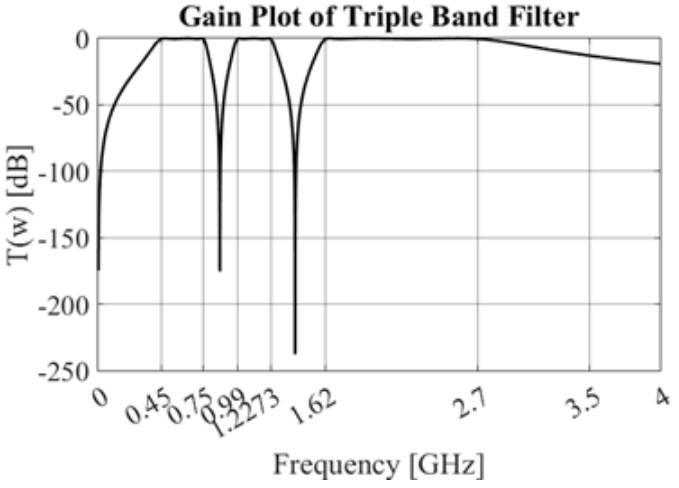

Figure 5.16: Gain response of the triple band filter.

The realizable model of the triple band filter is generated by performing EM simulation in ADS design environment. First the soldering pads and traces are drawn for assembling the lumped components. This structure inevitable brings extra parasitic capacitances and inductances. This causes degeneration on the performance of the filter. Therefore, to approach the response of the filter to

its ideal model, a certain fine tuning and acquisition is performed. The lumped components are chosen best possible commercially available counterparts. The C5 and C7 capacitances are replaced with distributed correspondings. Eventually, all circuit components are re-optimized for final production. The layout of the triple band filter is given in Figure (5.17). The component values and physical information of the distributed elements are given in Table (5.4).

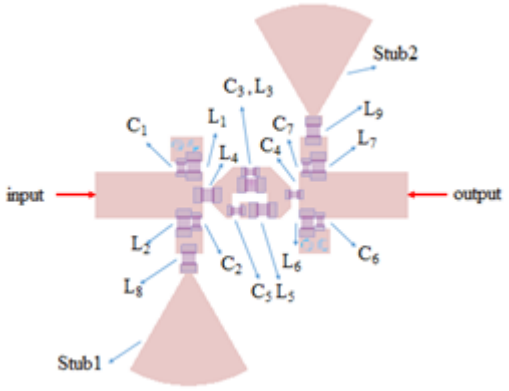

Figure 5.17: Layout of the implemented triple band filter.

Component Name	**Values**
C1, C6	0.6pF
L1, L6 ,L8, L9	10nH
C2, C7	5.6pF
L2, L7	3.9nH
Stub1, Stub2	L=7mm, Ang=60 Deg, Wi=0.5
C3	3.0pF
L3	5.1nH
C4	3.6pF
L4	3.3nH
C5	0.8pF
L5	23nH
PCB	FR4, 1.6mm, ε_r=4.8

Table 5.4: Element values of the manifactured triple band filter.

The lumped capacitors are provided from Murata brand 402 case GJM15 series and the lumped are provided from Coilcraft brand 603 case 06CS series. The images of the manufactured triple band filter and the measurement set-up are given in Figure (5.18)a and Figure (5.18)b respectively.

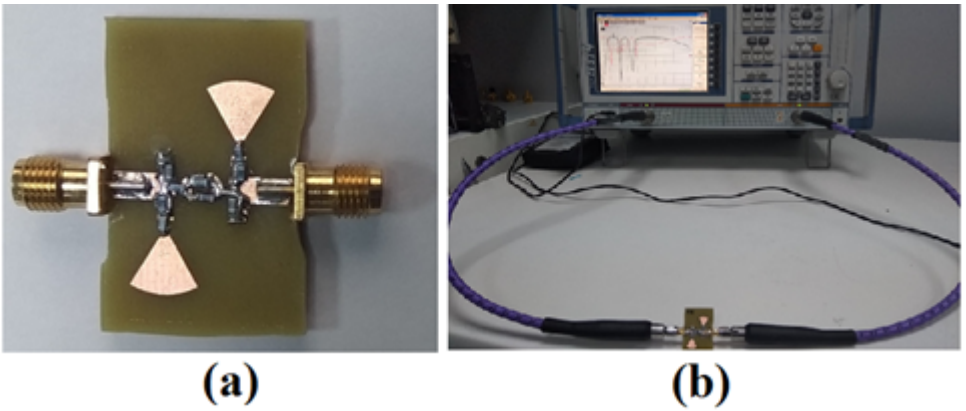

Figure 5.18: (a) Prototyped filter; (b) Measurement setup.

The manufactured filter is measured with by using Rohde&Schwarz ZVB14 network analyzer. The TPG and return loss responses of the measured filter and its ideal model filter are given in Figure (5.19) and Figure (5.20) respectively.

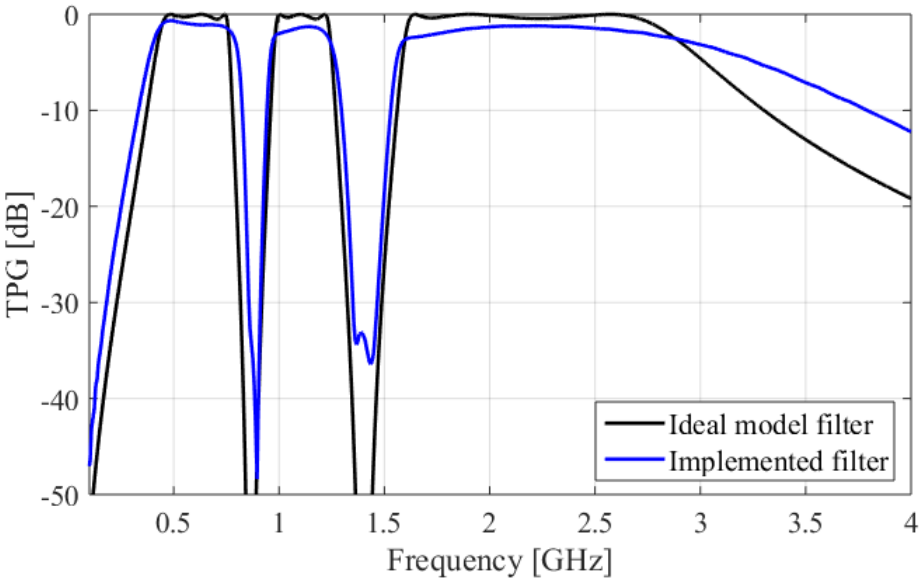

Figure 5.19: TPG response of the triple band filter.

The measured performance of the triple band filter is consistent with the performance of the its ideal lumped model. The shifts are due to approximations when converting lumped component to their distributed equivalencies, the tolerances

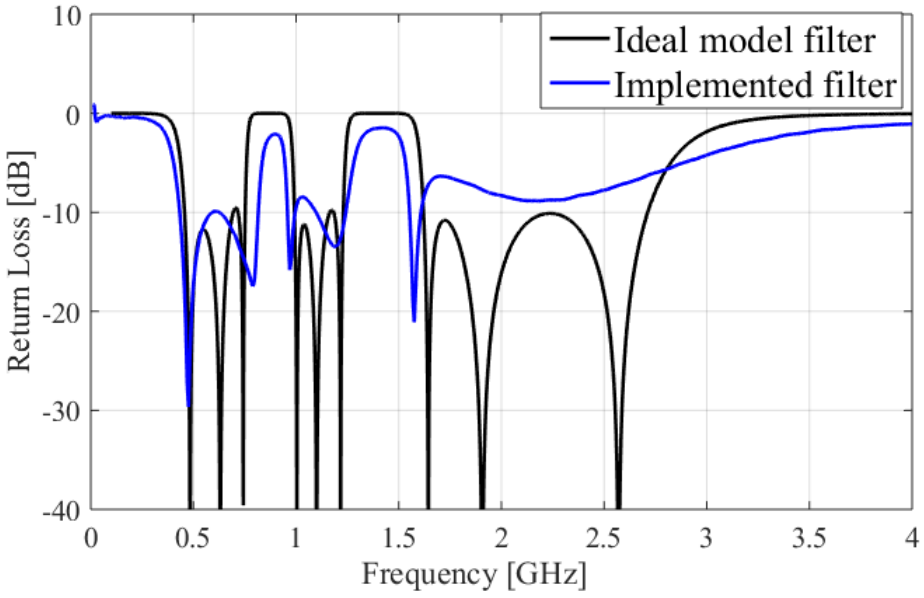

Figure 5.20: Return loss response of the triple band filter.

of lumped components, dielectric losses at high frequencies and measurement inaccuracies.

In this application, a triple band filter design and implementation is elaborated with using the proposed mapping function in Chapter 2. A 3rd degree Chebyshev LP prototype network is used to obtain triple band filter via the application of the constructed triple band mapping function on the elements of the LP filter. The explicit network topologies under the application of triple mapping function on ideal inductor and capacitor are taken from the obtained results in Section 3.3. After the determination of the triple band mapping function in accordance with the demanded band specification, the final triple band network is provided by incorporation of the triple band transformed resonator sections. The element values of the resonators are determined via given equations in Section 3.5. The implementation of the designed triple filter is obtained with mixed elements. Two lumped elements of designed ideal triple band filter are transformed into distributed equivalencies and several lumped elements are approximated to the

best possible commercially available values. The measurement results are presented. The performance characteristics of the designed ideal lumped filter and its manufactured prototype are consistent with each other.

Chapter 6

Conclusions

This thesis is arranged on the design of multiband concurrent lossless two-ports for impedance matching applications. The design technique employs only passive components due to concern on concurrent operations. The semi-analytical matching network design techniques which are called real frequency techniques are used for multiband matching problems. These techniques are efficient tools for the design of broadband matching applications. To implement RFT approaches for the design of multiband matching problem, new techniques are required to investigate. In this thesis, it is aimed to develop and formulate the design problem of multiband matching, based on semi-analytical techniques.

In Chapter 1, major multiband design approaches are summarized. Real frequency techniques of network theoretical foundations are discussed in Chapter 2.

In Chapter 3, a generalized multiband mapping function is introduced. The development steps and engagement of multiband mapping function with RFT algorithm are discussed for the design of multiband filter and matching networks. It has been shown that any arbitrary number of matching pass bands can be created by involving the proposed technique in multiband network design. In this discussion, a special emphasis is laid on the prototype network generation. Here, a parametric approach for bandpass prototype network generation is presented. Several multiband filter and matching network design examples are presented

to validate the proposed mapping functions and their performance for practical applications. As an extension of the proposed mapping technique, a dual band stop mapping function is also proposed.

The second part of the study deals with the synthesis based design of multiband ladders. In Chapter 4, the deriving point impedance and FTZs based characterization of the network function of multiband structure is discussed. The synthesis of Brune function (positive real function) is through FTZs extractions and associated negative values are impressed. The known parametric characterization of multiband network and associated synthesis routines are elaborated. A special emphasis is given to the removal of unrealizable elements of Brune sections, through appropriate network transformations or ad-hoc techniques. Examples are presented to display the application of the proposed approaches. A triple band matching example is elaborated with Norton transformations.

In Chapter 5, the application of the developed approaches to several filter design problems are given. In this context a dual band pass, dual band stop and triple band filter design, implementation and measurement works are presented.

Through the investigation and discussion of this study, we proposed transformation based and synthesis based RFT design approaches for multiband filter and matching network designs. The result of the algorithms are tested by implementations and simulations.

Even though successful results have been achieved, still further effort must be given to the improvements and developments of practical transformer-free multiband ladder networks. In the multiband frequency transformation approach, it is obvious that, the degree of complexity of the multiband network is increased by the number of assigned pass bands. Therefore, the realization with lumped resonators seems impractical for complex multiband designs. This issue can be elaborated by incorporation of different synthesis routines such as coupled cavity resonators, coupled distributed topologies etc.

On the other hand, in the synthesis based approach, although replacement techniques provide feasible and practical multiband designs, the development of constraints on Brune function and practical topologies are required for better the control of multiband characteristic of practical structures. As a future work to improve the design with practical realizations forms, the analytical functional constraints such as those of T. Fujisawa can be incorporated to practical designs.

Appendix A

Analysis of DBS Transformation

A.1 Dual Band Stop Frequency Transformation

The dual band stop frequency transformation is obtained by transforming a normalized LP prototype gain transfer characteristic in Ω domain to a band stop gain characteristic in w' domain by performing the low pass to band stop transformation given in (A.1).

$$\Omega(w') = \frac{B_1(w')}{(w')^2 - (w')_{01}^2}, \quad (w')_{01} = \sqrt{(w')_H (w')_L}, \quad B_1 = (w')_H - (w')_L \tag{A.1}$$

Then the dual band stop (DBS) gain characteristic in w domain is achieved by applying a low pass to band pass transformation on the previously generated band stop gain characteristic as illustrated in Figure (A.1)

By normalizing the band stop response in w' domain by setting $w'_H = 1$, the dual band stop transformation is as given in (A.2).

$$\begin{aligned} &\Omega'(w) = \frac{(w')}{1} = \frac{w^2 - w_0^2}{B_1 w}, \quad B_T = w_4 - w_1, \\ &w_0 = \sqrt{w_1 w_4}, \quad B_P = w_3 - w_2 \end{aligned} \tag{A.2}$$

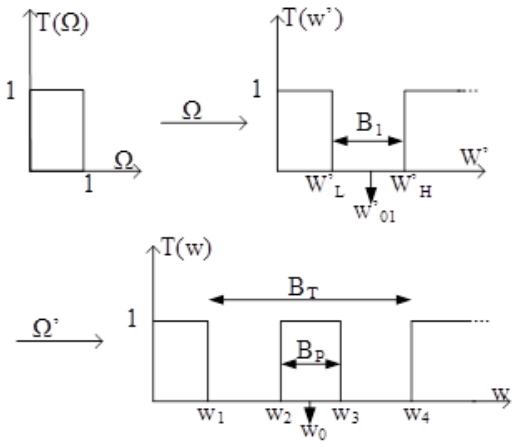

Figure A.1: The DBS transformation scheme [104].

These two sequential transformation process can be performed only one-step, which allows a direct transformation from low pass to dual band stop characteristic as given;

$$\Omega(w) = \frac{1}{\dfrac{1}{B_T - B_P}\left(\dfrac{w^2 - w_0^2}{w}\right) - \dfrac{1}{\dfrac{B_T - B_P}{B_T B_P}\left(\dfrac{w^2 - w_0^2}{w}\right)}} \tag{A.3}$$

The final form of DBS transformation $\Omega(w)$ provides a direct frequency mapping from low pass to dual band stop gain characteristic. The frequency mapping diagram of the DBS transformation is illustrated as given in Figure (A.2).

The $\{B_P, B_T, w_0\}$ parameters characterize the nonlinear mapping diagram. These parameters are also related with the corner frequencies of the DBS response as given in (A.2). The center frequencies of each notch band are expressed with the w_{z1}, w_{z2} parameters as illustrated in the DBS mapping diagram. The following relation must be satisfied between corner frequencies;

$$w_0 = \sqrt{w_1 w_4} = \sqrt{w_2 w_3}; \qquad w_1 < w_2 < w_3 < w_4 \tag{A.4}$$

This relation inherently determines the number of arbitrary selectable corner

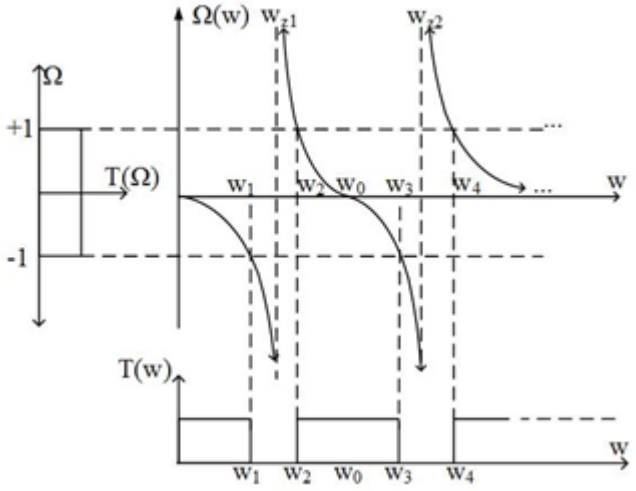

Figure A.2: The DBS mapping diagram [104].

frequencies. Under this relation only three corner frequencies are independent. The remaining corner frequency must be calculated by using the expression in (A.4).

Consider the normalized independent corner frequencies are chosen as $w_1 = 1$, $w_2 = 1.5$, $w_3 = 2$ the remaining corner is calculated by using (A.4) and it is found as; $w_4 = 3$. The parameters to define mapping function is calculated as; $B_T = 2$, $B_P = 0.5$ and $w_0 = 1.732$. Then the DBS mapping function is generated by using the relation (A.3) as;

$$\Omega(w) = \frac{1}{0.667\left(\frac{w^2-3}{w}\right) - \frac{1}{1.5\left(\frac{w^2-3}{w}\right)}} \tag{A.5}$$

This mapping function is applied on a 9th degree LP Chebyshev transfer function and the resulted DBS TPG response is achieved as given in Figure (A.3).

The lumped synthesis of a DBS filter is provided by successive application of the DBS mapping function on the each reactive components of the LP prototype network. The reactance functions of the DBS transformed inductor and inductor

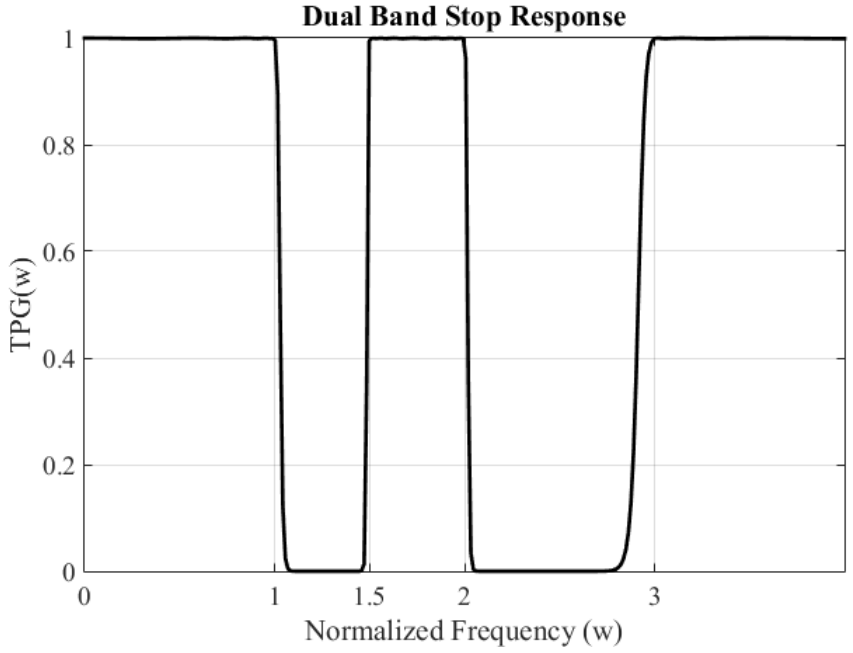

Figure A.3: DBS response generated with DBS mapping function.

are derived as;

$$Z_L = j\Omega(w)L = \frac{jL}{\frac{1}{B_T - B_P}\left(\frac{w^2 - w_0^2}{w}\right) - \frac{1}{\frac{B_T - B_P}{B_T B_P}\left(\frac{w^2 - w_0^2}{w}\right)}}$$

$$= \frac{1}{jwC_1 + \frac{1}{jwL_1} - \frac{1}{jwL_2 + \frac{1}{jwC_2}}} \tag{A.6}$$

$L_1 = {}^{L}\!/_{a_1 w_0^2}\,; C_1 = {}^{a_1}\!/_{L}\,; L_2 = a_2 L; C_2 = {}^{1}\!/_{L a_2 w_0^2}\,.$

$$a_1 = \frac{1}{B_T - B_P}; \qquad a_2 = \frac{B_T - B_P}{B_T B_P}$$

$$Y_C = j\Omega(w)C = \frac{jC}{\frac{1}{B_T - B_P}\left(\frac{w^2 - w_0^2}{w}\right) - \frac{1}{\frac{B_T - B_P}{B_T B_P}\left(\frac{w^2 - w_0^2}{w}\right)}}$$

$$= \frac{1}{jwL_1 + \frac{1}{jwC_1} - \frac{1}{jwC_2 + \frac{1}{jwL_2}}} \tag{A.7}$$

$$C_1 = {}^{C}\!/_{a_1 w_0^2}\ ; L_1 = {}^{a_1}\!/_{C}\ ; C_2 = a_2 C; L_2 = {}^{1}\!/_{C a_2 w_0^2}$$

Above DBS transformed impedance of inductor and admittance of capacitance is synthesized by employing one-port synthesis theorem [91] as given in Figure (A.4).

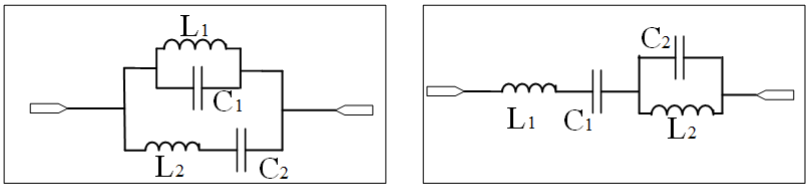

Figure A.4: (a) DBS transformed inductor (b) DBS transformed capacitor.

Therefore, by using the described procedure, any DBS filter can be analytically generated and synthesized by lumped resonators provided in Figure (A.4)

References

[1] I. I. Immoreev and P. D. V. Fedotov, "Ultra wideband radar systems: advantages and disadvantages," in *2002 IEEE Conference on Ultra Wideband Systems and Technologies (IEEE Cat. No. 02EX580)*. IEEE, 2002, pp. 201–205.

[2] J.-J. Deslise, "What is the difference between broadband and narrowband rf communications?" *Microwaves RF*, Nov 2014.

[3] R. M. Foster, "A reactance theorem," *Bell System technical journal*, vol. 3, no. 2, pp. 259–267, 1924.

[4] H. W. Bode, *Network analysis and feedback amplifier design*. D. Van Nostrand Company, 1945.

[5] R. M. Fano, "Theoretical limitations on the broadband matching of arbitrary impedances," *Journal of the Franklin Institute*, vol. 249, no. 1, pp. 57–83, 1950.

[6] D. Youla, "A new theory of broad-band matching," *IEEE Transactions on Circuit Theory*, vol. 11, no. 1, pp. 30–50, 1964.

[7] H. J. Carlin, *Wideband Circuit Design*. New York: CRC Press,, 1998.

[8] B. S. Yarman, *Design of ultra wideband power transfer networks*. Wiley, 2010.

[9] A. Aksen, "Design of lossless two-ports with mixed, lumped and distributed elements for broadband matching," Ph.D. dissertation, Lehrstuhl Für Nachrichtentechnik, Ruhr Universitaet, 1994.

[10] H. Dedieu, C. Dehollain, J. Neirynck, and G. Rhodes, "A new method for solving broadband matching problems," *IEEE Transactions on Circuits and Systems I: Fundamental Theory and Applications*, vol. 41, no. 9, pp. 561–571, 1994.

[11] T. R. Cuthbert, "A real frequency technique optimizing broadband equalizer elements," in *2000 IEEE International Symposium on Circuits and Systems. Emerging Technologies for the 21st Century. Proceedings (IEEE Cat No. 00CH36353)*, vol. 5. IEEE, 2000, pp. 401–404.

[12] H. Carlin, "A new approach to gain-bandwidth problems," *IEEE Transactions on Circuits and Systems*, vol. 24, no. 4, pp. 170–175, 1977.

[13] S. Best, "The foster reactance theorem and quality factor for antennas," *IEEE Antennas and Wireless Propagation Letters*, vol. 3, no. 1, pp. 306–309, 2004.

[14] I. Bahl, *Lumped elements for RF and microwave circuits*. Artech House, 2003.

[15] R. W. Rhea, *HF filter design and computer simulation*. McGraw-Hill, 1995.

[16] N. Dye and H. Granberg, *Radio frequency transistors: principles and practical applications*. Newnes, 2001.

[17] A. Aksen and B. S. Yarman, "A semi-analytical procedure to describe lossless two-ports with mixed lumped and distributed elements," in *Proceedings of IEEE International Symposium on Circuits and Systems-ISCAS'94*, vol. 5. IEEE, 1994, pp. 205–208.

[18] A. Sertbas, A. Aksen, and B. S. Yarman, "Construction of some classes of two-variable lossless ladder networks with simple lumped elements and uniform transmission lines," in *IEEE. APCCAS 1998. 1998 IEEE Asia-Pacific Conference on Circuits and Systems. Microelectronics and Integrating Systems. Proceedings (Cat. No. 98EX242)*. IEEE, 1998, pp. 295–298.

[19] C.-B. Vesna, *Advances in multi-band microstrip filters.* Cambridge Univ. Press, 2015.

[20] S.-F. Chang, W.-L. Chen, H.-C. Chen, S.-F. Tang, and A. Chen, "Concurrent triple-band gain amplifier for multi-standard coexist communications," *US Patent US7193477B2*, Dec 2006.

[21] Y. Li, T. Cantin, B. Derat, D. Pasquet, and J.-C. Bolomey, "Application of resonant matching circuits for simultaneously enhancing the bandwidths of multi-band mobile phones," in *2007 International workshop on Antenna Technology: Small and Smart Antennas Metamaterials and Applications.* IEEE, 2007, pp. 479–482.

[22] H. Hashemi and A. Hajimiri, "Concurrent multiband low-noise amplifiers-theory, design, and applications," *IEEE Transactions on Microwave Theory and Techniques*, vol. 50, no. 1, pp. 288–301, 2002.

[23] N. Nallam and S. Chatterjee, "Design of concurrent multi-band matching networks," in *2011 IEEE International Symposium of Circuits and Systems (ISCAS).* IEEE, 2011, pp. 201–204.

[24] J.-S. Lee, H. Rhyu, and B. Lee, "Design concept of multi-band antenna with resonant circuit on pcb," *Electronics Letters*, vol. 43, no. 6, pp. 5–6, 2007.

[25] W. E. Neo, Y. Lin, X.-D. Liu, L. C. De Vreede, L. E. Larson, M. Spirito, M. J. Pelk, K. Buisman, A. Akhnoukh, A. De Graauw *et al.*, "Adaptive multi-band multi-mode power amplifier using integrated varactor-based tunable matching networks," *IEEE Journal of Solid-State Circuits*, vol. 41, no. 9, pp. 2166–2176, 2006.

[26] C.-S. Lee and C.-L. Yang, "Matching network using one control element for widely tunable antennas," *Progress In Electromagnetics Research*, vol. 26, pp. 29–42, 2012.

[27] X. Yu and N. M. Neihart, "A 2–11 ghz reconfigurable multi-mode lna in 0.13 μm cmos," in *2012 IEEE Radio Frequency Integrated Circuits Symposium*. IEEE, 2012, pp. 475–478.

[28] C. Zhang and A. E. Fathy, "A novel reconfigurable power amplifier structure for multi-band and multi-mode portable wireless applications using a reconfigurable die and a switchable output matching network," in *2009 IEEE MTT-S International Microwave Symposium Digest*. IEEE, 2009, pp. 913–916.

[29] M. Kaynak, I. Tekin, and Y. Gurbuz, "A matching circuit tuned, multi-band (wlan and wimax), class—a power amplifier using 0.25 μm-sige hbt technology," in *2008 Ph. D. Research in Microelectronics and Electronics*. IEEE, 2008, pp. 169–172.

[30] R. Malmqvist, C. Samuelsson, P. Rantakari, T. Vähä-Heikkilä, D. Smith, J. Varis, and R. Baggen, "Rf mems and mmic based reconfigurable matching networks for adaptive multi-band rf front-ends," in *2010 IEEE International Microwave Workshop Series on RF Front-ends for Software Defined and Cognitive Radio Solutions (IMWS)*. IEEE, 2010, pp. 1–4.

[31] Y. Wu, Y. Liu, S. Li, C. Yu, and X. Liu, "A generalized dual-frequency transformer for two arbitrary complex frequency-dependent impedances," *IEEE Microwave and Wireless Components Letters*, vol. 19, no. 12, pp. 792–794, 2009.

[32] R. Fagotti, A. Cidronali, and G. Manes, "Concurrent hex-band gan power amplifier for wireless communication systems," *IEEE Microwave and Wireless Components Letters*, vol. 21, no. 2, pp. 89–91, 2011.

[33] A. Fukuda, H. Okazaki, S. Narahashi, and T. Nojima, "A concurrent multi-band power amplifier with compact matching networks," in *2011 XXXth URSI General Assembly and Scientific Symposium*. IEEE, 2011, pp. 1–4.

[34] F. Chiadini, A. Scaglione, and V. Fiumara, "Design of quarter-wave multi-section multi-band devices," in *ICECom 2013*. IEEE, 2013, pp. 1–4.

[35] H. Song, J. T. Aberle, and B. Bakkaloglu, "A mixed-signal matching state search based adaptive antenna tuning ic," *IEEE microwave and wireless components letters*, vol. 20, no. 10, pp. 581–583, 2010.

[36] Z. Wang and C.-W. Park, "Novel multiband matching network using resonators for multiband power amplifier applications," *Microwave and Optical Technology Letters*, vol. 55, no. 10, pp. 2469–2475, 2013.

[37] H. Rhyu, B. Jung, F. J. Harackiewicz, and B. Lee, "Design of a multi-band internal antenna using an open stub," in *2005 Asia-Pacific Microwave Conference Proceedings*, vol. 4. IEEE, 2005, pp. 4–pp.

[38] P. Sarkar, R. Ghatak, M. Pal, and D. Poddar, "Compact uwb bandpass filter with dual notch bands using open circuited stubs," *IEEE microwave and wireless components letters*, vol. 22, no. 9, pp. 453–455, 2012.

[39] T. G. Brand, P. Meyer, and R. H. Geschke, "Designing multiband coupled-resonator filters using reactance transformations," *International Journal of RF and Microwave Computer-Aided Engineering*, vol. 25, no. 1, pp. 81–92, Jan 2015.

[40] O. Brune, "Synthesis of a finite two-terminal network whose driving-point impedance is a prescribed function of frequency," *Journal of Mathematics and Physics*, vol. 10, no. 3, pp. 191–236, Aug 1931.

[41] R. Fletcher, *Practical methods of optimization*. J. Wiley, 1981.

[42] H. Dedieu, C. Dehollain, J. Neirynck, and G. Rhodes, "A new method for solving broadband matching problems," *IEEE Transactions on Circuits and Systems I: Fundamental Theory and Applications*, vol. 41, no. 9, pp. 561–571, 1994.

[43] Y. B. Sıddık, "Broadband matching a complex generator to a complex load," Ph.D. dissertation, 1982.

[44] H. Carlin and P. Amstutz, "On optimum broad-band matching," *IEEE Transactions on Circuits and Systems*, vol. 28, no. 5, pp. 401–405, 1981.

[45] B. Yarman and A. Fettweis, "Computer-aided double matching via parametric representation of brune functions," *IEEE Transactions on Circuits and Systems*, vol. 37, no. 2, pp. 212–222, 1990.

[46] B. Yarman and H. Carlin, "A simplified "real frequency" technique applied to broad-band multistage microwave amplifiers," *IEEE Transactions on Microwave Theory and Techniques*, vol. 30, no. 12, pp. 2216–2222, 1982.

[47] B. Yarman, "Modern approaches to broadband matching problems," *IEE Proceedings H Microwaves, Antennas and Propagation*, vol. 132, no. 2, pp. 87–92, 1985.

[48] A. Aksen and B. S. Yarman, "A semi-analytical procedure to describe lossless two-ports with mixed lumped and distributed elements," in *Proceedings of IEEE International Symposium on Circuits and Systems-ISCAS'94*, vol. 5. IEEE, 1994, pp. 205–208.

[49] C. Beccari, "Broadband matching using the real frequency technique," *IEEE Trans. CAS*, vol. 37, pp. 212–222, 1984.

[50] P. Jarry and A. Perennec, "Optimization of gain and vswr in multistage microwave amplifier using real frequency method," in *European Conference on Circuit Theory and Design*, vol. 23, 1987, pp. 203–208.

[51] A. Kilinç, H. Pinarbas, M. Sengul, and B. S. Yarman, "A broadband microwave amplifier design by means of immittance based data modelling tool," in *IEEE AFRICON. 6th Africon Conference in Africa,*, vol. 2. IEEE, 2002, pp. 535–540.

[52] B. S. Yarman, *Design of ultra wideband antenna matching networks: via simplified real frequency technique.* Springer, 2008.

[53] H. Carlin and J. Komiak, "A new method of broad-band equalization applied to microwave amplifiers," *IEEE Transactions on Microwave Theory and Techniques*, vol. 27, no. 2, pp. 93–99, 1979.

[54] B. Yarman, "Real frequency broadband matching using linear programming," *RCA Review*, vol. 43, pp. 626–654, Dec 1982.

[55] H. Carlin and B. Yarman, "The double matching problem: Analytic and real frequency solutions," *IEEE Transactions on Circuits and Systems*, vol. 30, no. 1, pp. 15–28, 1983.

[56] H. Carlin and P. Civalleri, "On flat gain with frequency- dependent terminations," *IEEE Transactions on Circuits and Systems*, vol. 32, no. 8, pp. 827–839, Aug 1985.

[57] A. Fettweis, "Parametric representation of brune functions," *International Journal of Circuit Theory and Applications*, vol. 7, no. 1, pp. 113–119, 1979.

[58] J. Pandel and A. Fettweis, "Broadband matching using parametric representations," in *IEEE International Symposium on Circuits and Systems*, vol. 36, 1985, pp. 143–149.

[59] J. PANDEL and A. Fettweis, "Numerical solution to brodband matching based on parameteric representations," *AEU. Archiv für Elektronik und Übertragungstechnik*, vol. 41, no. 1, pp. 202–209, 1987.

[60] A. Aksen, H. Pinarbasi, and B. S. Yarman, "A parametric approach to construct two-variable positive real impedance functions for the real frequency design of mixed lumped-distributed matching networks," in *2004 IEEE MTT-S International Microwave Symposium Digest (IEEE Cat. No. 04CH37535)*, vol. 3. IEEE, 2004, pp. 1851–1854.

[61] A. Aksen, E. G. Çimen, and B. S. Binboğa Yarman, "A numerical real frequency broadband matching technique based on parametric representation of scattering parameters," in *IEEE APCCAS98, Asia Pacific Conference on Circuits and Systems*. IEEE, 1998, pp. 351–354.

[62] B. S. Yarman and A. Aksen, "An integrated design tool to construct lossless matching networks with mixed lumped and distributed elements," *IEEE Transactions on Circuits and Systems I: Fundamental Theory and Applications*, vol. 39, no. 9, pp. 713–723, 1992.

[63] B. Yarman, "A simplified real frequency technique for broadband matching complex generator to complex loads," *RCA Review*, vol. 43, pp. 529–541, Sep 1982.

[64] Y. B. Siddik and N. RETDIAN, "Design of broadband matching networks," *ECT*, vol. 2007, no. 1, pp. 35–40, 2007.

[65] B. Yarman and A. Aksen, "Computer aided darlington synthesis of an all purpose immittance function," *IU-JEEE*, vol. 16, no. 1, pp. 2027–2037, 2016.

[66] J. A. G. Malherbe and A. Swiatko, "Modified chebyshev bandstop filter with transmission zeros at real frequencies," *Microwave and Optical Technology Letters*, vol. 53, no. 1, pp. 177–180, Jan 2011.

[67] H. Fujimoto, K. Murakami, and S. Kitazawa, "Equivalent circuits and transmission zeros of the coupled square-loop resonator," *IEICE Electronics Express*, vol. 4, no. 18, pp. 575–581, 2007.

[68] M.-H. Weng, S. Wu, S.-B. Jhong, Y.-C. Chang, and M.-S. Lee, "A novel compact dual-mode filter using cross-slotted patch resonator for dual-band applications," in *2007 IEEE/MTT-S International Microwave Symposium*. IEEE, 2007, pp. 921–924.

[69] X. Y. Zhang, Q. Xue, and B. J. Hu, "Planar tri-band bandpass filter with compact size," *IEEE Microwave and Wireless Components Letters*, vol. 20, no. 5, pp. 262–264, May 2010.

[70] H.-W. Wu, Y.-F. Chen, and Y.-W. Chen, "Multi-layered dual-band bandpass filter using stub-loaded stepped-impedance and uniform-impedance resonators," *IEEE Microwave and Wireless Components Letters*, vol. 22, no. 3, pp. 114–116, Mar 2012.

[71] R. J. Cameron, C. M. Kudsia, and R. R. Mansour, *Microwave filters for communication systems fundamentals, design and applications.* Wiley, 2007.

[72] A. Garcia-Lamperez and M. Salazar-Palma, "Single-band to multiband frequency transformation for multiband filters," *IEEE Transactions on Microwave Theory and Techniques*, vol. 59, no. 12, pp. 3048–3058, Dec 2011.

[73] J. Lee and K. Sarabandi, "A synthesis method for dual-passband microwave filters," *IEEE Transactions on Microwave Theory and Techniques*, vol. 55, no. 6, pp. 1163–1170, Jun 2007.

[74] S. Yıldız, A. Aksen, and S. B. Yarman, "Multiband matching network design via transformation based real frequency approach," in *2016 International Symposium on Fundamentals of Electrical Engineering (ISFEE).* IEEE, 2016, pp. 1–5.

[75] S. Yildiz, A. Aksen, and S. Yarman, "Dual band matching network design via real frequency technique by mapping from a band pass prototype," in *2016 16th Mediterranean Microwave Symposium (MMS).* IEEE, 2016, pp. 1–4.

[76] S. Yıldız, A. Aksen, B. S. Binboğa Yarman, O. Kaya, M. Koca, N. Su, S. Ulukuş, C. Yeşilyaprak, S. K. Yerli, O. Keskin *et al.*, "Srft ile frekans transformasyonunu kullanarak band geçiren filtre prototipi üzerinden

çokluband filtre tasarımı," in *International Conference on Electrical and Electronics Engineering, Bursa, Turkey*, 2016, pp. 01–03.

[77] G. Macchiarella and S. Tamiazzo, "Design techniques for dual-passband filters," *IEEE Transactions on Microwave Theory and Techniques*, vol. 53, no. 11, pp. 3265–3271, Nov 2005.

[78] S. C. Roy, "Network design for multiple frequency impedance matching by the frequency transformation technique," *IETE Journal of Research*, vol. 59, no. 6, pp. 698–703, Nov 2013.

[79] J. Lee and K. Sarabandi, "Design of triple-passband microwave filters using frequency transformations," *IEEE Transactions on Microwave Theory and Techniques*, vol. 58, no. 1, pp. 187–193, Jan 2008.

[80] S. Yildiz, A. Aksen, and B. Yarman, "Dual band filter design using real frequency technique and frequency transformation," *IU-JEEE*, vol. 17, no. 2, pp. 3343–3350, Jul 2017.

[81] A. Aksen, S. Yıldız, and S. B. Yarman, "A frequency transformation based real frequency design approach for dual-band matching," in *2017 International Symposium on Signals, Circuits and Systems (ISSCS)*. IEEE, 2017, pp. 1–4.

[82] S. Yıldız, A. Aksen, and S. B. Yarman, "Quad-band matching network design with real frequency technique employing frequency transformation," in *2017 IEEE First Ukraine Conference on Electrical and Computer Engineering (UKRCON)*. IEEE, 2017, pp. 143–147.

[83] "Symbolic math toolbox." [Online]. Available: https://www.mathworks.com/products/symbolic.html

[84] K. Su, *Analog Filters*. Springer US, 2003.

[85] K. Paramayudha, A. B. Putra, Y. Taryana, and Y. Wahyu, "Modified sierpinski patch antenna with co-planar waveguide feed for multiband wireless

applications," in *2015 IEEE International Conference on Aerospace Electronics and Remote Sensing Technology (ICARES)*. IEEE, 2015, pp. 1–6.

[86] S. Yıldız, A. Aksen, and B. S. Yarman, "Rft based multiband matching network design with foster resonance sections," in *2015 9th International Conference on Electrical and Electronics Engineering (ELECO)*. IEEE, 2015, pp. 911–915.

[87] N. Yildirim, *Filpro Manual: A textbook-like manual for the filter design software Filpro*. Middle East Technical University, 1997.

[88] J. Rhodes, J. Scanlan, and R. Levy, "Realisation of microwave brune sections," *Electronics Letters*, vol. 1, no. 9, pp. 268–269, Nov 1965.

[89] H. Fujimoto, K. Murakami, and S. Kitazawa, "Equivalent circuits and transmission zeros of the coupled square-loop resonator," *IEICE Electronics Express*, vol. 4, no. 18, pp. 575–581, 2007.

[90] J. Malherbe and T. Bopape, "Pseudo-elliptic bandpass filter with stepped impedance stubs," in *2016 46th European Microwave Conference (EuMC)*. IEEE, 2016, pp. 457–460.

[91] U. A. Bakshi, *Circuit Analysis II*. 1st Edition, Technical Publications Pune, 2009.

[92] S. Yıldız, A. Aksen, and S. B. Yarman, "Multiband and concurrent matching network design via brune sections," in *2017 24th IEEE International Conference on Electronics, Circuits and Systems (ICECS)*. IEEE, 2017, pp. 90–93.

[93] B. Silveira, C. Ouslis, and A. S. Sedra, "Passive ladder synthesis in filtorx," in *1993 IEEE International Symposium on Circuits and Systems*. IEEE, 1993, pp. 1431–1434.

[94] D. C. Youla, *Theory and synthesis of linear passive time-invariant networks*. Cambridge University Press, 2016.

[95] P. Pramanick and P. Bhartia, *Modern RF and microwave filter design*. Artech House, 2016.

[96] S. Darlington, "Synthesis of reactance 4-poles which produce prescribed insertion loss characteristics: Including special applications to filter design," *Journal of Mathematics and Physics*, vol. 18, no. 1-4, pp. 257–353, Sep 1939.

[97] T. Fujisawa, "Realizability theorem for mid-series of mid-shunt low-pass ladders without mutual induction," *IRE Transactions on Circuit Theory*, vol. 2, no. 4, pp. 320–325, 1955.

[98] H. Watanabe, "Synthesis of band-pass ladder network," *IRE Transactions on Circuit Theory*, vol. 5, no. 4, pp. 256–264, 1958.

[99] F. Lu and T. Nishi, "On the realizability of bandpass ladders composed of two kinds of lc resonant sections," in *ITC-CSCC: International Technical Conference on Circuits Systems, Computers and Communications*, 1996, pp. 158–161.

[100] J. Meinguet and V. Belevitch, "On the realizability of ladder filters," *IRE Transactions on Circuit Theory*, vol. 5, no. 4, pp. 253–255, 1958.

[101] H. Ozaki and J. Ishii, "Synthesis of transmission-line networks and the design of uhf filters," *IRE Transactions on Circuit Theory*, vol. 2, no. 4, pp. 325–336, Dec 1955.

[102] Z. Yang, Y. Yao, Z. Liu, M. Li, T. Li, and Z. Dai, "Design of high efficiency broadband continuous class-f power amplifier using real frequency technique with finite transmission zero," *IEEE Access*, vol. 6, pp. 61 983–61 993, 2018.

[103] S. Yildiz, A. Aksen, and S. B. Yarman, "A numerical approach for the design of matching networks consisting of brune sections based on fujisawa constraints," in *2018 18th Mediterranean Microwave Symposium (MMS)*. IEEE, 2018, pp. 171–174.

[104] S. Yildiz, A. Aksen, S. Kilinc, and S. Yarman, "Dual band stop filter design via frequency transformation and synthesiswith lumped resonators," *IET Circuits, Devices & Systems*, 2020.

[105] H. Uchida, H. Kamino, K. Totani, N. Yoneda, M. Miyazaki, Y. Konishi, S. Makino, J. Hirokawa, and M. Ando, "Dual-band-rejection filter for distortion reduction in rf transmitters," *IEEE Transactions on Microwave Theory and Techniques*, vol. 52, no. 11, pp. 2550–2556, Nov 2004.

[106] P. Castillo-Araníbar, A. Garca-Lampérez, S. Llorente-Romano, and D. Segovia-Vargas, "Dual-band band-stop microstrip filter with controllable bands based on unequal split ring resonators," *IET Microwaves, Antennas Propagation*, vol. 13, no. 12, pp. 2119–2128, Oct 2019.

[107] R. Cameron, M. Yu, and Y. Wang, "Direct-coupled microwave filters with single and dual stopbands," *IEEE Transactions on Microwave Theory and Techniques*, vol. 53, no. 11, pp. 3288–3297, 2005.